Impact of treated wastewater irrigation on soil structure and soil water dynamics

Dissertation
zur Erlangung des
Doktorgrades der Naturwissenschaften (Dr. rer. nat.)

der

Naturwissenschaftlichen Fakultät III
Agrar- und Ernärungswissenschaften,
Geowissenschaften und Informatik

der Martin-Luther-Universität Halle-Wittenberg

vorgelegt von

Herrn Leuther, Frederic
Geb. am 26.06.1987 in Lindenfels

1. Gutachter: Prof. Dr. Hans-Jörg Vogel
2. Gutachter: Prof. Dr. Jörg Bachmann
Verteidigung am: 29. April 2019

Summary

The usage of treated wastewater for agricultural irrigation has become most attractive for areas afflicted by water scarcity due to its year-round availability, the conservation of potable water, and recycling of nutrients. It has been observed that its higher loads of salts, sodium, organic matter, and suspended solids can have critical impacts on physical, chemical, and biological soil properties. However, little is known on the long-term effects on soil structure and soil water dynamics. The usage of reclaimed water may affect the soil pore network and the wettability of mineral surfaces and hence promotes flow instabilities and changes in hydraulic properties. These changes might influence the plant availability of water and nutrients, promote leaching of water and dissolved chemicals below the active root zone, and induce water loss by surface run-off.

In this study, the long-term effects of irrigation with treated wastewater on soil structure, wettability, and soil hydraulic properties were jointly analysed. In particular, the stability of infiltration fronts, water retention, and unsaturated hydraulic conductivity were measured and contrasted with changes in physicochemical and structural soil properties. Therefore, undisturbed samples from the topsoil of two different citrus orchards located in Israel were investigated: (i) a sandy clay loam that was irrigated with treated wastewater for more than 30 years; (ii) a loamy sand where irrigation was changed from fresh water to treated wastewater in 2008 and back to fresh water in 2012 at some experimental plots. At both locations, samples were taken below the irrigation drippers and from the non-irrigated soil between the rows of trees as a control.

Typically, soil structural and hydraulic characteristics have been determined in cylindrical soil cores to minimise the potentially disruptive surface area of the sampling containers. However, a non-destructive detection of water movement in soil cores have been difficult due to the opaque nature of soil. X-ray computed tomography and X-ray radiography are powerful tools for non-invasive and non-destructive investigation of soil structure and water dynamics in undisturbed samples. However, a direct derivation of soil moisture changes from X-ray attenuation has been impossible due to beam hardening and latency of the detector panel. A calibration protocol for the correction of beam hardening effects and panel latency was developed, which enables a quantitative determination of the changing average water content in two-dimensional projections of intact soil cores. Therewith, it was possible to investigate the impact of treated wastewater irrigation on infiltration instabilities caused by a decrease in soil wettability. A test series with decreasing initial water contents was run to simulate different irrigation strategies since water repellency is highly sensitive towards water content. Furthermore, seasonal dynamics were included to test for persistence of repellency, and the effect of reclaiming of water repellent soil by fresh water irrigation. Since samples

remained intact, measurements of soil structure, soil water retention, hydraulic conductivity, and physicochemical characteristics for the same samples were possible. The macro-pore network for pores larger than 19 µm was determined by X-ray computed tomography and analysed with regard to its depth profile, pore size distribution, and pore connectivity. Differences in soil structure, texture, and physicochemical characteristics were used to analyse how treated wastewater irrigation potentially changed soil hydraulic properties.

In summary, the thesis provides experimental evidence that long-term irrigation with treated wastewater affected soil structure and soil hydraulic properties of two common soils in Israel, but its severity was dependent on soil texture. By using a newly developed approach to detect changes in water content in undisturbed soil cores, it was possible to quantify the spatial pattern of infiltration fronts without any damage to the sample. The stability of infiltration fronts was dependent on the history of wastewater irrigation at the site and the initial water content. Organic substances contained in the irrigation water significantly changed the wettabilities of the soils. Changes in the pore space could be explained by differences in texture composition, soil physicochemical parameters, and hydraulic properties. The structure analysis showed that irrigation supported the development of a connected macro-pore network, but for the expense of clay loss, reduced water retention, and diminished unsaturated hydraulic conductivity. Overall, the investigated sandy clay loam was much more resistant to soil alteration by treated wastewater irrigation than the loamy sand.

Zusammenfassung

Die Verwendung von behandeltem Abwasser zur landwirtschaftlichen Bewässerung ist insbesondere für Regionen mit Wasserknappheit attraktiv geworden. Begründet ist dies durch dessen ganzjährige Verfügbarkeit, die Schonung von Trinkwasserressourcen und der Möglichkeit zur Wiederverwendung von Nährstoffen. Studien haben jedoch gezeigt, dass eine höhere Belastung mit Salzen, Natrium, organischen Stoffen und Schwebstoffen kritische Auswirkungen auf die physikalischen, chemischen und biologischen Bodeneigenschaften haben können. Derzeit ist noch unklar, ob die langfristige Verwendung von wiederaufbereitetem Wasser die Bodenstruktur und die Benetzbarkeit mineralischer Oberflächen beeinträchtigen und damit Fließinstabilitäten und Veränderungen der hydraulischen Eigenschaften begünstigen kann. In der Konsequenz könnte so die Pflanzenverfügbarkeit von Wasser und Nährstoffen beeinflusst, der Transport von Wasser und gelösten Chemikalien unterhalb der aktiven Wurzelzone gefördert sowie Wasserverluste durch Oberflächenabfluss hervorgerufen werden.

In dieser Studie wurden verschiedene Auswirkungen der Langzeitbewässerung mit behandeltem Abwasser auf die Bodenstruktur, die Benetzbarkeit und die bodenhydraulischen Eigenschaften analysiert. Insbesondere wurden die Stabilität der Infiltrationsfronten, die Wasserretention und die ungesättigte hydraulische Leitfähigkeit untersucht sowie den Veränderungen der physikalisch-chemischen und strukturellen Bodeneigenschaften gegenübergestellt. Hierfür wurden ungestörte Proben aus dem Oberboden zweier Zitrusplantagen in Israel untersucht: (i) ein sandig toniger Lehm, der seit mehr als 30 Jahren mit behandeltem Abwasser bewässert wird; (ii) ein lehmiger Sand, bei dem die Bewässerung 2008 von Frischwasser auf gereinigtes Abwasser und 2012 auf einigen Versuchsflächen wieder auf Frischwasser umgestellt wurde. An beiden Versuchsstandorten wurden Bodenproben unterhalb der Tröpfchenbewässerung entnommen, als Kontrolle dienten Proben aus dem nicht bewässerten Boden zwischen den Baumreihen.

Um das Risiko einer potenziellen Störung der Bodenprobe zu minimieren werden strukturelle und hydraulische Eigenschaften des Bodens typischerweise in zylindrischen Bodenkernen bestimmt. Jedoch ist eine störungsfreie Erfassung von Wasserbewegung in Bodenkernen aufgrund der Undurchsichtigkeit des Bodens schwierig. Die Röntgen-Computertomographie und Röntgen-Radiographie sind leistungsstarke Werkzeuge zur nicht-invasiven und störungsfreien Untersuchung von Bodenstruktur und Wasserdynamik. Eine direkte Ableitung der Bodenfeuchteänderungen aus der Strahlenabschwächung ist aufgrund der Strahlaufhärtung und der Latenz des Detektorpanels nicht möglich.

Zur Korrektur von Strahlaufhärtung und Panel-Latenz wurde ein Kalibrierprotokoll entwickelt, das die quantitative Bestimmung des sich ändernden durchschnittlichen Wassergehalts in zweidimensionalen Projektionen intakter Bodenkerne

ermöglicht. Mit diesem konnte der Einfluss von Abwasserbewässerung auf Infiltrationseigenschaften untersucht werden. Abwasser kann die Benetzbarkeit von Bodenpartikeln verändern, welche empfindlich gegenüber dem Wassergehalt im Boden ist. Daher wurde zur Simulation verschiedener Bewässerungsstrategien eine zusätzliche Versuchsreihe mit abnehmendem Anfangswassergehalt durchgeführt. Darüber hinaus wurden saisonale Dynamiken berücksichtigt, um die Persistenz der Hydrophobizität und die Regeneration durch Frischwasserbewässerung zu testen. Da die Proben intakt blieben, war es möglich Bodenstruktur, Bodenwasserretention, hydraulischen Leitfähigkeit und die physikalisch-chemischen Eigenschaften zu messen. Das Makroporen-Netzwerk für Poren größer 19 μm wurde mittels Röntgen-Computertomographie bestimmt und hinsichtlich des Tiefenprofils, der Porengrößenverteilung und der Porenkonnektivität analysiert. Unterschiede in Bodenstruktur, Textur und physikalisch-chemischen Eigenschaften wurden zur Analyse der hydraulischen Bodeneigenschaften genutzt.

Es konnte gezeigt werden, dass die Langzeitbewässerung mit behandeltem Abwasser die Bodenstruktur und die hydraulischen Eigenschaften des Bodens beeinflusste. Die Ausprägung war jedoch abhängig von der Bodentextur. Durch den neu entwickelten Ansatz zur Erfassung von Veränderungen des Wassergehalts in ungestörten Bodenkernen konnte das räumliche Muster von Infiltrationsfronten quantifiziert werden. Die Stabilität der Infiltrationsfronten war abhängig von der Historie der Abwasserbewässerung am Standort und dem Anfangswassergehalt. Die enthaltenen organischen Substanzen haben die Benetzungseigenschaften der Böden erheblich verändert. Anhand der festgestellten Unterschiede in der Texturzusammensetzung, den physikalisch-chemischen Bodenparametern und den hydraulischen Eigenschaften konnten Veränderungen im Porenraum erklärt werden. Die Bewässerung unterstützte die Entwicklung eines verbundenen Makroporen-Netzwerkes, jedoch auf Kosten von Tonverlust, geringerer Wasserretention und verminderter ungesättigter hydraulischer Leitfähigkeit. In der Gesamtbetrachtung war der untersuchte sandig tonige Lehm wesentlich widerstandsfähiger gegenüber Bodenveränderungen als der lehmige Sand.

Contents

List of Abbreviations

2D	two-dimensional
3D	three-dimensional
ASE	asymptotic standard error
BOD	biological oxygen demand
C	total carbon
Ca	calcium
CA	contact angle
Cl	chloride
DOM	dissolved organic matter
EC	electrical conductivity
e.g.	exempli gratia
Eq.	equation
FAO	Food and Agriculture Organisation of the United Nations
Feb	February
Fig.	figure
FW	fresh water
i.a.	inter alia
i.e.	id est
K	potassium

L	sandy clay loam
meq	milliequivalent
Mg	magnesium
N	total nitrogen
Na	sodium
NaN	not a number
NH_4-N	ammonium nitrogen
NoI	non-irrigated control
NO_3-N	nitrate nitrogen
Oct	October
p	level of significance
P	phosphorus
PLSR	partial least square regression
POM	particulate organic matter
PSD	pore size distribution
S	loamy sand
SAR	sodium-absorption-ratio
SO_4	sulphate
SWRC	soil water retention curve
s.m.	supplementary material
Tab.	table
TSS	total suspended solids
TWW	secondary treated wastewater
vol. %	percentage by volume
WDPT	water drop penetration time test

Variables and constants in equations are explained below the equations. Abbreviations for physical units are declared by the International System of Units.

List of Figures

List of Tables

Chapter 1

Introduction

1.1   Treated wastewater – a promising water resource?

Agriculture is by far the largest water consumer on a global scale (Winpenny et al., 2010). The use of non-conventional water resources like secondary treated wastewater (TWW) is a promising approach to mitigate the pressure on fresh water (FW) resources in water scarce regions (Assouline et al., 2015; Toze, 2006). In the Mediterranean and North African countries, TWW is considered as the only renewable water resource that will increase naturally over time driven by population growth, the extension of wastewater collection and treatment networks, and peoples' acceptance of its application (The World Bank, 2012). Due to its year-round availability, TWW can help to address inter-annual and inter-seasonal fluctuations in the availability of FW. Particularly in Mediterranean countries, that are typically marked by a hot and dry summer, and a rainy winter. Alternative strategies to bridge these fluctuations, such as sea water desalination and the construction of dams or reservoirs are comparably expensive in costs. On the other hand, the usage of raw sewage or saline water implements high risks for crops, environment, and human health (Rahman et al., 2018). The increasing need for water resources as a consequence of the demographic growth, economic development, improvement of living standards, climate change, and pollution, makes wastewater an increasingly valuable resource rather than a waste product (Becerra-Castro et al., 2015; Winpenny et al., 2010). Furthermore, by recycling the remaining organic and inorganic nutrients in plant production, the discharge of effluents into the environment and their degradation can be reduced, particularly the eutrophication of natural water bodies such as lakes, rivers, and the coastal marine environments (Toze, 2006).
In the past decades, Israel has become the promoting pioneer country in TWW reusage. In 2015, 75 % of the wastewater was treated to secondary, and tertiary levels and reused for irrigation, which covered 50 % of total water consumption

by agriculture (OECD, 2015). Worldwide, the agricultural sector is responsible for 70 % of FW abstraction, therefore, also in more humid regions TWW has been considered as a water resource to bridge temporal water shortage (WWAP, 2017). In 2016, the German Environment Agency published a report issuing the boundary conditions for the sustainable reuse of TWW for agricultural irrigation in Germany to build resilience to climate change (Seis et al., 2016).

Although wastewaters are roughly composed of 99 % water and 1 % of suspended, colloidal, and dissolved solids, the reduction of pollutants by water treatment is essential to prevent negative impacts on soil, plants, and human health (WWAP, 2017). In contrast to industrial wastewaters, municipal wastewaters primary of domestic areas are more similar in their physicochemical composition. Moreover, the physicochemical composition becomes more similar with the stage of the sewage treatment (Feigin et al., 1991). During the preliminary and primary stage of a treatment plant, water quality is improved by the sedimentation of solids, removal of large objects and floating materials such as oil and grease. In a secondary stage, organics are degraded in a biological reactor (aerobic or anaerobic). A chemico-physical treatment for nutrient removal or disinfection is classified as a tertiary stage. In Table 1.1 typical parameters of fresh water, untreated, and secondary treated wastewater from three different treatment plants in Israel are presented (Ben-Hur, 2004; Lado and Ben-Hur, 2009), i.e. salinity as electrical conductivity (EC), sodicity as sodium absorption ratio (SAR), total suspended solids (TSS), and organic pollution separated in biological oxygen demand (BOD) and dissolved organic matter (DOM). The secondary treatment of municipal wastewater mainly reduced organic material (including micro-organisms and pathogens), while inorganic substances and physicochemical characteristics were not affected. Secondary treated wastewater has become the standard in developed countries and considered as the sufficient treatment for reuse in agriculture by most institutions (Iannelli and Giraldi, 2011; WWAP, 2017).

The availability of TWW needs to be addressed when considering TWW as a sustainable water resource. Many developing countries are still unable to implement comprehensive wastewater treatment programs, and untreated sewage effluent is a common source for agricultural irrigation (Qadir et al., 2010). While only 8 % of wastewaters produced in low-income countries are treated, up to 38 % in upper-middle income countries and 70 % in high-income countries are treated (Sato et al., 2013). Therefore, an extension of treatment networks is a prerequisite to close the gap between availability and demand on recycled water in many water scarce regions. Although most effluent discharge requirements and regulations are of interest in water pollution control and human health, they do not address agricultural concerns. Informations about specific chemical elements and compounds that affect plant growth and physicochemical soil properties are important for farmers and decision-makers to prevent land degradation (Pedrero et al., 2010).

Table 1.1: Average values of pH, electrical conductivity (EC), sodium absorption ratio (SAR), biological oxygen demand (BOD), total suspended solids (TSS), and dissolved organic matter (DOM) of fresh water, raw sewage, and after secondary treatment of three different treatment plants located in Israel (Lado and Ben-Hur, 2009).

Location and water quality	pH	EC $[\text{dS}\,\text{m}^{-1}]$	SAR $[(\text{meq/L})^{0.5}]$	BOD $[\text{mg}\,\text{L}^{-1}]$	TSS $[\text{mg}\,\text{L}^{-1}]$	DOM $[\text{mg}\,\text{L}^{-1}]$
Fresh water	7.2	0.9	2.5	0	0	4.3
Raw sewage						
Haifa	7.5	2.4	8.5	650	605	191
Tel Aviv	7.8	2.0	4.9	547	330	194
Netania	8.0	1.6	3.8	500	330	144
Secondary treated wastewater						
Haifa	7.9	2.3	7.2	38	47	50
Tel Aviv	8.0	2.0	5.6	6.7	4.4	31
Netania	7.6	1.5	3.5	8.0	6.0	26

1.2   Chances and risks for agricultural reuse

Former studies have concluded, that protection of human health, prevention of environmental degradation, and reduction of adverse effects on crop yield are the main issues that must be considered when TWW is used for irrigation (Paranychianakis et al., 2011). However, the wide variety of chemicals, organics, and micro-pollutants in TWW can have different effects, positive or negative, on crops and soils.

Beneficial substances for agricultural reuse are nutrients, trace elements, and organic matter which can contribute to soil fertility, especially for regions where farmers cannot afford a sufficient fertilisation. For citrus, Hadas and Kislev (2011) calculated that seasonal irrigation with TWW can replace nitrogen-fertilisers up to 55 %, phosphorous up to 21 %, and potassium up to 90 %. Chen et al. (2008) determined an enhanced enzyme activity in soils irrigated with TWW for over 10 years, which is an integrative indicator of soil biological health. As a consequence of the continuous nutrient supply, TWW irrigation can promote an increase in yield on the short-term (Bedbabis et al., 2015). On the long-term, these benefits are often diminished by adverse effects, "a complex interplay of chemical, physical, and biological soil attributes affecting plant production" (Assouline et al., 2015). Depending on the nutrient availability in the soil and the sensitivity of the crop, TWW irrigation can cause overfertilisation, which reduces yield or affects growing

cycles (Iannelli and Giraldi, 2011). The presence of salt ions in soil solution can also prevent the uptake of nutrients and water by plants due to an increase in osmotic potential. Paudel et al. (2016) have shown that the osmotic stress reduced root growth of citrus trees uo to 50 % in a heavy clay soil and up to 20 % in a loamy sand. In their study about the long-term effect of TWW irrigation on the root zone environment, Assouline and Narkis (2013) reported a decline in avocado yield due to the combined effects of reduced water availability, aeration, and physicochemical changes of the rhizosphere.

Adverse effects can occur due to particular types of contaminants: (i) pathogenic micro-organisms can harm workers and consumers health, and contaminate crops; (ii) suspended solids, which are difficult to handle in irrigation systems due to clogging of pipes, drippers, sprinklers, and eventual also soil pores (Ben-Hur, 2004; Lado and Ben-Hur, 2010; Schacht and Marschner, 2015); (iii) dissolved organic matter which can reduce the wettability of soil particle surfaces (Doerr et al., 2000; Wallach et al., 2005); (iv) salts, mainly from sodium, chloride, potassium, calcium, ammonium, and sulphate, increase soil solution salinity and change soil structure (Halliwell et al., 2001; Levy, 2011); (v) the (bio-)accumulation of heavy metals and of organic contaminants such as polycyclic aromatic hydrocarbons, phenols, pesticides, or pharmaceuticals (Müller et al., 2007; Pedrero et al., 2010).

These potentially beneficial and harmful substances can have immediate specific effects, for instance nutrition or toxicity of plants, or the impact of viruses and bacteria on human health. Potential hazards to workers and crops can often be limited by adapting agricultural practises, i.e. reducing exposure of human and crop, using an adequate choice of irrigation systems and crop types for specific tolerances and physical barriers. While intensive research efforts have been invested on the short-term effects of effluent irrigation on plant health and soil chemical properties, the long-term effects on soil structure and soil hydraulic properties are still not fully understood, especially not as a synergistic approach. More specifically, there are only a few studies concerning soil structure alteration due to TWW irrigation and non of them directly measured soil structural attributes. Changes in saturated hydraulic conductivity, clay mineral loss, or aggregate stability were used as indicators to describe the effect of TWW irrigation on soil structure (Levy, 2011; Lado and Ben-Hur, 2009). Specific TWW pollutants were shown to potentially affect soil structure and soil hydraulic properties, which are depict in Figure 1.1 and introduced in the following sections.

1.2.1   Impact on soil structure

The structure of soils and its stability are important properties that contribute to many soil physical processes, such as water retention, infiltration, aeration, root penetration, erosion, and organic matter and nutrient dynamics (Jury et al., 1991).
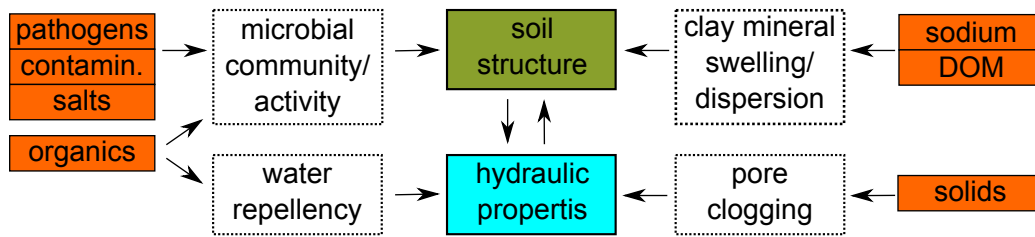
Figure 1.1: Potential effects of treated wastewater pollutants on soil structure and soil hydraulic properties.

Independent of water quality, irrigation generally increases the amount of water passing through the soil compared to natural conditions and can accelerate mineral weathering, mass transfer, and soil structure alteration (Murray and Grant, 2007). In Israel, irrigation water supply is usually adjusted to the calculated daily evaporation rate, hence soil is kept moist and undergoes less swelling-shrinking and wetting-drying cycles than under natural conditions.

It is well known that soil structure is to a large extent formed by soil biota, and that microbial communities play a critical role in organic matter decomposition, in shaping the physical characteristics of the soil, and in stabilising soil structure (Bottinelli et al., 2015; Minz et al., 2011; Oades, 1993). Studies about the impact of TWW irrigation on soil microbiology have shown that salts, contaminants, additional micro-organisms, and the quality and quantity of organic matter in irrigation water can shape the formation of soil biological communities (Adrover et al., 2012; Frenk et al., 2014; Ibekwe et al., 2018), and could therefore affect soil structure. In addition to its nutritional value, organic matter also contributes to the formation and stabilisation of soil architecture as a cementing agent. However, higher loads of organic matter in the effluents are reported to result in inconsistent effects on the carbon concentrations of the topsoil in the field. While in some soils, the organic carbon concentration was increased (Jueschke et al., 2008), in others the effect was marginal (Lado et al., 2012) or it was reduced by priming effects due to the stimulation of microbial activity (Adrover et al., 2012). Despite affecting the total content of soil organic matter, their composition can change towards an increase in aliphatic substances, which are known to affect the wettability of soil minerals (Tarchitzky et al., 2007).

Soil water salinity can have a positive effect on soil particle aggregation and stabilisation since charged cations promote the flocculation of soil colloids. However, TWW often contains high amount of sodium ions which have an opposite effect on structure as they promote clay dispersion, surface sealing, and swelling of clay minerals. In comparison to calcium and magnesium ions, sodium in soil solution is a strongly hydrated monovalent ion that forms weak outer-sphere surface complexes and disrupts the binding energies between clay particles by penetrating the

silicate layers. In addition, the presence of dissolved organic matter can promote clay dispersivity as negatively charged humic substances bind to the positively charged edges of clay minerals and prevent their flocculation (Tarchitzky et al., 1999). Studies have shown that the usage of TWW increased the salinity and sodicity of soils at depth down to 1.5 m (Lado and Ben-Hur, 2009; Levy, 2011; Bedbabis et al., 2014) together with clay migration due to the dispersion of clay minerals in the topsoil (Bardhan et al., 2016). The latter can enhance soil sealing, reduces infiltration, increases soil loss in sandy soils, and enhances slaking in clay soils (Lado et al., 2005). Studies have shown that the impact of TWW irrigation on soil structure may result from a variety of biological, physical and physicochemical mechanism, and that the severity of different pollutants seems to be soil-dependent. However, there is a gap in research about how these changes affect soil structure and thereby soil water dynamics, especially on the long-term. One explanation for the lack of studies in that area could be that the detection of soil structure is a rather difficult procedure (Díaz-Zorita et al., 2002).

In this study, a pore perspective description of soil structure was followed, where soil structure is defined by different type of pores and where the surfaces of soil particles mark the walls of the pore space (Elliott and Coleman, 1988; Rabot et al., 2018). According to their origin, pores can be classified into primary and secondary pores. Primary pores are defined by the arrangement of primary soil particles, their sizes are smaller than 20 µm. Larger secondary pores (structural pores) result from environmental stresses such as biological activity, climate, and management practises (Rabot et al., 2018). The stability describes the ability of the soil to retain its arrangement of pores and solid particles when exposed to these stresses.

The methods used to characterise structural attributes of a soil often depend on the research questions, as there is no universally accepted way to measure soil structure (Díaz-Zorita et al., 2002). One direct method is the use of X-ray computed tomography (CT), where the pore space of an opaque, undisturbed soil sample can be evaluated by non-destructive radiation with high accuracy (Wildenschild and Sheppard, 2013). Imaging techniques enable a quantitatively description of the soil samples structural components, such as macro-porosity and pore size distribution. In addition, this method allows for attributes analyses of single features, such as their spatial distribution and connectivity. Therefore, samples must be taken with caution in order to avoid disturbances. The reconstructed 3D images often need to be processed and optimised to receive unbiased information about the structural features (Schlüter et al., 2014). The information gained using imaging techniques are limited to the selected resolution, which is defined by the sample size and the detector panel.

1.2.2   Impact on soil hydraulic properties

The availability of soil to store, release, and transport water is strongly related to soil structure and therefore affected by changes within the pore system. The amount of water contained in a volume of soil at a certain free energy (water potential) is one of the fundamental relationships in soil physics, often expressed as the soil water retention curve. The second relationship is the hydraulic conductivity as a function of changing water content or water potential. Both relationships are highly non-linear, soil specific (soil structure, textural composition, organic matter, salinity), and affected by the direction and rate of change of soil moisture (Hillel, 1998). In the unsaturated zone, water is retained by both capillary forces in soil pores and absorption onto solid phase surfaces. Capillarity results from the surface tension of water and its contact angle with the solid particles.

In a simplified conceptual capillary model, where the pore system of a soil is described as a bundle of cylindrical capillaries with different radii, soil structure alteration as described in the section above would directly change soil hydraulic properties (Lado and Ben-Hur, 2009). Defined by the Young-Laplace equation, both the capillary pressure (ρ_c),

$$\rho_c = \frac{\sigma_w}{r},$$
(1.1)

and the capillary rise (h),

$$h = \frac{2\sigma_w cos\gamma}{\rho_w gr},$$
(1.2)

against gravity (g) of a single pore are directly related to its pore radius (r). σ_w is defined as the surface tension, ρ_w the water density, and γ the contact angle between the solid–liquid interface and the liquid–gas interface. Both a reduction in pore radii and in surface wettability of the solid phase ($\gamma > 0$), would reduce the ability of soil to retain water.

Also the quantity of water percolating through a pore per unit of time (Q), as described by Hagen-Poiseuille equation,

$$Q = \frac{\pi r^4 \Delta \psi}{8\eta l},$$
(1.3)

and its conductivity (K),

$$K = \frac{r^2}{8\eta},$$
(1.4)

are strongly dependent on the pore radius ($\Delta \psi$ = difference in hydraulic potential, η = viscosity of the fluid, and l = flow section).

By using this simplified model it becomes apparent that changes in pore radius and

wettability affect soil hydraulic properties. Water retention and movement of water and solutes through soils are strongly determined by the capillarity of soil pores. In a non-idealised soil pore network further attributes have to be accounted, the solid and liquid interfacial properties, the connectivity of the pore system, pore orientation, aggregation, and the spatial distribution of components with different hydraulic properties such as roots, organic matter, or stones (Hillel, 1998; Or and Tuller, 2005; Rabot et al., 2018).

The complexity of the system makes it difficult to distinguish between different effects and mechanisms driven by TWW irrigation. Thus, previous studies mainly concentrated on single effects of TWW irrigation on soil structure and hydraulic properties. They concluded, that a reduction in hydraulic conductivity and water retention could be related to: (i) the retention of organic matter on pore walls and clogging of pores by suspended solids and biomass (Aiello et al., 2007; Coppola et al., 2004; Gharaibeh et al., 2016; Lado and Ben-Hur, 2010; Levy et al., 1999); (ii) deflocculation, dispersion, and transport processes of clay minerals due to sodium and dissolved organic matter (Assouline et al., 2016; Coppola et al., 2004; Mace and Amrhein, 2001; Tarchitzky et al., 1999); (iii) a reduced wettability of mineral surfaces by organics (Schacht et al., 2014; Tarchitzky et al., 2007; Wallach et al., 2005; Wallach and Graber, 2007). Furthermore, it was shown that water repellency by organics and the development of surface crusts by sodium reduced water infiltration and caused preferential flow (Arye et al., 2011; Gonçalves et al., 2007; Rye and Smettem, 2017; Wallach and Jortzick, 2008).

There is an extensive body of literature on the impact of TWW on soil physical properties but their results were not entirely consistent. One explanation for the inconsistency is that the severity of different mechanisms was dependent on soil texture, sample depth, and the history of TWW irrigation. Another explanation is, that the wide mixture of different substances in TWW affected soil physical properties differently, i.e. they could have enhanced or counteracted each other.

Vinten et al. (1983) and Levy et al. (1999) have shown, that the accumulation of suspended solids and the accompanied reduction in hydraulic conductivity was greatest for fine textured soil, while sandy soils were only slightly affected. Most solids accumulated close to the soil surface, while deeper soil layers were not affected. Both studies concluded that the higher carbon and nitrogen input by TWW could have enhanced the impact on hydraulic conductivity due to bioclogging, a stimulation of bacteria growth occupying the pore space. Conversely, Mathan (1994) reported an increase in hydraulic conductivity for a sandy clay loam due to higher loads of organic material supporting soil aggregation and structural stability. The effect of salinity and sodicity on soil hydraulic properties have been studied intensively concluding that, "the effect of salinity (EC) on soil permeability oppose those of sodicity (SAR): permeability increases with increasing EC, whereas permeability decreases with increasing SAR" (Assouline et al., 2016). Although

soils irrigated with TWW were usually not classified as sodic soils, the seasonal fluctuation from high saline TWW to low saline rain water harmed hydraulic conductivity and infiltration properties on the long-term (Bedbabis et al., 2014; Ben-Hur et al., 2009; Coppola et al., 2004; Levy et al., 2005; Mace and Amrhein, 2001). Sodium affects clay minerals, therefore, a reduction in hydraulic conductivity by TWW irrigation was mainly found in fine textured soils. The presence of DOM in soil solution intensified the impact of sodium on soil structure (Suarez and Gonzalez-Rubio, 2017; Tarchitzky et al., 1999).

Soil water repellency has been commonly associated with certain vegetation types rich in lipids (i.a. citruses), plant root exudate, fungal hyphae, and as a consequence of forest fire (Doerr et al., 2000). However, Wallach et al. (2005) have shown that the significant concentrations of organics in TWW changed the wettability of soil particle surfaces. The coating of soil particles with hydrophobic, long-chained organic molecules and the interstitial accumulation of particulate organic matter can change soil water dynamics (Bauters et al., 2000). The level of repellency depends on the extend of particle surfaces coated with hydrophobic molecules, hence coarse textured soils are more prone to water repellency than fine textured soils (Doerr et al., 2000). The impact of reduced wettability on soil hydraulic properties can drastically change with soil water content. Aliphatic molecules consist of a hydrophobic non-polar hydrocarbon chain and a hydrophilic polar functional group. When exposed to water, these molecules can change their orientation due to the attraction of their functional group to water and render the mineral surface from non-wettable to wettable (Doerr and Thomas, 2003).

Studies have shown, that water repellency destabilised soil water infiltration, which caused preferential flow and surface run-off (Bughici and Wallach, 2016; Dekker and Ritsema, 1994; Ganz et al., 2013; Lamparter et al., 2006; Rye and Smettem, 2018; Wallach et al., 2013). Further, it reduced soil water retention (Bauters et al., 2000; Diamantopoulos et al., 2013; Rahav et al., 2017), inhibited evaporation (Or et al., 2013; Rye and Smettem, 2017; Shokri et al., 2008), and decreased hydraulic conductivity (Arye et al., 2011; Lado and Ben-Hur, 2009; Schacht and Marschner, 2015). These alterations could increase with time, especially when soils are not tilled (Müller et al., 2016). Although many research have already been done on the causes of water repellency and their affect on soil hydraulic properties, little attention has been paid to the possible impact of irrigation with TWW on water repellency (Levy and Assouline, 2011). Furthermore, most laboratory studies issuing water repellency and its impact on water movement in soils neglected a potential effect of soil structure.

In Israel, orchards are usually irrigated via drip irrigation and soil cultivation is reduced to inorganic fertilisation without any tillage. On the long-term, the locally concentrated application of TWW could have a high impact on the water and nutrient availability for plants.

1.3   Objectives and outlines of the thesis

The main objective of this thesis was to jointly analyse the effect of long-term irrigation with TWW on soil structure, wettability, and soil water dynamics in undisturbed soils. Studies have indicated that organic matter in recycled water affected, either positively or negatively, the soil's structure and on an independent manner decreased the soil wettability. Further, higher contents on sodium may enhance clay mineral swelling and dispersion, while suspended solids can cause pore clogging. Both, soil structure alteration and contact angle increase have a significant influence on soil physical properties, e.g. water retention characteristics, soil sorptivity, water flow, and solute transport regimes. These changes in soil properties could affect the water and nutrient availability to plant roots and may enhance leaching of water and dissolved chemicals below the active root zone and contaminate groundwater. Yet, the knowledge about the synergistic effect of soil structure alteration and reduced wettability on water infiltration, retention, and flow in soil is still lacking. To narrow this gap, physicochemical soil properties, infiltration characteristics, water retention, unsaturated hydraulic conductivity, and structural properties of undisturbed soil columns were investigated. Samples were taken from 2 citrus orchards irrigated with TWW for more than 7 years were investigated.

This research followed the hypotheses that TWW irrigation may change water retention and flow regime in the topsoil due to

   (i) the alteration of wettability and herewith the development of preferential flow path,

  (ii) the change in soil biological communities and their structure forming potential,

 (iii) the physicochemical alteration due to higher loads of salts and organic material.

As discussed in the introduction, all three aspects need to be considered to evaluate the impact of effluent irrigation on the soil water budget and solute leaching. A combined analysis of changes in wettability and soil structure in response to effluent irrigation could open new possibilities for steering soil functions and optimising management strategies in water scarce areas.

To investigate a variety of soil characteristics at the same undisturbed samples by different methods, non-destructive techniques had to be used to analyse soil structure and water flow. Hitherto, no non-destructive approach for the quantification of water flow in cylindrical soil cores via common X-ray radiography was available. Most X-ray systems are using a polychromatic beam, a range of energy

spectrum, which prevents to quantify changes in water content straight by changes in attenuation. Therefore, a correction protocol for beam hardening and panel latency was developed, which is presented in **Chapter 2**. A non-destructive method to determine changes in water content using X-ray radiography, which bases on a direct, soil specific calibration for the full range of soil and water content along the beam line.

This suitable approach was used to study how long-term TWW irrigation had changed water infiltration characteristics in undisturbed soil columns, which is presented in **Chapter 3**. Therefore, samples were taken from the topsoil of two study sites in Israel with different soil textures and different irrigation regimes (TWW-irrigated, FW-irrigated, and non-irrigated control). To include seasonal affects on water repellency and on infiltration characteristics, samples were taken at the end of the dry season and the rainy season. Additionally, a test series with different initial water contents was run to detect the influence on water movement at different wettabilities and to simulate different irrigation strategies.

In **Chapter 4**, the soil structure of the studied samples are presented and contrasted with soil hydraulic properties, water retention characteristics, and unsaturated hydraulic conductivity. Additionally, soil texture, physicochemical parameters (pH, EC, SAR), water repellency, and carbon and nitrogen concentrations were investigated to explain differences in these soil attributes. Therefore, the multivariate regression method 'Partial Least Squares Regression' was used as an exploratory analysis tool to select suitable predictor variables for soil hydraulic properties at field capacity.

In **Chapter 5**, the determined results of long-term irrigation on soil structure, wettability, and soil hydraulic properties are summarised by reconsidering the stated hypotheses. The findings of this thesis were used to identify further research questions and to provide recommendations for farmers and decision makers.

Chapter 2

Quantitative analysis of water infiltration in soil cores using X-ray

This chapter has been published as a co-first authorship publication of Frederic Leuther and Ulrich Weller who contributed equally to this work: Weller, U., Leuther, F., Schlüter, S., and Vogel, H.-J., 2018. Quantitative analysis of water infiltration in soil cores using X-ray. Vadose Zone J. 17

2.1 Abstract

X-ray radiography is a suitable approach to study water dynamics in undisturbed soil. However, beam hardening impairs the deduction of soil moisture changes from X-ray attenuation, especially when studying infiltration of water into cylindrical soil columns. We developed a calibration protocol to correct for beam hardening effects that enables the quantitative determination of changing average water content in two-dimensional projections. The method works for a broad range of materials and is easy to implement. Moreover, we studied the drift of X-ray attenuation values due to the detector latency and eliminated its contribution to the quantitative analysis. Finally we could visualise the dynamics of infiltrating water into undisturbed cylindrical soil samples.

2.2 Introduction

Knowledge about the patterns of infiltration fronts in soil is important for a better understanding of the translocation of nutrients and pollutants (Hendrickx and Flury, 2001; Jarvis, 2007). However, direct, non-destructive observation of infiltration fronts in opaque soil is difficult. The visualisation of water dynamics is important for a substantial understanding of many processes, such as water storage and

solute transport. X-ray radiography and tomography can be used to determine differences in material density, and as such it is useful not only to investigate soil structure (Wildenschild and Sheppard, 2013) but also to study changes in water content (Hainsworth and Aylmore, 1983). Unfortunately, the measurement signal is small because water has a much lower attenuation of X-ray than mineral soil materials. The signal can be increased by adding tracers (Luo et al., 2008; Mori et al., 1999); however, high concentrations of heavy salts need to be applied for substantial improvement. This may lead to structural damage of the soil. Another approach uses the differences in X-ray attenuation at different energy levels, under the assumption that water attenuation has a constant value in Hounsfield units for any energy (Rogasik et al., 1999).

Another difficulty results from beam hardening as a critical feature when using polychromatic X-ray sources. Each wavelength has a specific attenuation coefficient, and with increasing path length through a sample the spectrum of the ray is shifted toward shorter wavelengths with a lower interaction probability. This has a strong influence on the attenuation coefficient of water along the cross-section of the sample, especially if the soil samples are cylindrical, as is typical for experiments on minimally disturbed soil cores. For circular cross-sections, the range of path lengths through the sample and therefore the range of attenuation values is very large. This effect has been neglected in previous studies (e.g. Bayer et al., 2004) but needs to be accounted for if quantitative results on changing water contents are to be analysed. This is why it has been stated in the past that X-ray cannot be used for quantification of water infiltration (Allaire et al., 2009). Some researchers have overcome this limitation by applying three-dimensional computed tomography (CT) reconstruction, where the elimination of the beam hardening is part of the reconstruction process (Mooney, 2002). For high-resolution CT images, it is now possible to determine the distribution of water in the coarse pore space (e.g., Tracy et al., 2015). This is limited to steady-state images and to very small sample volumes.

Because X-ray attenuation by water is small, some researchers have shifted to the application of neutron radiography (Moradi et al., 2011; Snehota et al., 2015). Kaestner et al. (2016) gave an overview of the different methods applied. While neutron probing is an excellent tool for imaging water, the availability of neutron beam lines is limited. In the past, X-ray studies of water infiltration were mainly performed using flat, quasi-two-dimensional Hele-Shaw cells to minimise beam hardening effects and to homogenise the attenuation field. It is, however, close to impossible to obtain flat and rectangular soil samples that are only minimally disturbed, and the boundary effects of such samples are critical for flow and transport experiments. This is why flow and transport in soil is typically investigated in the laboratory using cylindrical samples (Allaire et al., 2009). Moreover, for cylindrical cores a sampling technology exists that minimises structural disturbance

Table 2.1: Grain size distribution for the studied materials.

soil	sand	silt	clay
loamy sand	84 %	7 %	9 %
sandy loam	65 %	16 %	19 %
coarse sand	94 %	6 %	0 %

(Kuka et al., 2013): a drill guided by a tripod cuts out the cylindrical shape, and short after the cutting blade a steel cylinder is guided over the soil column.

In this study, we developed a methodological approach to quantify water dynamics in terms of volumetric water content during transient infiltration experiments in cylindrical soil cores. It is based on a direct and sample-specific calibration procedure for the full range of soil and water content along the beam line through the circular cross-section of the cores.

2.3   Materials and methods

2.3.1   Soil samples

The approach was tested for 21 soil cores. In this study, we concentrated on three rather contrasting samples. They differed in soil material and in initial water content: two undisturbed soil samples with different textures (a sandy loam and a loamy sand according to FAO taxonomy) and a column filled with dry coarse sand. The sample cylinders were made of polycarbonate, with a wall thickness of 3 mm and an outer diameter of 100 mm. The sample heights were 100 mm for the undisturbed loamy sand and the coarse sand and 200 mm for the sandy loam. The loamy sand column was dried for 7 d in an oven at 50 °C to reduce the initial water content, the sandy loam was at field moisture, and the coarse sand was oven dried at 105 °C prior to the infiltration experiment. In this way, our approach could be tested for different situations ranging from a wet sandy loam where little change in moisture can be expected to a dry coarse sand with potentially strong gradients and sharp infiltration fronts. The soil textures of the different materials are given in Table 2.1.

2.3.2   Experimental design

The setup followed the multi-step flux configuration according to Weller and Vogel (2012). An irrigation device with 21 evenly distributed needles was installed on top of the samples to homogeneously spread the water on the entire surface. A

constant water flux was provided by a peristaltic pump at a flux rate of $j = 8\,\mathrm{mm\,h^{-1}}$. For the coarse sand with its high hydraulic conductivity, we increased the flux rate to $j = 16.2\,\mathrm{mm\,h^{-1}}$ after 168 min and to $j = 64.8\,\mathrm{mm\,h^{-1}}$ after 242.5 min to detect further changes in water content. At the lower boundary, the cylindrical samples were covered with a perforated lid to stabilise the core and placed on a funnel-shaped support that was filled with saturated foamed clay pellets. Thus, percolating water drained freely (seepage boundary) and was transported to the outflow, where water was removed immediately using the same pump as for the irrigation system. To independently measure the total change in water content during infiltration, the entire experimental setup was mounted on a balance and the weight was automatically recorded every 20 s. The experiments were stopped when the total mass remained constant, assuming that an equilibrium of outflow and inflow was reached.

2.3.3   Radiography

The analysis was performed in an X-ray microtomograph (X-TEK XT H 225, Nikon Metrology) with classical radiography to monitor the two-dimensional projection of infiltrating water so that the shape and stability of wetting fronts were detected. To exploit the full range of grey values, slightly different energy settings were chosen for the different materials: loamy sand (140 keV, 470 μA), sandy loam (160 keV, 520 μA), and coarse sand (128 keV, 450 μA). To prevent overexposure at the lateral margins of the detector panel, we used a 2.0 mm (sandy loam), a 1.5 mm (loamy sand), and a 0.5 mm (coarse sand) copper filter. Radiographs were automatically taken every 150 s by averaging 16 frames with an exposure time of one frame per second. In between two records, the source of radiation was switched off to reduce grey value shifts due to latency of the panel.

The complete experimental setup was installed inside the X-ray chamber. To allow for calibrating the measured X-ray attenuation with respect to volumetric water content, the first image was made with an additional water column (radius 27 mm) installed horizontally behind the vertical soil core, which was relatively dry (see Fig. 2.1). Due to the cylindrical forms of the sample and the water column, this image provides (i) a water gradient in the vertical direction across the diameter of the water column and (ii) a gradient in soil thickness in the horizontal direction across the diameter of the soil sample. Afterward, the water column was removed and an image of the dry sample was taken. The sample was not moved during the entire experiment, which is critical for the following analysis.

A drawback of X-ray radiography is slight drifts in grey values due to charging or discharging of the panel while recording the images. The effect of latency varies in time and space because it is highly sensitive to the absorption of radiation from the penetrated material and to the history of the previous images. To reduce the

(a) Schematic setup   (b) Radiography
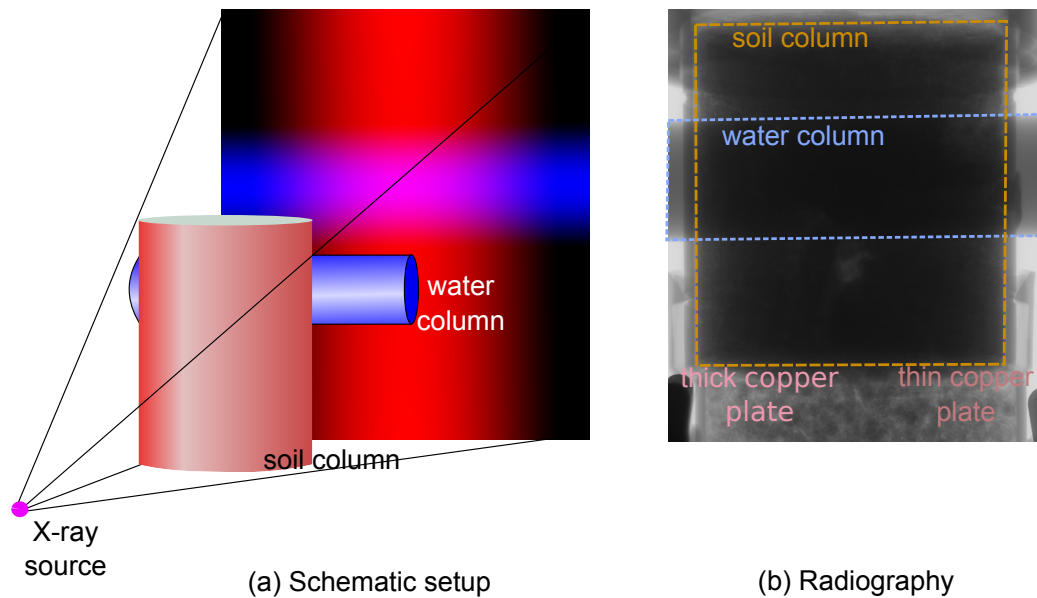
Figure 2.1: Calibration setup with water column added.

influence of grey value shifts during the experiment, we preradiated the panel without the sample for 15 min using the same energy settings as for the subsequent experiment. Thus, the imaging started with a fully charged panel and the grey value drifts were limited to discharging processes. To detect the grey value drift, we installed two flat copper disks of different thicknesses close to the sample cylinder. The thicknesses of the disks were chosen such that their X-ray attenuation corresponded approximately to the minimum and maximum attenuation caused by the soil core (Fig. 2.1b). For the loamy sand, we used 1.5- and 11 mm-thick copper disks and 2.0- and 14 mm-thick disks for the sandy loam.

2.3.4   Image analysis

The calibration procedure was based on the radiography of the soil columns at initial moisture content in combination with the water column (Fig. 2.1). This setup produced a broad range of well-defined water contents above the initial moisture according to the beam length within soil and water. For each pixel of the radiography, the X-ray beam has passed known lengths through soil and through additional water. This can be used for calibration. All image processing was done using the open source software packages QtQuantIm (Vogel et al., 2008) and Fiji ImageJ V. 1.50d (Schindelin et al., 2012) in four steps:

1. *Image generation (QtQuantIm)*: A cylindrical projection for both the water column and the soil column was calculated. Additionally, the radiography of the dry soil with the water column was divided by the dry soil without the water column to obtain the attenuation due to the water column (water attenuation image c). Here, *dry* means the initial soil moisture of the sample before the irrigation had started.

2. *Fitting (Gnuplot)*: An automatic, randomised point data sampling of $300\,000$ pixels within the area of the projected water column was performed. For each pixel, the projected length of the water column (w), the initial grey value due to the soil column (s_0), and the value of the water attenuation image (c) was obtained. This gives the attenuation curve for the amount of water, where the attenuation coefficient is dependent on the initial attenuation by the soil column. The fit was based on minimising the sum of squared residuals of the hyperbola exponential function and the sampled data by varying h_1, h_2, and h_3:

$$c = e^{w\left(\frac{h_1}{(s_0+h_2)}+h_3\right)} \tag{2.1}$$

Equation 2.1 needs fewer parameters and had a lower sum of errors of all the tested curves (exponential, polynomial, and rational).

3. *Image correction (Fiji)*: To eliminate the effect of grey value drifts due to latency of the panel, we calculated the mean grey value for the thick (m) and thin (a) copper disks for every single time step (t) and corrected the initial grey values of the soil column (s_0) for the specific drift by assuming a linear relation between the drifts:

$$s_d = s_0 + \frac{s_0 - a_0}{m_0 - a_0}(m_t - m_0) + \left(1 - \frac{s_0 - a_0}{m_0 - a_0}\right)(a_t - a_0) \tag{2.2}$$

where m_0 and a_0 are the mean initial grey values, m_t and a_t are the mean grey values for the single time step (t), and s_d is the final grey value.

4. *Water quantification (QtQuantIm)*: The amount of water (w_t) added during the experiment along the beam line was quantified in QtQuantIm for every single time step using

$$w_t = \frac{\ln\left(\frac{s_t}{s_d}\right)}{\left(\frac{h_1}{(s_d+h_2)}+h_3\right)} \tag{2.3}$$

where s_t is the grey value for the single time step, and s_d is the driftcorrected initial grey value.

Finally, the quantified water had to be translated into volumetric water content by dividing the result by the projection length of the soil column. For numerical

Table 2.2: Fitting parameters for radiography evaluation for the three soil types. Asymptotic standard error in parentheses [%].

Fitting parameter	h_1	h_2	h_3
loamy sand	3.65×10^{-5} (1.6)	6.96×10^{-2} (3.8)	-2.75×10^{-4} (0.1)
sandy loam	4.89×10^{-5} (1.0)	8.89×10^{-2} (2.3)	-2.64×10^{-4} (0.1)
coarse sand	3.45×10^{-5} (1.2)	6.02×10^{-2} (2.7)	-2.77×10^{-4} (0.1)

reasons, the division image and the projection images were multiplied by an appropriate factor to use the full grey value range of a 16-bit image.

To check the accuracy of the method, water mass balance was calculated both by the mean volumetric water content across the entire soil sample calculated from the radiography and by the increase in total mass.

2.4 Results

2.4.1 Fitting

The relations between grey values of soil, water content, and their division is described by a hyperbola exponential function with three parameters: h_1, h_2, and h_3. Data points and the fitting curve of the loamy sand are plotted in Figure 2.2; the colour scheme of the single dots illustrates the individual vertical distance to the optimised curve. The method of sum of squared residuals provides a parameter fit for the different soils and moisture levels with an asymptotic standard error (ASE) not higher than 4 % (Tab. 2.2). The fit for the sandy loam had the least maximum ASE of 2.3 % for h_2. In comparison to the sandy loam and the coarse sand with a maximum error of 2.7 % for h_2, the fit for the loamy sand has a higher instability, which results in a maximum error of 3.8 %. The higher residuals of the single data points are evenly distributed across the entire range; therefore no systematic trend across the observed fitting range can be detected.

Applying the attenuation coefficient for water without correction for beam hardening in the dark parts, where the attenuation by soil is 0.1, would result in an underestimation of the water content. For the loamy sand and coarse sand only 25 % and for sandy loam only 15 % of the actual water would be detected.

2.4.2 Grey value drift

Figure 2.3 shows the mean grey value drifts with time of the 1.5- and 11.0 mm copper disks during $n = 11$ repetitions with the same experimental settings and
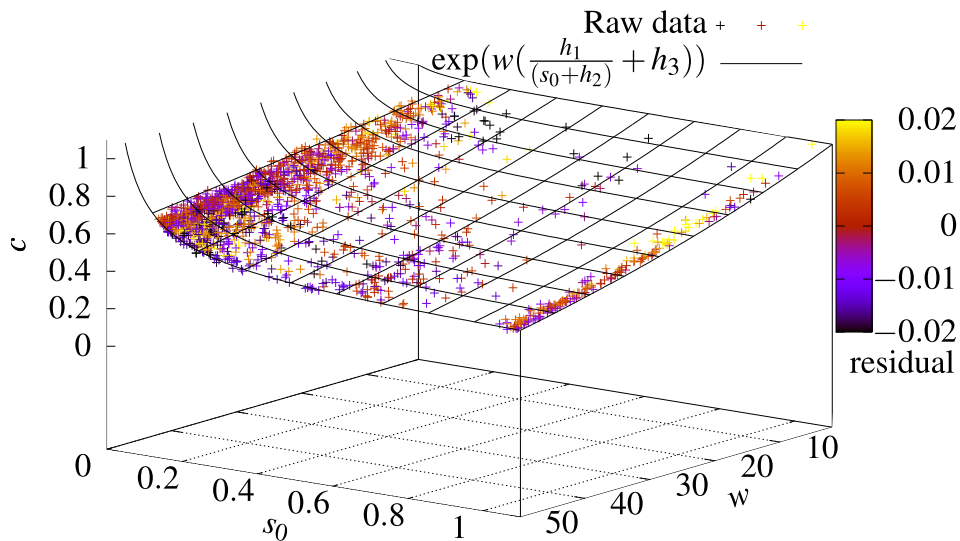
Figure 2.2: Fitted hyperbola exponential function for X-ray attenuation by water: attenuation due to added water column (c), initial attenuation by soil column (s_0), and the projected path length in the water column (w in mm).

their standard deviation. To start with a well defined latency, we pre-radiated the panel for 15 min to charge the panel. During the experiment, the radiation is absorbed by the material and therefore reduced in energy at the panel. This effect is enhanced by a discharging of the panel with time-the grey values are getting lower and therefore the drifts are negative. The thicker copper disks had a mean grey value of around 4300, the thinner of 23 800. These values correspond to the brighter and darker areas in the image of the soil core. For the 11.0 mm copper disks, the mean grey values decrease by $-3.5\,\%$, the 1.5 mm copper disks by $-1.1\,\%$. The grey values of the soil are in between the grey value range of the copper disks and therefore are affected by the drift likewise. The data show a clear negative trend of the grey value drifts, which are related to the density of the radiated material. Hence, correction is necessary to prevent an overestimation of the water front because a negative drift would be interpreted as an increase in water content.

2.4.3   Infiltration fronts via 2D X-ray radiography

Infiltration front propagation and the spatial moisture distribution of the different experiments are shown in Figure 2.4. Three images per sample from different time steps are presented from left to right for the loamy sand (A), the coarse sand (B), and the sandy loam (C). The images give the mean values of water content along
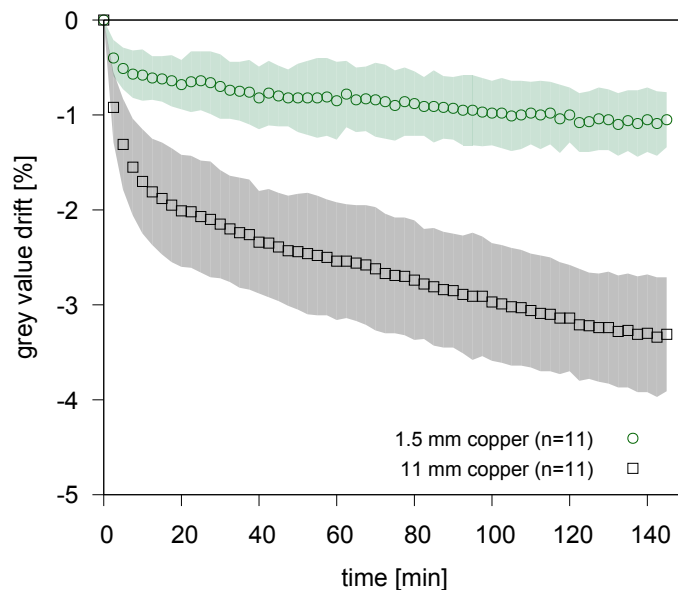
Figure 2.3: Drift of the grey values due to panel latency. Shaded areas indicate the standard deviation; boxes give the mean value for the replicates.

the projected path length; local heterogeneities are pronounced in the lateral parts, but are more leveled out in the central region. The colour code illustrates changes in water content in a range from 0 to 65 vol. %; the values were calculated for every single pixel. Because the velocity of the infiltration front is primarily determined by the change in water content ($\Delta\theta$) across the infiltration front, this front passes much faster in the wet sandy loam than in the dry sandy soils. Therefore, different points in time are presented to better compare the spatial infiltration patterns for the different materials. The wetting front of the dried loamy sand is distributed across the entire sample width and proceeds homogeneously through the soil. The boundary between dry and completely wet soil is sharp. The final increase in water content for the entire sample was about 28.9 vol. %, while at the boundaries and in the uppermost part of the sample this increase was up to 55 vol. % because here the soil was initially drier.

The coarse sand represents an excellent example of preferential flow in unsaturated, coarse-textured soils. Three narrow paths are sufficient to conduct the water to an artificial layer, where water accumulates before flowing to a second layer. In this experiment, the calculated change in water content is equal to the absolute water content because the filled coarse sand was oven dried. The paths on top and the one between the two layers have a mean water content of 7 vol. %, the upper water lenses up to 36 vol. % and the lower up to 55 vol. %. The experiment shows high gradients in water contents and demonstrates the huge heterogeneity of the flow
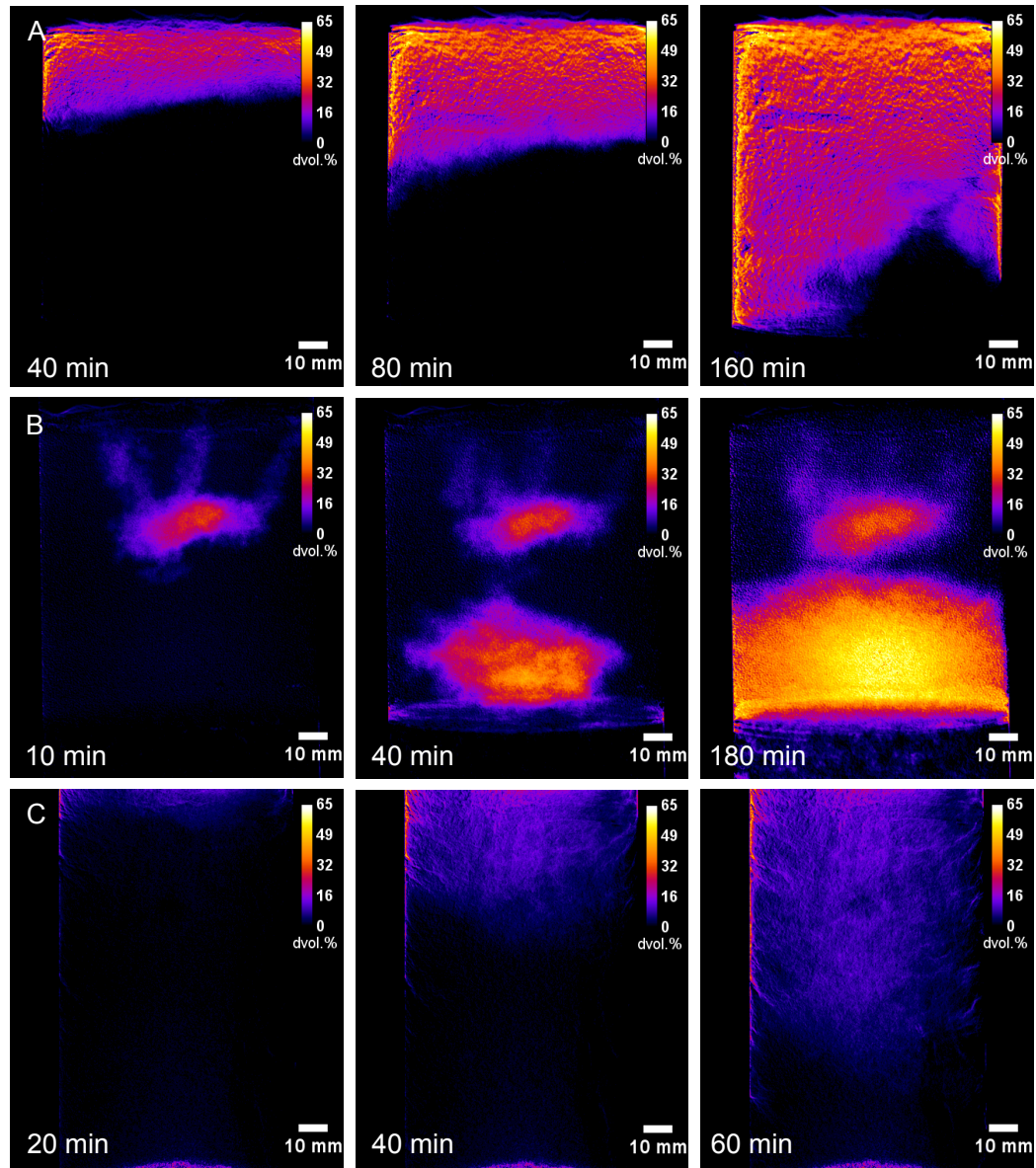
Figure 2.4: Infiltration for three different soils: (A) loamy sand, (B) filled coarse sand, and (C) sandy loam.

field in quantitative terms.

The total increase of soil moisture in the sandy loam was 5.6 vol. %; the infiltration front is clearly detectable for all time steps. Due to higher initial soil moisture in the column, the initial hydraulic conductivity ahead of the infiltration front is higher, the gradient in water content at the front is small (0 to 6 vol. %), and therefore the front is less sharp. Because the clay minerals were already water saturated, artefacts of a swelling soil are negligible.

2.4.4   Quantification of infiltrated water

Figure 2.5 shows the change in water contents calculated by weight gain per volume and the mean determined grey value of the entire sample. The results demonstrate the applicability of the method but also a systematic overestimation of the water content. For the sandy loam the data are most reliable, with a maximum discrepancy of 1.9 vol. % after 90 min. The coarse sand has a maximum discrepancy after 95 min (3.0 vol. %), the loamy sand after 145 min (3.8 vol. %). It was possible to detect the water dynamics in the sandy loam and the changes in water content due to increasing flux rates in the coarse sand after 168 and 242.5 min, respectively. The consistency of the determined changes in water content were verified in a series of soil columns under two conditions (Fig. 2.6). The dried loamy sand had lower deviations and no drift with time, whereas the initially wetter sandy loam had up to 2 vol. % of mean drift.

2.5   Discussion

The differences in water content derived from radiography were in good agreement with the ones obtained via gravimetry. Also, the resulting images of water infiltration showed no lateral gradient due to the cylindrical shape of the soil column. Only at the very edge can an overestimation of water be assumed. Parts of the oversaturation at the boundaries are artefacts due to swelling processes of the soil into former air-filled areas. The method is based on density changes and cannot separate the radiation reduction due to increasing water content from that due to particle movement. The artefacts are therefore predominant at the edges where the radiated soil is thin and small changes have a strong impact on the mean grey value. Therefore, the first 10 pixel rows had to be excluded from further analysis. It can be assumed that the reconstruction of the water content is feasible and that beam hardening has been eliminated with the hyperbolic correction. However, there is no obvious explanation why the correction function should be a hyperbola. The calibration method allows the study of infiltration fronts in minimally disturbed soil columns, which is an advantage over cubic setups that have been studied previously
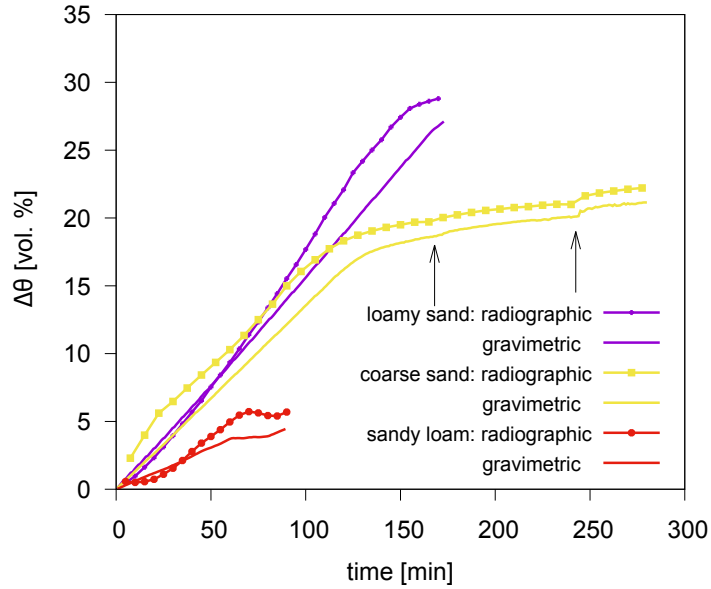
Figure 2.5: Comparison of the change in water content ($\Delta\theta$) using gravimetric and radiographic methods for 3 different columns. Arrows indicate increasing flux rates.
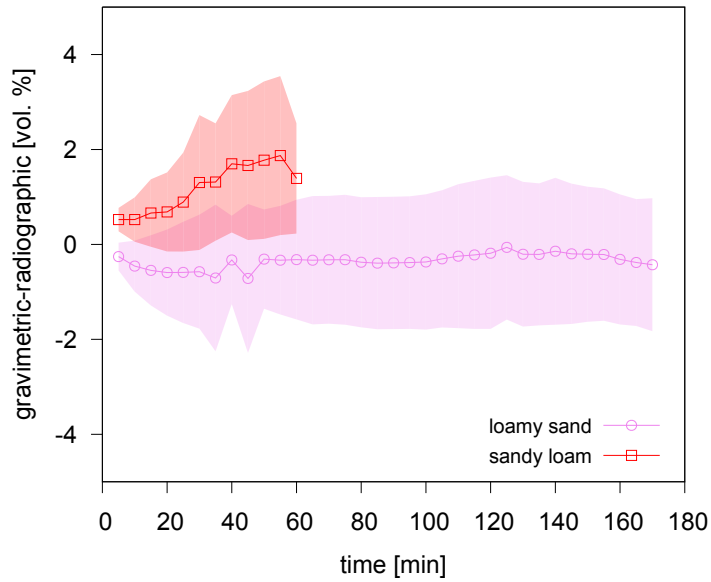
Figure 2.6: Differences between radiometrically and gravimetrically determined changes in water content. Shaded areas indicate the standard deviation; boxes give the mean value for the replicates.

based on radiography.

An obvious drawback of using radiography is the projection of the water content along the sample thickness such that details in the spatial patterns are blurred. This could be overcome with three-dimensional reconstruction of the water content. We did this experiment, calculating the water content for the whole set of 500 radiographs and recalculating the water contents into artificial attenuation images, which were then used for CT reconstruction using conventional filtered back-projection. The quality of the resulting images was, however, as noisy as direct CT reconstruction images and subsequent difference calculation of the Hounsfield values. The main disadvantage for the three-dimensional reconstruction remains: the series of radiographs has to be captured very fast if the water fronts are moving fast. In this case, the two-dimensional reconstruction is clearly superior.

2.6   Conclusions

With the presented procedure, it was possible to quantify changes in water content across the whole range of studied materials. We could eliminate the effects of beam hardening, which enabled us to use minimally disturbed, cylindrical soil cores for our infiltration studies. This technique enables the visualisation and quantification of fast-moving water fronts. It enables the quantitative study of heterogeneous water flow and of nonequilibrium dynamics with simple polychromatic X-ray radiography at a resolution that could be achieved before only by neutron probing or with monochromatic X-ray sources.

Chapter 3

Soil water repellency and its impact on infiltration front stabilities

3.1 Abstract

Irrigation with treated wastewater (TWW) is a common practise in agriculture, mainly in arid and semiarid areas as it provides a sustainable water resource available at all-season in general and at freshwater shortage in particular. However, TWW still contains abundant organic material which is known to decrease soil wettability, which in turn may promote flow instabilities that lead to the formation of preferential flow paths. We investigate the impact of long-term TWW irrigation on water wettability and infiltration into undisturbed soil cores from two commercially used orchards in Israel. Changes of water content during infiltration were quantitatively analysed by X-ray radiography. One orchard (sandy clay loam) had been irrigated with TWW for more than 30 years. In the other orchard (loamy sand) irrigation had been changed from freshwater to TWW in 2008 and switched back in some experimental plots to freshwater in 2012. Undisturbed soil cores were taken at the end of the dry and the rainy season to investigate the seasonal effect on water repellency and on infiltration dynamics in the laboratory. The irrigation experiments were done on field moist samples. A test series with different initial water contents was run to detect the influence on water movement at different wettabilities. In this study we show that the infiltration front stability is dependent on the history of wastewater irrigation at the respective site and on the initial water content.

3.2   Introduction

Crop irrigation with treated wastewater has become a common practise in arid and semiarid areas to deal with water scarcity and to reduce the usage of fresh water. In Israel, the reuse of former wastewater already provides more than 50 % of total water consumption by agriculture (OECD, 2015). Besides the advantages as a sustainable water resource and recycling of nutrients, it has been observed that TWW irrigation may have critical impact on soil hydrological properties mainly induced by the load of organic compounds (DeBano, 1981; Doerr et al., 2000; Wallach et al., 2005). A reduced affinity of soil to water, so called soil water repellency, may lead to reduced infiltration capacities, intensify overland flow, and formation of preferential flow paths that render the spatial wetting pattern uneven (Rahav et al., 2017).
Previous studies have shown these effects as a result of forest fires, decomposing of litter from plants rich in lipids and waxes, root exudates, fungal hyphae, and the usage of irrigation water of poor quality (Bughici and Wallach, 2016; Dekker and Ritsema, 2000; Horne and McIntosh, 2000; Lado and Ben-Hur, 2009; Zavala et al., 2009), concluding that mainly hydrophobic organics influences soil hydraulic properties. The occurrence of water repellency is induced by hydrophobic molecules coating mineral surfaces and by the presence of hydrophobic particles in the pore space (Doerr et al., 2000). The hydrophobic effect of amphipathic coatings depends on soil water content as their non-polar hydrocarbon chains are changing the orientation during drying. Hydrophobicity of soil can become a persistent attribute over time when supply is larger than degradation or leaching of these substances. The occurrence of water repellency and their affect on soil water dynamics is still not fully understood (Doerr et al., 2007). One reason is that the detection of wetting front characteristics and, furthermore, quantifying preferential flow in undisturbed soils is a challenge (Allaire et al., 2009). Therefore, infiltration studies in the past were mainly carried out by using flat, quasi two-dimensional Hele-Shaw cells (Carrillo et al., 2000; Rye and Smettem, 2017; Wallach and Jortzick, 2008; Wang et al., 2000; Xiong et al., 2012), by detecting wetting pattern of soil profiles and transects (Dekker and Ritsema, 1994; Kobayashi and Shimizu, 2007; Lipsius and Mooney, 2006), or by solute transport experiments (Clothier et al., 2000). The impact of water repellency on the wetting behaviour of the soil and the occurrence of preferential flow is already described, but is mainly limited to two-dimensional detection of a three-dimensional process, to a single scenario in the field by destroying the structure, or to point measurements. Rahav et al. (2017) have shown the occurrence of uneven wetting and preferential flow on the field scale via non-invasive ERT-measurements.
A new approach developed by Weller et al. (2018) enables a direct, non-destructive quantification of water infiltration into undisturbed soil cores via X-ray radiography

without the usage of chemical tracers. Compared to X-ray computer tomography image recording takes only seconds, this enables the detection of fast moving water fronts. The results are 2D projections of mean changes in water content along the beam line, i.e. the horizontal sample depth.

The objective of this study was to use this method to investigate influences of long-term TWW irrigation on the stability of infiltration fronts in undisturbed, cylindrical soil cores under different moisture conditions and, therefore, simulate diverse irrigation strategies. Furthermore, we included seasonal dynamics and soil textural differences to test for persistence of repellency, and the effect of reclaiming of water repellent soil by fresh water irrigation.

3.3   Materials and methods

3.3.1   Study sites and soil sampling

The study sites were located in Israel's coastal plain which is dominated by brown-red (degrading) sandy soils and marked by two pronounced climate seasons, a hot and dry summer where orchards are irrigated, and a rainy winter without irrigation. The first sampling location was close to Rehovot, where soil texture is loamy sand (denoted in the following as S). Here, three different treatments of irrigation were investigated: fresh water (FW), treated wastewater (TWW), and no irrigation (NoI). Bulk density and carbon content were different in the irrigated parts ($\rho_b = 1.31\,\mathrm{g\,cm^{-3}}$, $C = 1.2\,\%$) compared to the non-irrigated part ($\rho_b = 1.64\,\mathrm{g\,cm^{-3}}$, $C = 0.6\,\%$), shown in Table 3.1. Soil pH under TWW irrigation ($pH = 5.7$) was reduced compared to NoI ($pH = 7.4$) and FW irrigation ($pH = 7.2$). The second location was close to Hadera, where sandy clay loam (denoted in the following as L) was the predominant soil texture. At this site, no freshwater irrigation was available, only treated wastewater (TWW) and no irrigation (NoI). Bulk density $\rho_b = 1.48\,\mathrm{g\,cm^{-3}}$ and soil $pH = 7.4$ were independent of the irrigation regime. The carbon content under NoI $C = 1.7\,\%$ was higher than under TWW irrigation $C = 0.8\,\%$ (Tab. 3.1). At both study sites, citrus fruit (grapefruit in Rehovot and mandarin in Hadera) were produced. Soil cultivation was mainly reduced to inorganic fertilisation without any tillage. In Rehovot, the water management was changed from fresh water to secondary treated wastewater irrigation in 2008. In 2012, single plots of a block design experiment were converted to ground water irrigation for soil reclamation (Rahav et al., 2017). In Hadera, farmers have used secondary treated wastewater for more than 30 years. At both study sites, the amount of irrigation was adjusted to the daily evapotranspiration rates.

The first sampling was done at the end of dry season (October 2015), when soils were irrigated with the different treatments for seven months. The second campaign

Table 3.1: Site conditions (sites: S=loamy sand, L=sandy clay loam; treatments: NoI=non-irrigated control, FW=fresh water, TWW=treated wastewater): texture (FAO, LS =loamy sand, SCL=sandy clay loam), grain size distribution, bulk density, soil pH_{H_2O}, and carbon content (C).

treatment	texture	sand	silt	clay	bulk density	pH	C
S-NoI	LS	81.4 %	7.8 %	10.8 %	1.64 g cm^{-3}	7.4	0.6 %
S-FW	LS	80.7 %	8.5 %	11.1 %	1.31 g cm^{-3}	7.2	1.2 %
S-TWW	LS	86.2 %	5.9 %	7.9 %	1.32 g cm^{-3}	5.7	1.2 %
L-NoI	SCL	63.4 %	14.3 %	22.3 %	1.48 g cm^{-3}	7.5	1.7 %
L-TWW	SCL	65.5 %	12.6 %	21.8 %	1.48 g cm^{-3}	7.4	0.8 %

was scheduled in February 2016, after four months of the rainy season without irrigation. The samples were taken within the wet soil along the dripper lines (FW and TWW) and between the tree rows beyond the reach of irrigation water (NoI). Soil cores were sampled from the topsoil (0 to 200 mm depth) by using a custom-made drill (UGT GmbH, Germany) for undisturbed sampling of cylindrical soil cores (Kuka et al., 2013). The sample cylinders were made of polycarbonate with a wall thickness of 3 mm and an outer diameter of 100 mm. Depending on the difficulty to take undisturbed samples below the trees we used columns of different height, 100 mm and 200 mm. The samples were immediately stored in plastic bags to keep them field moist, carefully packed, and shipped to Germany. Overall, 13 minimally disturbed soil cores (2 S-FW, 4 S-NoI, 2 S-TWW, 5 L-TWW) were taken in October 2015 and 23 (5 S-FW, 1 S-NoI, 6 S-TWW, 4 L-TWW, 7 L-NoI) in February 2016. Additional 77 undisturbed samples (50 mm in diameter and 50 mm in height) were taken from the topsoil in the vicinity of larger soil cores to test the soil for water repellency.

3.3.2   Soil water repellency

The persistence and intensity of soil water repellency was characterised by two methods, the water drop penetration time test (WDPT) (Doerr, 1998; Letey et al., 2000) and the sessile drop contact angle (CA) (Bachmann et al., 2000). The small (50 mm in diameter) undisturbed soil samples were placed in an oven at 50 °C until a reference water content corresponding to that of air dried soil was reached. WDPT and CA were measured for the upper 50 mm of the soil in an interval of 10 mm following Bughici and Wallach (2016).
The WDPT was determined by placing three drops of 50 µL distilled water on the soil surface and recording the required time for their complete infiltration. The

average time was used to classify their water repellency (Bisdom et al., 1993): class I, not water repellent (infiltration within 5 s); class II, slightly water repellent ($5 < \text{WDPT} \leq 60$ s); class III, strongly water repellent ($60 < \text{WDPT} \leq 600$ s); class IV, severely water repellent ($600 < \text{WDPT} \leq 3600$ s); class V, extremely water repellent ($\text{WDPT} > 3600$ s).

The initial contact angle and its variation in time was measured with a goniometer (EasyDrop DSA20E, KRÜSS GmbH, Germany) for a flat surface of air dried, sieved soil ($< 50\,\mu\text{m}$) from every 10 mm layer. The soil was glued to a double-sided tape attached to a pathology slide to form a flat single layer of soil particles and a drop volume of 15 μL was placed on the single particle layer. The change in drop shape was translated to a change in CA by the Easy Drop Software. The decrease in CA during the contact time $\phi(t)$ of the liquid with soil particles can be influenced by conformational changes, hydration, or rearrangement of organic molecules, coating soil-particle surfaces as a result of contact with water (Graber et al., 2007). Double-exponential-decrease functions were fitted to describe the dynamics of changing CA (Eq. 3.1), as an additional quantification of water repellency persistence.

$$\phi(t) = a * e^{-b*t} + c * e^{-d*t} \tag{3.1}$$

where b, and d represents the rate at which the CA ($a + c$) varies with time (t). The sum of parameter a and c at time point zero is the initial CA, and their ratio describes the relevant dominance of the tailing.

3.3.3   Infiltration experiments

The detection of infiltration fronts in the larger cylindrical, undisturbed soil cores followed the approach developed by Weller et al. (2018). 36 samples were tested for their infiltration characteristics while they were still field moist. Afterwards, a test series with 12 loamy sand samples (6 TWW and 6 FW) at reduced initial soil water content was investigated. Therefore, soil cores were dried in an oven at 50 °C for 3 and for 7 days. All irrigation experiments were performed inside an X-ray microtomograph (X-TEK XT H 225, Nikon Metrology) with the same irrigation rate (Fig. 3.1 a). A peristaltic pump provided a constant flux of $j = 8\,\text{mm}\,\text{h}^{-1}$ which was equally distributed over the soil surface by an irrigation device with 21 needles installed on top of the sample. The applied flux correspond to the irrigation rate of one dripper in the field. To prevent effects on soil chemistry and structure, like dispersion of clay minerals, the salt concentrations of the irrigation water were adapted to the field specific water characteristics (S-FW $EC = 857\,\mu\text{S}\,\text{cm}^{-1}$, S-TWW $EC = 1735\,\mu\text{S}\,\text{cm}^{-1}$, and L-TWW $EC = 1386\,\mu\text{S}\,\text{cm}^{-1}$). At the lower boundary, two different experimental setups were chosen for the field moist samples and the dryer series.
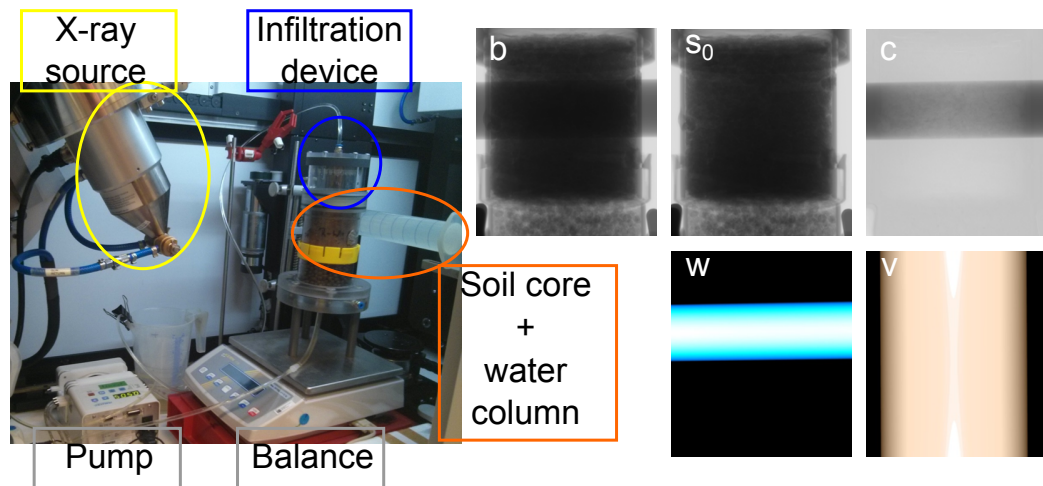
Figure 3.1: Workflow of water quantification: *a*) experimental setup inside X-ray microtomograph *b*) radiography of initial soil plus water column s_0) radiography of initial soil column *c*) water attenuation *w*) projected water column *v*) projected soil column.

Field moist samples: At the lower boundary a prescribed matrix potential was applied through a pressure control system via a ceramic plate. Therefore, matrix potentials were monitored by two tensiometers installed along the vertical profile at 25 mm and 75 mm depth. By adapting the lower boundary to the potential measured by the topmost tensiometer, the flow conditions were forced towards gravity-flow (Weller and Vogel, 2012). The outflow was removed immediately using the same pump as for the irrigation system. To independently measure the total change in water content during infiltration, the entire experimental setup was mounted on a balance and the mass was automatically recorded every 20 s. The experiments were stopped when total mass remained constant, assuming that an equilibrium of outflow and inflow was reached and a stable flow field was established inside the column.

Dry initial conditions: The setup for the dried soil samples was slightly different as the pressure control system could not be used due to the low water potential. The tensiometers were removed and the lower boundary was changed to free drainage conditions (seepage boundary). Therefore, the cylindrical samples were covered with a perforated lid to stabilise the core and placed on a funnel-shaped support which was filled with saturated foamed clay pellets.
Radiographs were taken with different, soil specific energy settings and copper filters to gain a wide grey value distribution: loamy sand 140 keV, 470 μA, and 1.5 mm copper filter, and sandy clay loam 160 keV, 520 μA, and 2.0 mm copper filter. The temporal progress of the fronts were repeatedly captured via constant

imaging of radiograms at time steps of 150 to 600 s by averaging 16 frames with an exposure time of 1 frame per second. Latency of the detector panel can cause artificial grey value drifts during the experiments which impairs the quantification of water movement. To reduce this effect, the radiation source was switched off in between two records and 2 reference copper discs (loamy sand: 1.5 mm and 11.0 mm, sandy clay loam: 2.0 mm and 14.0 mm) were installed next to the samples to correct the images by a linear interpolation between the grey value drifts of the disks.

3.3.4   Quantification of water infiltration

Infiltrating water was quantified as 2D projections of the mean changes in water content along the beam line for every pixel following the work-flow developed by Weller et al. (2018). The method is based on a direct, soil specific calibration of grey values for the full range of soil and water content. Therefore, a radiography was required with an additional water column (radius of 27 mm) mounted perpendicular to the soil column in the background of the sample to calibrate the method before starting the irrigation experiment (Fig. 3.1 b).

This projection provides a broad range of defined water contents because of the cylindrical form of both columns: a water gradient in vertical direction and a soil gradient in horizontal direction. At first, cylindrical projections for the water and soil column were created to store the information of the specific spatial paths length of radiation in an image file (Fig. 3.1 w and v). The attenuation caused by different water contents was obtained by a division of the radiographs with and without the water column (Fig. 3.1 c). A pixel-wise point data sampling of the projected water column (w), the initial soil column (s_0) and the value of water attenuation (c) were used to determine the sample specific variables h_1, h_2, and h_3 of the hyperbola e function (Eq. 3.2).

$$c = e^{w\left(\frac{h_1}{(s_0+h_2)}+h_3\right)}$$ (3.2)

Before calculating the change in water content for every single time step, the radiographs were corrected for the grey value drift due to panel latency by linear interpolation between the drifts of the two copper discs. Finally, the change in water content (w_t) was determined as an integral along the beam line using Equation 3.3, where s_t denotes the grey value for the single time step, and s_d the drift corrected initial grey value.

$$w_t = \frac{\ln\left(\frac{s_t}{s_d}\right)}{\left(\frac{h_1}{(s_d+h_2)}+h_3\right)}$$ (3.3)

The translation into volumetric water content was done by dividing the calculated water image by the projection length of the soil column (v).

Table 3.2: Soil specific fitting parameters.

Fitting Parameter	h_1	h_2	h_3
loamy sand	3.26×10^{-5}	5.95×10^{-2}	-2.78×10^{-4}
sandy clay loam	4.98×10^{-5}	9.02×10^{-2}	-2.70×10^{-4}

This method was developed only after the irrigation experiments for field-moist samples from the first sampling campaign. For these samples the radiographs including the calibration based on the water column was not available. Therefore, a sample specific determination of the variables in Equation 3.2 was not possible. Instead, mean values of soil specific fitting parameters determined from the second sampling campaign were used (Tab. 3.2).For each time step, the average change in water content for the entire sample projection as calculated by image analysis was verified by comparison to the changes in total mass recorded by the balance.

The projections were analysed in a 16 bit format were the maximum value (65 535) corresponds to a change in water content, $\Delta\theta$, of 66 vol. %. Hence, we rescaled the values to a range between 0 to 66 vol. %. To illustrate the change in water content we used a continuous colour code where blue refers to small and yellow to large changes, while black equals no change. The spatial resolution is 0.065 mm per pixel and their values are mean changes $\Delta\theta$ along the beam line. Disturbances at the lower part of the single images were due to the experimental setup. Movements of a bolt or the socket caused artefacts which were detected as changes in water content. Therefore, the values of the lower 20 mm were not considered in analyses of the infiltration characteristics. Furthermore, it should be noticed that the projections are more sensitive to detect preferential flow at the edges of the projected cylindrical body as the averaged soil volume is smaller.

To quantify patterns of water infiltration, a statistical description of the projected flow field at the end of experiments was done. Specifically, the change in mean water content $\Delta\bar{\theta}$ and its standard deviation, sd, was measured for a squared area of 40 000 pixel where water flow was detected. A threshold of $\Delta\bar{\theta} - 3 * sd$ was used to divide the images into areas with and without detected water flow.

3.4   Results

3.4.1   Soil water repellency

WDPT greater than 5 s were detected for all sampling locations except for the non-irrigated part of the loamy sand, indicating marks of water repellency. Figure 3.2 presents the WDPT classifications for the topsoil (0 to -50 mm) of the different

locations, treatments, and seasons. Table 3.3 lists the median WDPT-class for the single layers. For the loamy sand, most FW soil samples were classified as slightly to strongly water repellent and TWW samples as slightly to severely water repellent. Including seasonal dynamics, a reduction of WDPT at the end of the rainy season was detected at the FW irrigated plots, while repellency stayed high under TWW irrigation. In February, most FW samples were classified as not to slightly water repellent, TWW samples as slightly to severely water repellent. For all loamy sand samples water repellency was not changing with depth, independent of the season. For the sandy clay loam, the irrigated samples were mostly classified as not to slightly water repellent. Only after the dry season 14 % of the measurements conducted at TWW samples were classified as strongly water repellent. Samples taken from the non-irrigated parts provided a wide range from not to severely water repellent. This wide spread of classes was also detected for individual layers. L-NoI was the only treatment where WDPT decreased with depth.

The initial contact angles (CA) of the soil surfaces provide similar results in terms of water repellency distribution (Fig. 3.3, top left). Except for NoI of the loamy sand, all measured CA were above $0°$ and therefore classified as sub-critical water repellent ($<90°$) and water repellent ($\geq90°$). To compare the different treatments statistically, an analysis of the initial contact angles measured at the soil surfaces were done by testing Tukey Honestly Significant Differences with a 95 % family-wise confidence level. For the loamy sand, there was a statistical significant ($p < 0.001$) decrease of CA from S-FW October (mean CA $79.8°$ with a standard deviation of ±8.6) to S-FW February ($59.0° \pm13.4$) and no significant difference between S-TWW Oct ($88.7° \pm6.5$) and S-TWW Feb ($91.9° \pm7.2$). Comparing between the irrigated treatments, CA measured in February were significantly higher at TWW-irrigated plots compared to FW-irrigated plots, but no differences in October. For the sandy clay loam, a significant decrease of CA was determined for L-TWW between the two sampling occasions, the mean CA for October was $67.0°$ (±16.4) and for February $39.7°$ (±19.3). Furthermore, the CA at the soil surface of the non-irrigated part ($112.1° \pm7.1$) was significantly higher compared to the irrigated part, and overall the highest. The parameters of the fitted double-exponential-decrease functions of changing CA, $\phi(t)$, with time are presented in Table 3.4. Residuals of the measurements provided an R^2 to evaluate the quality of the fit. The mean values and standard errors were determined for all replications where R^2 was larger than 0.75 and used to plot the decrease in CA with contact time for the different treatments and depths from 0 to -50 mm (Fig. 3.3). Missing values in layer 3 (L-TWW) are due to insufficient qualities of the fits and in layer 5 (L-NoI) due to the wettability of the soil. The rate of decreasing CA (b) was lowest on the top layers for all treatments. For the loamy sand, the rate of decrease for FW soil was two to four times larger than for the TWW soil, especially in -40 to -50 mm depth. For the sandy clay loam, the rate of decrease for the L-TWW was
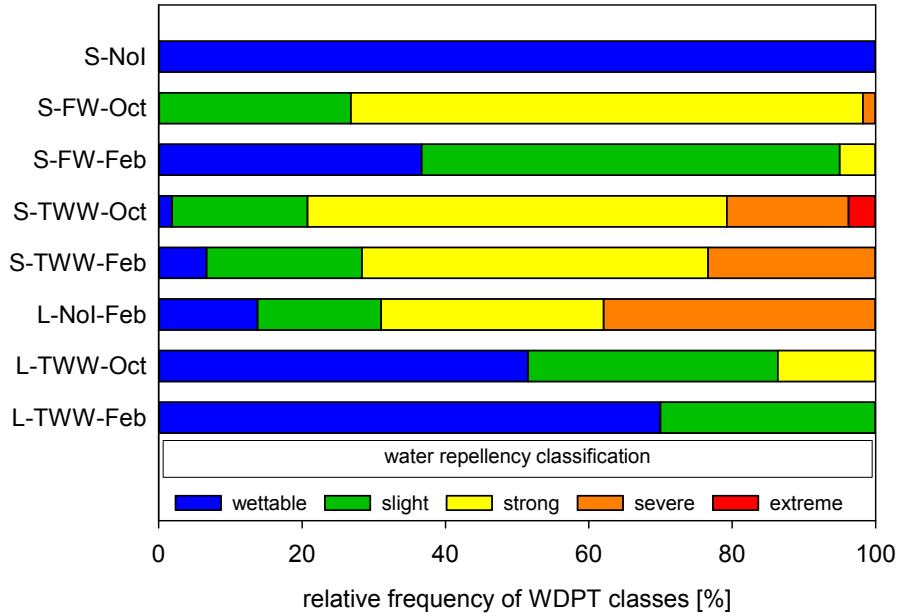
Figure 3.2: Relative frequency of water drop penetration time (WDPT) classes for the topsoil (sites: S=loamy sand, L=sandy clay loam; treatments: NoI=non-irrigated control, FW=fresh water, TWW=treated wastewater; seasons: Oct=October, Feb=February).

Table 3.3: Median water drop penetration time classes for single layers of the topsoil (sites: S=loamy sand, L=sandy clay loam; treatments: NoI=non-irrigated control, FW=fresh water, TWW=treated wastewater; seasons: Oct=October, Feb=February).

Depth	0 mm	−20 mm	−30 mm	−40 mm	−50 mm
S-NoI	1.0	1.0	1.0	1.0	1.0
S-FW Oct	2.0	3.0	3.0	3.0	3.0
S-FW Feb	1.0	2.0	2.0	2.0	2.0
S-TWW Oct	3.0	3.0	3.0	3.0	3.0
S-TWW Feb	3.0	3.0	3.0	3.0	3.0
L-NoI Feb	3.5	4.0	3.0	2.5	1.0
L-TWW Oct	2.0	1.0	1.0	2.0	1.0
L-TWW Feb	2.0	1.0	1.0	1.0	1.0
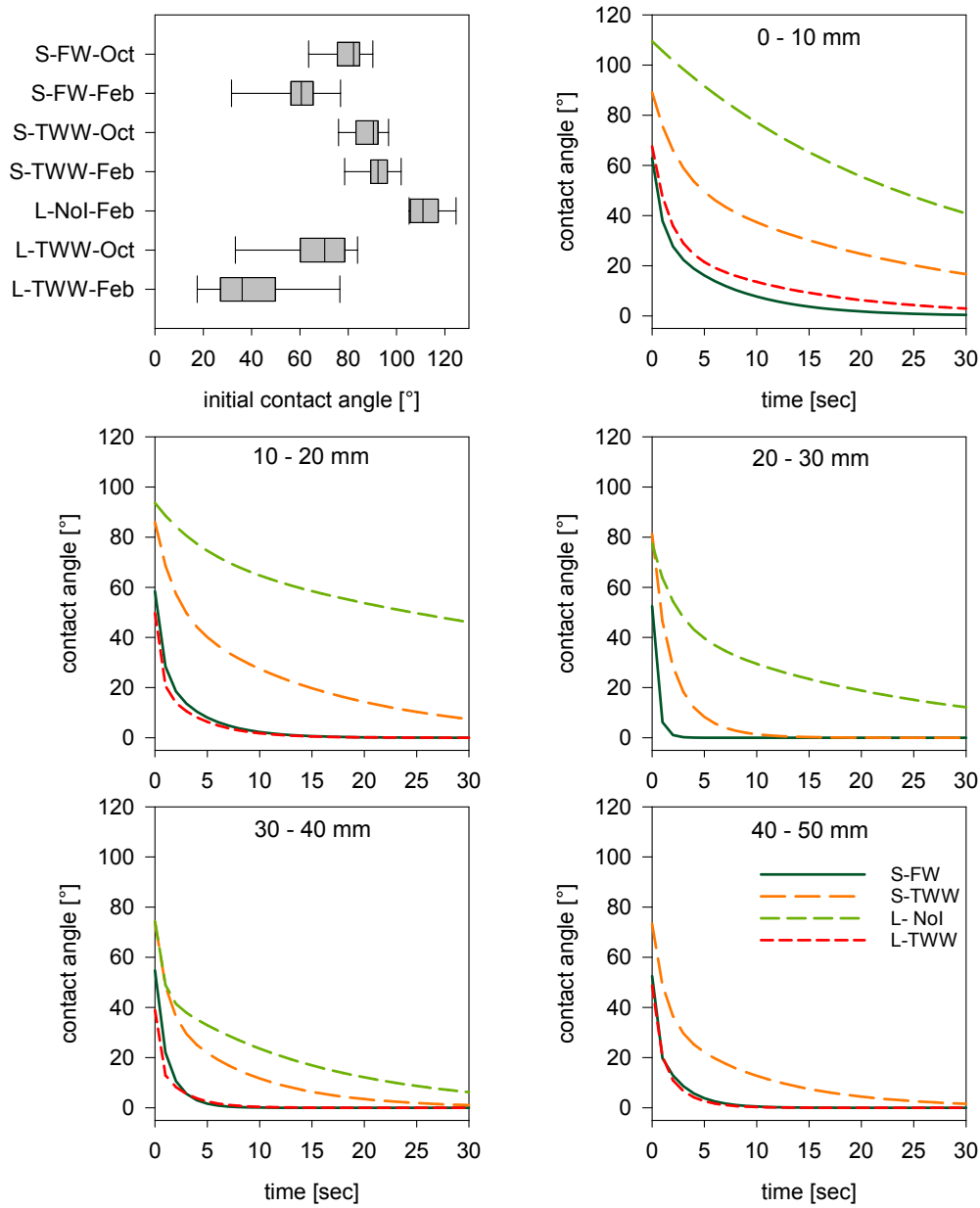
Figure 3.3: Initial CA at soil surface (top left) and averaged dynamic CA-fit for single layers of the topsoil (sites: S=loamy sand, L=sandy clay loam and treatments: NoI=non-irrigated control, FW=fresh water, TWW=treated wastewater).

Table 3.4: Averaged fitting parameters for single layers of the topsoil (sites: S=loamy sand, L=sandy clay loam; treatments: NoI=non-irrigated control, FW=fresh water, TWW=treated wastewater). Values in parenthesis are coefficient of variation.

Parameter	depth [mm]	S-FW	S-TWW	L-NoI	L-TWW
a	0 - 10	29.5 (0.2)	34.7 (0.2)	45.0 (0.7)	38.7 (0.2)
b	0 - 10	1.18 (0.8)	0.39 (1.3)	0.05 (0.8)	0.62 (0.6)
c	0 - 10	33.4 (0.3)	54.4 (0.1)	64.5 (0.5)	28.8 (0.2)
d	0 - 10	0.15 (0.9)	0.04 (1.6)	0.02 (2.1)	0.08 (0.6)
$\phi_0 = 0$/n	0 - 10	0/12	0/12	0/6	2/16
a	10 - 20	30.1 (0.2)	33.7 (0.2)	22.2 (0.3)	27.2 (0.5)
b	10 - 20	1.55 (0.9)	0.54 (1.4)	0.20 (0.7)	2.17 (1.1)
c	10 - 20	28.3 (0.3)	52.3 (0.2)	71.5 (0.3)	22.6 (0.3)
d	10 - 20	0.25 (1.0)	0.07 (1.4)	0.01 (1.2)	0.26 (0.9)
$\phi_0 = 0$/n	10 - 20	0/12	0/12	0/6	5/16
a	20 - 30	26.2 (0.5)	34.8 (0.3)	32.5 (0.2)	NaN
b	20 - 30	3.19 (1.0)	0.91 (1.9)	0.44 (1.1)	NaN
c	20 - 30	26.3 (0.6)	46.3 (0.3)	44.9 (0.5)	NaN
d	20 - 30	1.64 (2.5)	0.35 (2.4)	0.04 (1.2)	NaN
$\phi_0 = 0$/n	20 - 30	0/12	0/12	0/6	7/16
a	30 - 40	22.1 (0.7)	34.5 (0.3)	28.4 (0.8)	20.6 (0.6)
b	30 - 40	1.71 (11.6)	0.95 (1.1)	1.55 (1.5)	3.57 (1.3))
c	30 - 40	32.7 (0.4)	39.6 (0.3)	45.9 (0.4)	18.4 (0.7)
d	30 - 40	0.60 (3.2)	0.12 (1.2)	0.07 (1.3)	0.40 (1.2)
$\phi_0 = 0$/n	30 - 40	1/12	0/12	2/6	12/16
a	40 - 50	23.6 (0.4)	36.7 (0.3)	NaN	23.2 (1.1)
b	40 - 50	3.93 (0.9)	0.83 (1.0)	NaN	1.69 (0.9)
c	40 - 50	28.9 (0.4)	36.6 (0.5)	NaN	25.6 (0.5)
d	40 - 50	0.40 (1.0)	0.11 (1.4)	NaN	0.46 (1.3)
$\phi_0 = 0$/n	40 - 50	1/12	0/12	5/6	13/16

two to ten times larger than for L-NoI. Overall, L-NoI provided the lowest decrease in CA, but *b* was increasing with depth and complete wettability was reached in layer 5.

3.4.2   Infiltration front at field moisture

The propagation of water infiltration in 20 field moist samples from Rehovot (7 x S-FW, 8 x S-TWW, 5 x S-NoI) and 10 samples from Hadera (7 x L-TWW, 3 x L-NoI) were successfully determined. The detection of mean changes in water content, $\Delta\bar{\theta}$, along the sample profile via radiography were confirmed by the recorded mass data. In October, samples of irrigated areas (TWW and FW) were taken during or shortly after the daily irrigation while in February the soils were still moist from rain. Therefore, the initial water contents were close to field capacity and changes due to infiltrating water consequently low. In Rehovot (loamy sand), the mean initial water contents of FW and TWW-irrigated samples were about 25 vol. % and of NoI-samples about 18 vol. %. When saturated, the maximum water holding capacity of the topsoil at FW/TWW plots is 42 vol. % and at NoI 34 vol. %. The constant irrigation rate of $j = 8\,\mathrm{mm\,h^{-1}}$ increased the water content for irrigated samples by 7 vol. % and 11 vol. % for NoI. In Hadera (sandy clay loam), the sampled soil under the drippers contained 29 vol. % of water and the non-irrigated part 21 vol. %. $\Delta\bar{\theta}$ was about 6 vol. % for TWW samples and 9 vol. % for NoI. The maximum water holding capacity of the topsoil in the irrigated part is 38 vol. %, and 31 vol. % between the tree rows. Here, the samples were close to saturation at the end of experiment. Figure 3.4 shows the calculated projections of changes in water content, $\Delta\theta$, due to infiltrating water as a time series (rows) of one representative sample of each treatment and location (columns). The results of all infiltration experiments are provided in the appendix, supplementary material A (s.m.).

For the loamy sand (S, Fig. A1, and A2, s.m.), infiltration fronts were clearly detectable and water was infiltrating homogeneously, independent of treatment (FW, TWW, NoI) and season (Oct=dry, Feb=rainy season). After 60 to 80 min of irrigation the infiltration fronts had passed the samples and water contents had increased uniformly from top to the bottom. Projections of samples H, K, L, and N provided a drift in $\Delta\theta$ along the vertical profile from 6 to 1 vol. %, furthermore areas with low change in water contents were detected, especially in the lower parts. At sample J, a layer of 30 mm in height, starting 20 mm under the sample surface, was determined where water content did not change, an increase was detected only for single pathways. Sample P also provided a layer of 40 mm with higher increase of $\Delta\theta$, located at the sample top, but the measurement was biased by an experimental error where a constant lower boundary of 350 hPa was applied. Nevertheless, also here the infiltration front propagated uniformly.
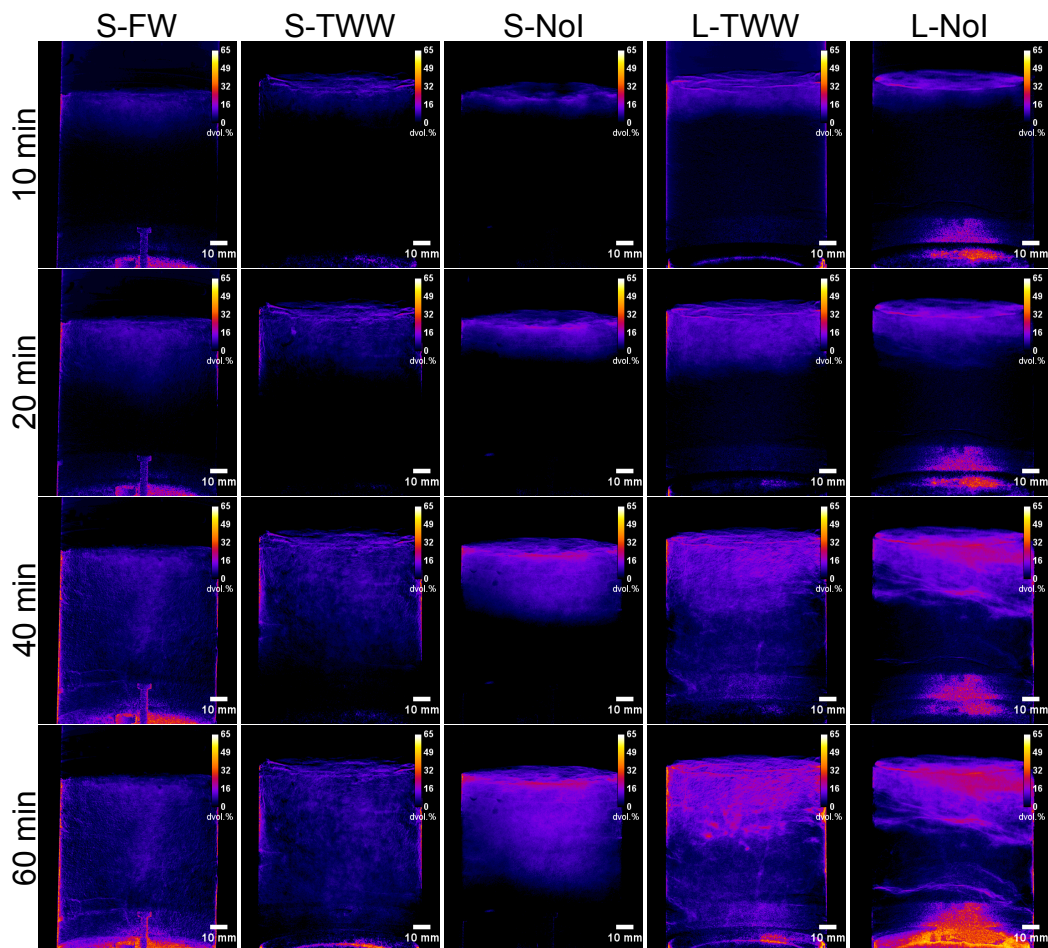
Figure 3.4: Changes in water content $\Delta\theta$ (vol. %) during infiltration experiments. Columns separate samples from different locations and treatments. From left to right: loamy sand: fresh water (S-FW), treated wastewater (S-TWW), non-irrigated control (S-NoI); sandy clay loam: treated wastewater (L-TWW), non-irrigated control (L-NoI). Rows illustrate the progress of infiltrating water in time: after 10 min, 20 min, 40 min, and 60 min of irrigation.

For the sandy clay loam (L, Fig. A3), samples from the TWW-irrigated plots show similar results as water was infiltrating homogeneously along the entire sample projection. No larger areas without changes in water contents were detected, independent of the season. At the surfaces of samples A, B, and C thin layers of high change in water content (30 to 65 vol. %) were captured after 40 min due to ponding of water. In contrast to the irrigated area, NoI samples provided slight heterogeneities in $\Delta\theta$. Patterns of lower changes in water content were distributed over the samples projections and a gradient of larger $\Delta\theta$ from the top to lower changes at the bottom was detected. Furthermore, layering of $\Delta\theta$ was observed for samples H and J. After 60 min of irrigation, at most areas of the samples a change in water content was detected.

3.4.3   Infiltration front at reduced initial water content

The reduced initial water content had a significant effect on the observed flow fields. 3 days of drying reduced the initial water content of the loamy sand to 13 vol. % and after 7 days to 1.5 vol. %. It should be noticed that this water was not equally distributed due to small-scale heterogeneities in hydraulic properties. Figure 3.5 shows the results of the different infiltration experiments for the same two samples presented already in Figure 3.4. Figure 3.6 shows the associated relative changes in water content over time detected via gravimetric data. Projections of all experiments are attached in the supplementary material. As water was infiltrating slower due to increasing $\Delta\theta$, the presented time series were adjusted to the infiltration front propagation.

After 3 days of drying, water was infiltrating the FW samples mostly uniform from top to bottom (Fig. A4, s.m.). An exception is sample E, where water flow was concentrated at one side. Samples A, B, and G show a gradient in change of water content from top (high) to bottom (low), due to the initial conditions with a high gradient of water loss from the sample top (dry) to the bottom (moist). At the end of experiments changes in water content were detected over the entire FW samples. In contrast, preferential flow was observed for all samples of the TWW treatment, except for sample H. Single pathways conducted the water from top to the lower boundary, where it spread. Subsequently samples were wetted from both, the top and bottom. At the end of experiments, when water inflow and outflow was equilibrated, water content was increased in most parts of the samples with exception in I, L, and N. The gravimetric data (Fig. 3.6) confirm the observed changes in water flow due to the drying process. While relative changes in water content for S-FW was systematically increasing with drying time, the change in water content for S-TWW was lower after 7 days of drying than after 3 days of drying.

After 7 days of drying, the differences between the treatments became more
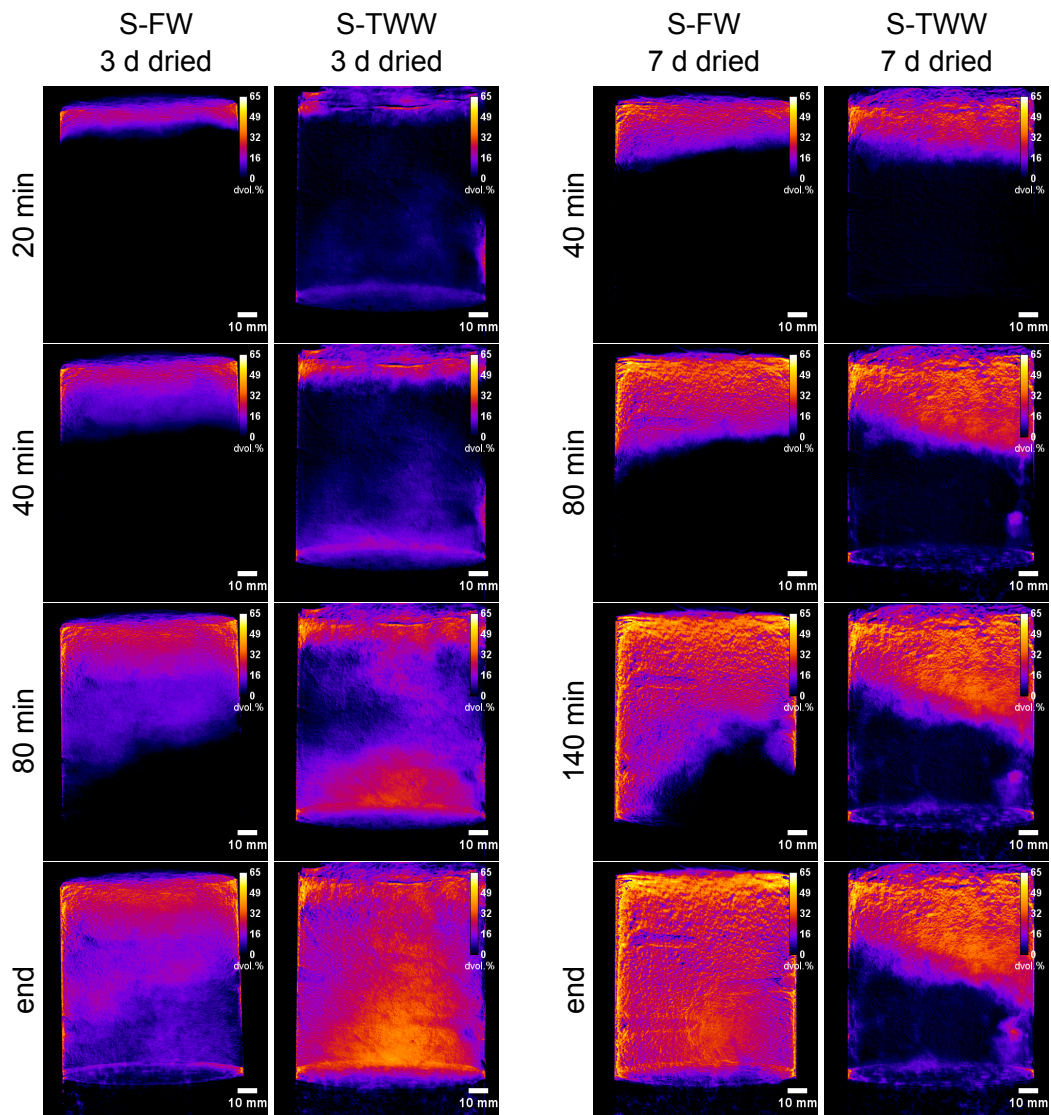
Figure 3.5: Changes in water content $\Delta\theta$ (vol. %) during infiltration experiments of dried loamy sand samples (50 °C). On the left side: S-FW and S-TWW dried for 3 days. On the right side: same samples dried for 7 days (FW=fresh water, TWW=treated wastewater).

pronounced (Fig. A5, s.m.). For FW samples A, B, C, and G the infiltration fronts were very sharp and mostly stable for the first 80 min. After that, they became slightly unstable. At the end of the experiment, except for sample G, all FW samples were uniformly and homogeneously wetted. In contrast, under TWW irrigation the instabilities of the infiltration front occurred already after 40 to 80 min for all samples. In a depth of 20 to 50 mm the infiltration fronts propagation stopped and water flowed through single path ways to the lower boundary. At sample I, L, N, and O, large areas with no change in water content were detected. Patterns of water infiltration at the end of the experiment were quantified via a threshold of $\Delta \bar{\theta} - 3 * sd$. Figure 3.7 shows the reduction of used area for the samples due to the drying process as a relative value of the projected sample area. After 3 days of drying the median of TWW flow fields was reduced to 86.1 % of the projection area, after 7 days to 50.4 %. Whereas for FW samples the area used for water flow did not significantly change due to drying.

Changes in absolute soil water holding capacities at this specific infiltration rate were determined by gravimetric data. Figure 3.8 illustrates the relation of water loss through drying to water gain by infiltration, so called rewetting ratio. Thus, the water content after irrigation at field moisture was used as reference. The rewetting ratios of 1 as obtained for the completely wettable samples confirmed the validity of this approach. The determined ratios show that the capacity of TWW samples for water uptake was reduced by the drying process. After 3 days the median rewetting ratio of TWW samples was reduced to 0.83, after 7 days to 0.57. FW samples re-established their water contents after 3 days (1.08) and after 7 days (0.94). Some samples slightly increased their water contents (rewetting ratio > 1) due to the change of the lower boundary from gravity flow to seepage. A statistical analysis (ANOVA, Tukey multiple comparisons of means, $\alpha = 5 \%$) provided a significant difference in the rewettability between FW and TWW treatment after 7 days ($p < 0.05$), but not after 3 days.

3.5   Discussion

Soil water repellency was detected for all sampling locations except for S-NoI, independent of the season, irrigation treatment or soil texture, but with variation in severity and frequency of occurrence. While FW samples in Rehovot (loamy sand) provided a seasonal dynamic in hydrophobicity, water repellency at TWW irrigation plots were not reduced by rain. Hydrophobicity seems to have become a persistent soil characteristic under TWW irrigation. Furthermore, for loamy sand the initial contact angles close to soil surface were significantly increased by TWW irrigation compared to FW plots. However, as FW plots were irrigated from 2008 to 2012 with TWW, the topsoil was still classified as water repellent.
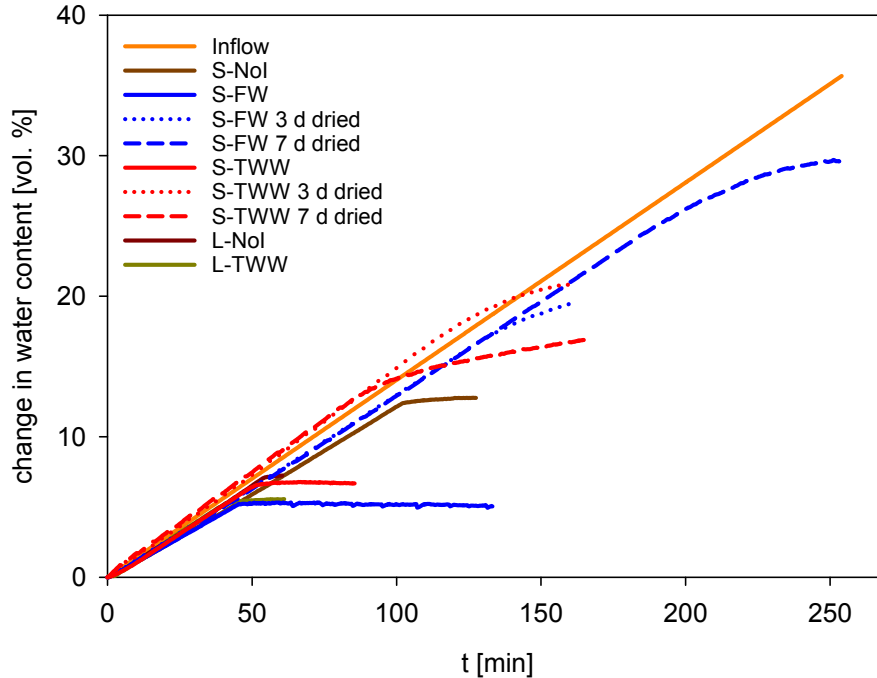
Figure 3.6: Gravimetric changes in water content $\Delta\theta$ (vol. %) as a function of time for all presented samples (sites: S=loamy sand, L=sandy clay loam and treatments: NoI=non-irrigated control, FW=fresh water, TWW=treated wastewater).

By comparing the decrease of CA with time, it has been shown that the persistence of water repellency in TWW plots was two to four times larger than in FW plots, especially at larger depths. 3 years of 700 mm FW irrigation and 550 mm of precipitation were not sufficient to turn the soil hydrophilic, but changed the persistence of repellency. The sandy clay loam in Hadera provided different results. Here, soil under TWW irrigation was mostly defined as wettable to slightly water repellent and the analysis of CA showed a significant reduction of repellency at the end of rainy season. Moreover, the non-irrigated part was significantly more affected by water repellency at the end of the winter than the irrigated part at all season, and provided by far the highest CA at the soil surfaces of all measurements.

By analysing water repellency of the single layers it has been shown that hydrophobicity detected by WDPT in samples taken under irrigation (FW and TWW) was equally distributed over the entire sampling depth, whereas in L-NoI repellency concentrated in the top layers and decreased with depth. This was confirmed by the dynamic CA measurements which decreased more rapidly with depth. Compared to the other treatments a higher amount of litter and humic substances with local
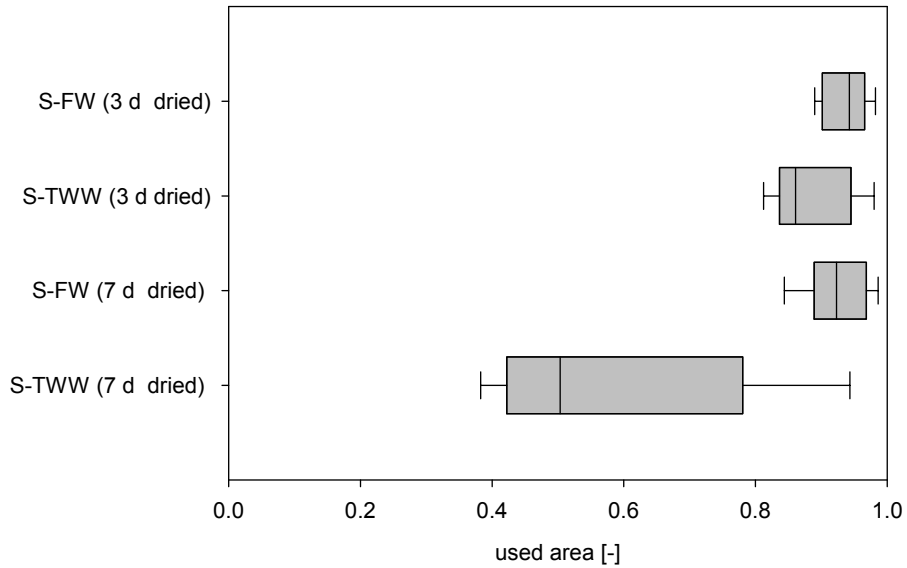
Figure 3.7: Relative area of $\Delta\theta$ within a 99.8 % confidence interval of water flow (S=loamy sand, FW=fresh water, TWW=treated wastewater).
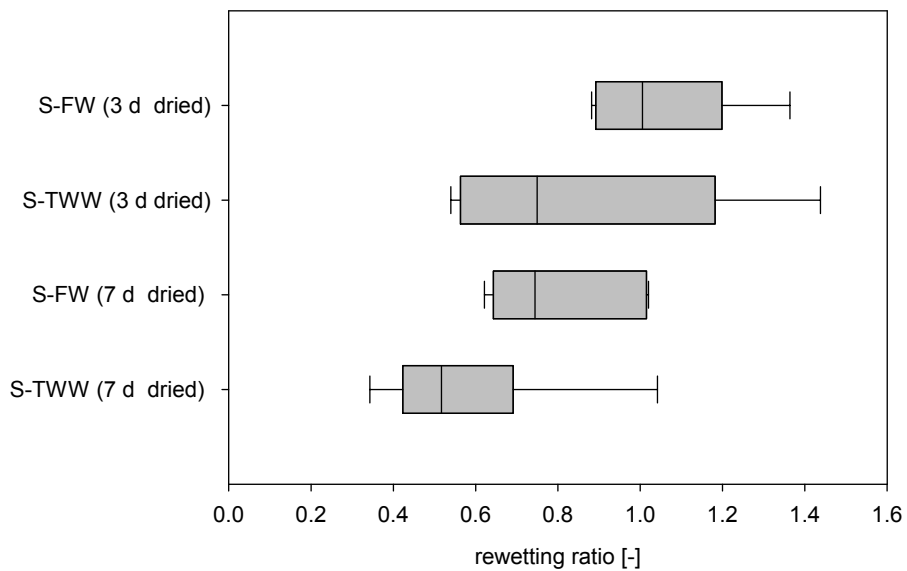
Figure 3.8: Capacity of the sample to reach the water content of the completely wetted initial experiment (S=loamy sand, FW=fresh water, TWW=treated wastewater).

heterogeneities were observed in the upper 30 mm of L-NoI which was covered with leafs at all season. Besides the organic input by TWW irrigation, hydrophobicity can be established by other organic materials such as input of organic litter from citrus trees, which contain waxes and other amphipathic substances (González-Peñaloza et al., 2012; Scott, 2000; Zavala et al., 2009). Furthermore, in summer 2015 patterns of moist soil were leading from the drippers to the non-irrigated rows, which indicates an impact of TWW to L-NoI. In Hadera, the irrigated part of the orchard is kept moist over the year, therefore the micro-biological activity is probably higher as compared to the non-irrigated part where degradation of organic substances can be reduced by limitation of water. Water repellency detected in L-NoI can be explained by a combination of accumulation of organic material with high contents of amphiphilic substances and surface run-off from TWW irrigated plots. Here, a more detailed look into the distribution of organics, their characteristics, and their occurrence inside soil structure is needed to determine their sources and appearances, which is beyond the scope of the current study.

The potential water repellency was measured at dried soil comparable to the 7 days dried samples of the infiltration test series. Our experiments mimicked different field conditions in terms of initial water content. The field moist samples of both study sites mainly showed a homogeneous propagation of water infiltration fronts and an increase in water content over the entire sample heights. For the sandy clay loam, the NoI samples provided some slight heterogeneities in flow pattern. Here, local heterogeneities of organic material in the topsoil might have influenced the capacity of water uptake and water flow. It should be noticed that field moist samples from Hadera were close to saturation behind the infiltration front and therefore larger macro-pores were probably activated and dominated water distribution.

At both study sites, some samples showed a decreasing change in water content from top to bottom or areas with low changes. This can be attributed to the high initial water content with a water gradient along the sample height due to gravity, and to local heterogeneities in soil density. In this case, little changes in water content are required to conduct the applied water flux. Hence, small variabilities in density can have a considerable influence on the detection of the flow field since our method is only sensitive to changes in water content. Furthermore, changes of soil structure e.g. due to shrinking and swelling of clay minerals or particle transport might be interpreted as changes in water content (sample I Fig. A3, s.m.). Nevertheless, even small changes in water content were captured for the entire sample areas of all field moist samples which could be confirmed by gravimetric measurements.

No preferential flow was detected for field moist soil, independent of the water quality and the season. An exception was sample J (S-FW) where water flow was dominated by layering of different soil textures. In contrast to field moist samples, uneven wetting front propagation and preferential flow was detected for most of

the TWW samples from Rehovot after reducing the soil water content to 13 vol. %. This was not the case for FW samples. After 7 days of drying (1.5 vol. %) the influence of the long-term irrigation of TWW became even more severe, as large areas of the samples were excluded from water flow and staid dry. The analysis of gravimetric data supports these findings, as the rewetting capacity of TWW was reduced in average about 12 % and 27 %, one sample even lost 59 % of water storage capacity. These results confirm the findings of other studies where water repellency was found to be closely linked to low initial water contents (Bauters et al., 2000; Wallach and Jortzick, 2008; Xiong et al., 2012). No systematic characteristic of flow fields was observed, they were highly individual. It is noted that the FW samples from October were classified as strongly water repellent, similar to TWW samples, which, however, did not influence the infiltration propagation. The persistence of water repellency measured by CA dynamics may explain this phenomenon as CA measured for FW samples were decreasing much faster than for TWW, especially in the detected critical zone of 20 to 50 mm. Here, the reorientation of hydrophobic molecules by water seems to be fast enough to enable a more homogeneous wetting of the samples.

3.6   Conclusion

Long-term treated wastewater irrigation causes potential water repellency in soils. Its severity is dependent on soil texture and its effect on water infiltration is more pronounced when soil is dry. In soil column experiments, we found that the presence of water repellency may not be a noticeable problem for water dynamics as long as the soil is kept moist. Once soil is exposed to water shortage, the risk of preferential flow, surface run-off, and reduced water storage increases severely. For a loamy sand irrigated with TWW for more than 7 years, it was clearly shown that water flow became highly preferential when water contents drop below some 13 vol. %. By using the new approach to detect changes in water content via X-ray radiography, it was possible to quantify the spatial pattern of infiltration fronts in undisturbed, cylindrical soil cores. This provides more substantial information on the heterogeneity of water flow as compared to chemical tracers or by using quasi-two-dimensional Hele-Shaw cells. Moreover, we could demonstrate that measurement of the dynamic contact angle is a useful parameter to explain the occurrence of different flow regimes in dry samples which were classified as water repellent by water drop penetration time and initial contact angle.

Chapter 4

Soil structure alteration and hydraulic properties

4.1 Abstract

Secondary treated wastewater, a commonly used water resource in agriculture in (semi-)arid areas, often contains salts, sodium, and organic matter which may affect soil structure and hydraulic properties. The main objective of this study was to jointly analyse the effects of long-term irrigation with treated wastewater on physicochemical soil characteristics, soil structure, and soil water dynamics in undisturbed soils. X-ray microtomography was used to determine changes in macro-porosity ($> 19\,\mu m$), pore size distribution, and pore connectivity of a sandy clay loam and a loamy sand. Differences in the pore network among soils irrigated with treated wastewater, fresh water that replaced treated wastewater, and non-irrigated control plots could be explained by changes in textural composition, soil physicochemical parameters, and hydraulic properties. In this study we showed that irrigation led to the development of a connected macro-pore network, independent of the studied water quality. The leaching of silt and clay particles in the sandy soil due to treated wastewater irrigation resulted in an increase of pores $< 130\,\mu m$. While this change in texture reduced water retention, the unsaturated hydraulic conductivity was diminished by physicochemical alteration, i.e. induced water repellency and clay mineral swelling. Overall, the fine textured sandy clay loam was much more resistant to soil alteration by treated wastewater irrigation than the loamy sand.

4.2   Introduction

The utilisation of treated wastewater (TWW) has become an important source of irrigation water in many countries, primarily in arid and semiarid areas where water scarcity is severe. In Israel, already 75 % of wastewater is treated and re-used for irrigation, covering 50 % of the water consumption in agriculture (OECD, 2015). Compared to fresh water (FW), TWW is generally characterised by a higher load of dissolved organic matter, suspended solids, sodium adsorption ratio, and considerable levels of salinity. Therefore, irrigation with TWW can increase salinity and sodicity of soils at depths down to 1.5 m (Lado and Ben-Hur, 2009; Levy, 2011; Bedbabis et al., 2014), accompanied with clay migration due to dispersion of clay minerals in the topsoil (Bardhan et al., 2016). The latter can enhance soil sealing, reduce infiltration, increase soil loss in sandy soils, and enhance slaking in clay soils (Lado et al., 2005).

At the same time, higher loads of organic matter in the effluents are reported to result in inconsistent effects on the carbon concentrations of the topsoil. While in some soils the organic carbon concentrations were increased (Jueschke et al., 2008), in others the effect was marginal (Lado et al., 2012) or it was reduced by priming effects due to the stimulation of microbial activity (Adrover et al., 2012). It is well known that soil structure is to a large extent formed by soil biota (Oades, 1993) and that the quality and quantity of organic matter in irrigation water can shape the structure of soil biological communities (Adrover et al., 2012; Frenk et al., 2014; Ibekwe et al., 2018). Hence, organic compounds introduced through TWW irrigation are expected to affect soil structure and thereby soil water dynamics.

Lado and Ben-Hur (2009) and Levy (2011) reported that TWW irrigation decreased soil structural stability and significantly altered soil pore architecture. This resulted in a reduction in saturated hydraulic conductivity in clay and loamy soils due to clogging of the pores with suspended solids while sandy soils were not affected. Bardhan et al. (2016) reported that the conductivity of clay soil was reduced in a water potential range of 0 down to -100 hPa, suggesting that the volume fraction of macro- and meso-pores were affected by pore narrowing through dissolved organic matter that may have led to enhanced clay swelling. Halliwell et al. (2001) hypothesised that changes in the pore system of the soil due to TWW seem to be the dominant factor for the reduction in soil hydraulic conductivity. Moreover, it has been shown that TWW contains hydrophobic compounds which can cause water repellency and can effect soil water dynamics such as reduced infiltration capacity, overland flow, formation of preferential flow path, and reduced water retention (Bauters et al., 2000; Diamantopoulos et al., 2013; Wallach and Jortzick, 2008). For the loamy sand soil discussed in this paper, an impact of reduced wettabiliy on the stability of water infiltration and the occurrence of preferential flow has been confirmed by heterogeneous water distributions in the field (Rahav et al., 2017)

and infiltration experiments in undisturbed soil columns (Leuther et al., 2018). The main objective of this study was to jointly analyse the effects of long-term irrigation with TWW on soil structure and soil water dynamics in undisturbed soils which integrates effects of changes in microbial communities, clay mineral swelling and dispersion, clogging of pores, and induced water repellency by loads of organics, suspended solids, and sodium. We used X-ray microtomography to determine the undisturbed macro-pore network of a sandy clay loam and a loamy sand irrigated with TWW for more than 7 years. The measurements were concentrated on the topsoil, assuming that this is the most affected region under drip irrigation (Assouline and Narkis, 2011; Elifantz et al., 2011; Wallach et al., 2005). Furthermore, we determined differences in soil texture and physicochemical characteristics to analyse how TWW irrigation potentially had changed clay content, and analysed the effect on soil hydraulic properties as integrative soil characteristics reflecting changes in soil wettability, soil texture, and soil structure.

4.3   Materials and methods

4.3.1   Study sites and soil sampling

The topsoils of two commercial orchards located in the coastal plain of Israel were investigated. The region is dominated by Lovisols (Singer, 2007) of a sandy texture and has two pronounced climate seasons, a hot and dry summer where orchards are irrigated, and a rainy winter without irrigation. At the study sites, water was applied via drip irrigation and the amount was adjusted to the daily evapotranspiration rates, approximately 700 mm per dry season. Soil cultivation was mainly inorganic fertilisation without any tillage. To capture seasonal dynamics due to the irrigation schemes, the sampling was carried out in October 2015 and February 2016. We investigated the topsoil (0 to 200 mm depth) of a loamy sand close to Rehovot (31°53'59.0"N, 34°51'00.0"E) , denoted in the following as S, and a sandy clay loam close to Hadera (32°24'48.0"N, 34°58'02.3"E), denoted as L.
For the S-site, the water management was changed from fresh water (FW) to secondary treated wastewater irrigation (TWW) in 2008. In 2012, single plots of a block design experiment were converted back to FW irrigation for soil reclamation (Rahav et al., 2017). For the L-site, farmers have used TWW for more than 30 years. Soil samples were randomly taken within the wet soil along the dripper lines (FW and TWW) and between the tree rows beyond the reach of irrigation water (NoI) as a control for untreated soil. The study sites enclosed an area of $4500\,m^2$ at the S-site and of $1500\,m^2$ at the L-site. The chemical properties of the different water treatments are given in Table 4.1.
Cylindrical polycarbonate containers with a wall thickness of 3 mm and an outer

Table 4.1: Irrigation water characteristics (EC=electrical conductivity, SAR=sodium absorption ratio) for the two study sites (S=loamy sand, L=sandy clay loam, FW=fresh water, TWW=treated wastewater): mean values based on two measurements in 2014 and 2015 (S-site adapted from Rahav et al. (2017)).

Site	pH	EC $[\mathrm{dS\,m^{-1}}]$	SAR $[(\mathrm{meq/L})^{0.5}]$	Na $[\mathrm{mg\,L^{-1}}]$	Ca $[\mathrm{mg\,L^{-1}}]$	Mg $[\mathrm{mg\,L^{-1}}]$
S-FW		0.77	1.73	65.32	61.00	28.31
S-TWW	7.2	1.65	4.61	164.68	61.80	21.02
L-TWW	7.4	1.32	3.96	153.00	85.00	16.80

	Cl $[\mathrm{mg\,L^{-1}}]$	NO_3-N $[\mathrm{mg\,L^{-1}}]$	NH_4-N $[\mathrm{mg\,L^{-1}}]$	SO_4 $[\mathrm{mg\,L^{-1}}]$	P $[\mathrm{mg\,L^{-1}}]$	K $[\mathrm{mg\,L^{-1}}]$
S-FW	108.20	< 1.50	0.63	253.92	< 0.01	3.58
S-TWW	231.60	< 1.50	53.82	487.20	7.38	26.00
L-TWW	175.50	2.26	8.32	369.50	5.20	22.10

diameter of 100 mm were used for soil sampling. These had a height of either 100 mm or 200 mm, depending on the feasibility of undisturbed sampling in the presence of woody roots below the trees. Soil samples were excavated by using a sampling device for undisturbed soil cores manufactured by UGT GmbH, Germany (Kuka et al., 2013). The method is adapted from an excavation technology for large soil monoliths, where surrounding soil is pre-cut and continuously removed by a rotating cutting sleeve. While slowly penetrating the soil, the remaining, undisturbed soil core is taken in by a sampling cylinder placed inside the sleeve. All samples were immediately covered with a lid, stored in plastic bags to keep them field moist, carefully packed and shipped to Germany. Overall, 17 soil cores (3 S-FW, 4 S-NoI, 3 S-TWW, 7 L-TWW) were taken in October 2015 and 26 soil cores (6 S-FW, 2 S-NoI, 6 S-TWW, 5 L-TWW, 7 L-NoI) in February 2016. Additional 77 undisturbed samples (50 mm in diameter and 50 mm in height) were taken from the topsoil in the vicinity of larger soil cores to measure soil water repellency.

4.3.2   Physicochemical soil properties

The total carbon (C) and nitrogen (N) concentrations in air dried soil were measured for each sample. To exclude a possible impact of carbonates on the measured C values, the soil was tested for lime content via hydrochlorid acid (10 %) with a negative result (Jahn et al., 2006). C and N were determined by elemental analysis using gas chromatography (Vario EL Cube, Elementar). Three replicates per

sample were ground, weighed (60 mg) and burned at 950 °C.

Particle size distribution in mineral soil was analysed by sedimentation following DIN ISO 11277 (2002). Samples had been dried in an oven at 105 °C, and separated from carbonates and organic substances before sedimentation.

Three different parameters were determined to describe changes in soil chemical properties by TWW irrigation: acidity (pH), electrical conductivity (EC), and sodium adsorption ratio (SAR) following the protocol described by Rowell (1994). Oven dried soil samples were mixed and sub-samples of 10 g were suspended in 25 mL distilled water and shaken for 15 min to measure soil pH_{H2O} in a 1:2.5 suspension with a pH meter. The pH was recorded after 1 min time of stabilisation. Afterwards, 25 mL more distilled water was added, the reagent was shaken for 30 min, and the EC was measured in the supernatant of the 1:5 suspension. By multiplication with a factor of 6.4, the measured value was converted to EC of a saturation extract, the reference water content to describe soil salinity (Rowell, 1994). After filtering the extraction (Whatman No.1), Na^+, Ca^{2+}, and Mg^{2+}-ion concentrations were analysed via ion chromatography (DIONEX Aquion, Thermo Fisher). The SAR was determined via

$$SAR = \frac{Na^+}{\sqrt{\frac{(Ca^{2+}+Mg^{2+})}{2}}}, \qquad (4.1)$$

all concentrations were expressed in millimol per kilogram.

Soil water repellency at soil surface was determined by two methods, the water drop penetration time test (WDPT) (Doerr, 1998) and the sesille drop contact angle (CA) (Bachmann et al., 2000). Therefore, additional soil samples were placed in an oven at 50 °C until a reference water content corresponding to that of air dried soil was reached. The WDPT was determined by placing 3 drops of 50 µL distilled water on the soil surface and recording the required time to their complete infiltration. The initial contact angle of a 15 µL-water drop was measured with a goniometer (EasyDrop DSA20E, KRÜSS GmbH, Germany) for a flat single-grain of air dried, sieved soil.

4.3.3   Soil structure analysis via X-ray microtomography

All samples were scanned using an X-ray microtomograph (X-TEK XT H 225, Nikon Metrology) to capture the undisturbed soil structure. The samples were scanned with energy settings of 140 kV and 470 µA, and a 1.5 mm copper filter to reduce beam hardening artefacts and prevent overexposure at the lateral margins of the detector panel. The exposure time for each image was 1000 ms with two frames per projection and a total of 2748 projections. The reconstruction of three-dimensional images was done with the CT Pro 3D software package (version 3.1)

at a spatial resolution of 60 μm. Four additional sub-samples (30 mm in height and in diameter) of each irrigation treatment were taken from the midst of the large 100 mm soil cores and scanned at a resolution of 19 μm to widen the spatial scale of structure analysis. Here, a 0.1 mm copper filter was used and the energy settings were changed to 115 kV and 170 μA.

Image processing and analysis were done with the open source software packages QuantIm (Vogel et al., 2008) and Fiji ImageJ V. 1.50d (Schindelin et al., 2012) and mainly followed the workflow described by Schlüter et al. (2016). At first the raw image volumes were filtered with a 2D-Nonlocal Means filter from every dimension (x, y, and z) to reduce image noise equally in all directions. Second, the images were corrected for vertical differences in average image intensity due to shading and cone beam artefacts. Third, images were segmented into three classes: pore system, particulate organic material, and soil matrix, following Schlüter et al. (2014).

Macro-porosity, here defined as the CT derived porosity, and the amount of particulate organic material (> 2 voxels), such as roots and litter, were determined as the ratio of segmented voxels to total number of voxels within the sample. The segmented pore network was analysed in terms of change in porosity over sample depth, pore size distribution, and connectivity. The pore size distribution was determined with the maximum inscribed sphere method in the BoneJ plugin for Fiji ImageJ (Doube et al., 2010). The pore size distribution of every sample was classified in one-voxel increments. This allowed to combine the pore sizes determined at different resolution (Vogel et al., 2010). The connectivity of the pore network was defined by their Γ-indicator (Eq. 4.2), reflecting the probability of two randomly chosen pore voxels to belong to the same pore cluster (Renard and Allard, 2013).

$$\Gamma(p) = \frac{1}{n_p^2} \sum_{i=1}^{N(X_p)} n_i^2 \tag{4.2}$$

Here, n_p is the total number of pore voxels in the analysed volume X_p and n_i is the number of voxels per cluster. Therefore, $\Gamma(p)$ is dominated by the proportion of pores which are connected to the biggest pore cluster. Overall, the undisturbed pore networks were analysed for 23 S-samples (8 x FW, 9 x TWW, 6 x NoI), 15 L-samples (9 x TWW, 6 x NoI), and 10 sub-samples (4 x S-FW, 4 x S-TWW, 2 x L-TWW). The topsoil (0 to 10 cm) was analysed for all samples while for the depth between 10 and 20 cm this was possible only for 3 replicates from the L-NoI and L-TWW plots, respectively.

4.3.4   Soil hydraulic properties

The soil water retention curve (SWRC) and unsaturated hydraulic conductivity were measured with the HYPROP device for larger soil cores (METER Group, Inc. USA) for a potential range from 0 to -5000 hPa using the evaporation method developed by Schindler et al. (2010). For the dry end of the SWRC ($< -10\,000$ hPa), soil water retention was determined with a WP4C (METER Group, Inc. USA). For hydraulic conductivity close to saturation the evaporation method is limited, therefore, the measurements were supplemented by Multi-Step-Flux experiments for a potential range from -2 to -35 hPa (Weller and Vogel, 2012). To prevent changes in soil chemistry and structure during the experiment, the salt concentrations of the irrigation water were adapted to the field specific water characteristics. At the end of the experiments, soil samples were dried at 105 °C to determine bulk density, total porosity, and saturated water content.

4.3.5   Statistical analysis

The comparisons of means for each soil property were done by analysing the variance of each treatment (ANOVA) using the lsmeans package in R Version 3.4.2 (Lenth, 2016). Parameters were tested for equality of variances with Levene's test for homogeneity of variance and the means were compared by Tukey's multiple comparison of means based on a 95 % family-wise confidence level. Furthermore, the multivariate regression method Partial Least Squares Regression (PLSR) implemented in the pls package in R Version 2.6-0 (Wehrens and Mevik, 2007) was used as an exploratory analysis tool to select suitable predictor variables for soil hydraulic properties. Therefore, the physicochemical and textural soil properties were grouped into texture, water repellency, and salinity. These were used as predictor variables for soil water retention and hydraulic conductivity at field capacity (water potential -100 hPa). Finally, a combination of the potential most influential parameter according to literature were tested for its predictive power (sand concentration, SAR, and initial contact angle at soil surface). All predictors were tested for cross-validation by leave-one-out cross-validation.

4.4   Results and discussion

4.4.1   Physicochemical soil properties

According to FAO classification, all treatments at the S-site were classified as loamy sand and at the L-site as sandy clay loam (Tab. 4.2, Fig. A7 in the appendix, supplementary material B (s.m.)). For both locations, no significant differences in

Table 4.2: Study sites characteristics (S=loamy sand, L=sandy clay loam and treatments: NoI=non-irrigated control, FW=fresh water, TWW=treated wastewater): grain size distribution, chemical soil parameters (EC=electrical conductivity, SAR=sodium absorption ratio), total carbon (C) and nitrogen (N) concentrations, and water repellency characteristics (CA= initial contact angle, WDPT = water drop penetration time). Values in parentheses are the standard errors.

Parameter	S-NoI (n=4)	S-FW (n=9)	S-TWW (n=9)	L-NoI (n=6)	L-TWW (n=9)
sand [g 100 g^{-1}]	81.4 (2.0)	79.1 (2.1)	86.1 (1.6)	65.5 (2.3)	63.8 (0.7)
silt [g 100 g^{-1}]	7.8 (0.9)	9.0 (1.0)	5.7 (0.6)	12.6 (0.2)	14.6 (0.7)
clay [g 100 g^{-1}]	10.8 (1.2)	11.9 (1.2)	8.2 (1.1)	21.8 (2.0)	21.6 (0.9)
bulk density [g cm^{-3}]	1.64 (0.02)	1.31 (0.04)	1.32 (0.06)	1.48 (0.03)	1.48 (0.03)
pH [-]	7.4 (0.1)	7.2 (0.1)	5.7 (0.2)	7.5 (0.1)	7.6 (0.1)
SAR	0.6 (0.1)	1.4 (0.2)	2.7 (0.3)	0.5 (0.0)	3.6 (0.1)
EC [dSm^{-1}]	0.9 (0.1)	1.7 (0.2)	2.0 (0.2)	1.6 (0.1)	1.4 (0.1)
C_{tot} [g 100 g^{-1}]	0.55 (0.08)	1.18 (0.19)	1.21 (0.17)	1.74 (0.33)	0.83 (0.09)
N_{tot} [g 100 g^{-1}]	0.07 (0.01)	0.13 (0.02)	0.13 (0.02)	0.17 (0.03)	0.10 (0.01)
C/N-ratio	8.28 (0.51)	9.18 (0.32)	8.96 (0.34)	9.96 (0.49)	8.54 (0.32)
CA [°]	NaN	69.3 (3.6)	91.1 (2.3)	113.3 (3.2)	48.8 (7.3)
WDPT [s]	0 (0)	41.4 (20.4)	144.9 (71.8)	882.8 (190.1)	12.4 (2.7)

soil texture were found between non-treated NoI and irrigated topsoil due to high variations within the treatments. Nevertheless, at the S-site a significant increase in sand content was determined for the S-TWW soil compared to S-FW ($p = 0.02$) most likely caused by eluviation of silt and clay particles. For the L-soil, no differences in soil texture classes between the TWW irrigated and the non-irrigated treatments were found.

TWW had an effect on soil acidity (pH) and salinity (EC) in the sandy S-soil but not in loamy L-soil, where pH remained around 7.5 and EC around $1.5\,\mathrm{dS\,m^{-1}}$ for both treatments. Soil pH under S-FW irrigation (pH 7.2) was slightly reduced compared to non-treated soil (pH 7.4), but under TWW irrigation the soil was significantly acidified to a mean pH of 5.7 ($p < 0.001$). Compared to the control, a significant increase in soil salinity occurred in both irrigation treatments. Soil sodicity was affected most. In both textures the SAR ratios were the greatest for TWW plots, yet with considerable variations in the S-TWW treatment. Also, some S-FW samples showed an increased sodium content compared to the non-irrigated treatments. The inequality in variance of the measured SAR values within the single treatments prevented a statistical analysis.

Due to their high variances, both the total carbon and nitrogen concentrations of the S-soil were not significantly different below drip-irrigation compared to the non-irrigated plot. In contrast, for the L-soil, both the total carbon and nitrogen concentrations of the NoI-samples were significantly increased compared to TWW irrigation ($p = 0.05$). The C/N ratio was around 9:1 for all samples, independent of the location and the irrigation regime.

All sampling locations except for the S-NoI were classified as sub-critical water repellent ($35° < \mathrm{CA} < 90°$) to water repellent ($\mathrm{CA} \geq 90°$). Both water repellency characteristics, WDPT and CA, were significantly greater in S-TWW compared to S-FW and S-NoI as reported in detail by Leuther et al. (2018). For the L-soil, the surfaces of L-NoI samples were classified as strongly to severely water repellent by WDPT, while L-TWW samples were classified as wettable to slightly water repellent.

In summary, changes in physicochemical soil properties due to long-term irrigation with TWW were mostly found for the S-soil. Here, changes in pH and SAR were highly significant, while increase in carbon content and electrical conductivity, in combination with slight changes in textural composition were also found in FW irrigated plots. Due to high evaporation in summer, the low salt contents of the fresh water can still increase salinity in topsoil. Furthermore, 3 years of TWW application prior to FW could have affected the soil as well. This might explain the high variance in SAR and the reduced wettability. Although sodicity increased in TWW plots, soils in all treatments from both sites can be classified as non-salt affected, with $\mathrm{EC} < 4.0\,\mathrm{dS\,m^{-1}}$ and $\mathrm{SAR} < 6\,(\mathrm{meq/kg})^{0.5}$ (Rengasamy, 2010).

30 years of TWW irrigation on the L-soil did not change soil texture, pH, and EC.

It seems that the annual precipitation was sufficient to prevent an increase in total salinity but not for Na accumulation. The greater C and N concentrations in the L-NoI control might be explained by the observed accumulation of organic litter and reduced biological decomposition during dry summers. For S-NoI, no litter accumulation was observed.

Except for acidification of S-TWW, all measured changes in soil properties were in agreement with previous studies on TWW effects with similar soil textures (Lado et al., 2012; Tarchouna et al., 2010; Schacht and Marschner, 2015). While most studies reported that soil pH increased with TWW irrigation due to accumulation of alkalis, here, pH dropped significantly. Similar, but less intense reductions in pH were also reported by Bedbabis et al. (2014). In both studies ammonium dominated the nitrogen supply in irrigation water, which can cause soil acidification due ammonium uptake by plants and microbial nitrification (Marschner et al., 1986). Due to the low amount of silt in the S-soil, the pH buffer capacity was reduced compared to the L-soil.

Differences in soil carbon and nitrogen concentrations due to a priming effect or due to higher loads of organics by TWW could not be detected due to high variability within the treatments. The narrow C/N-ratio of 9:1 was found for all treatments which is close to the ratio of citrus leaves (Pedrero et al., 2010). This indicates that the carbon and nitrogen storage in the soils was dominated by the input and accumulation of organic litter from the trees and not by the quality of irrigation water.

4.4.2   Soil structure

The soil structure of a representative 10 cm sample of every treatment and one 3 cm sub-sample is shown in Figure 4.1 to provide a visual impression of the structural heterogeneities. This heterogeneity manifests itself by looser and denser regions, refilled pores, cracks, small stones, roots and particulate organic matter distributed over the samples (for details on POM abundance and distribution see Fig. A6, s.m.). Figure 4.2 shows the depth profiles of the averaged macro-porosities (pores $> 60\,\mu m$) for every treatment (a), their macro-pore connectivity (b), total porosity determined by dry weight (c), and total porosity as a function of macro-porosity (d). The visible macro-porosity of the different S-treatments decreased with depth while for the L-soil the depth profiles were more uniform. A significant increase in macro-porosity due to irrigation (FW and TWW) was determined for the sandy S-soil, but not for the more loamy L-soil. The Γ-connectivity of the pore network increased with increasing macro-porosity due to connected biopores. For the S-soil, macro-porosity ($> 60\,\mu m$) contributed 11 % to the total soil porosity, and only 6 % for the L-soil. Thus, the relations between macro-porosity and total porosity were different for the two orchards. While for the S-treatments, the visible macro-
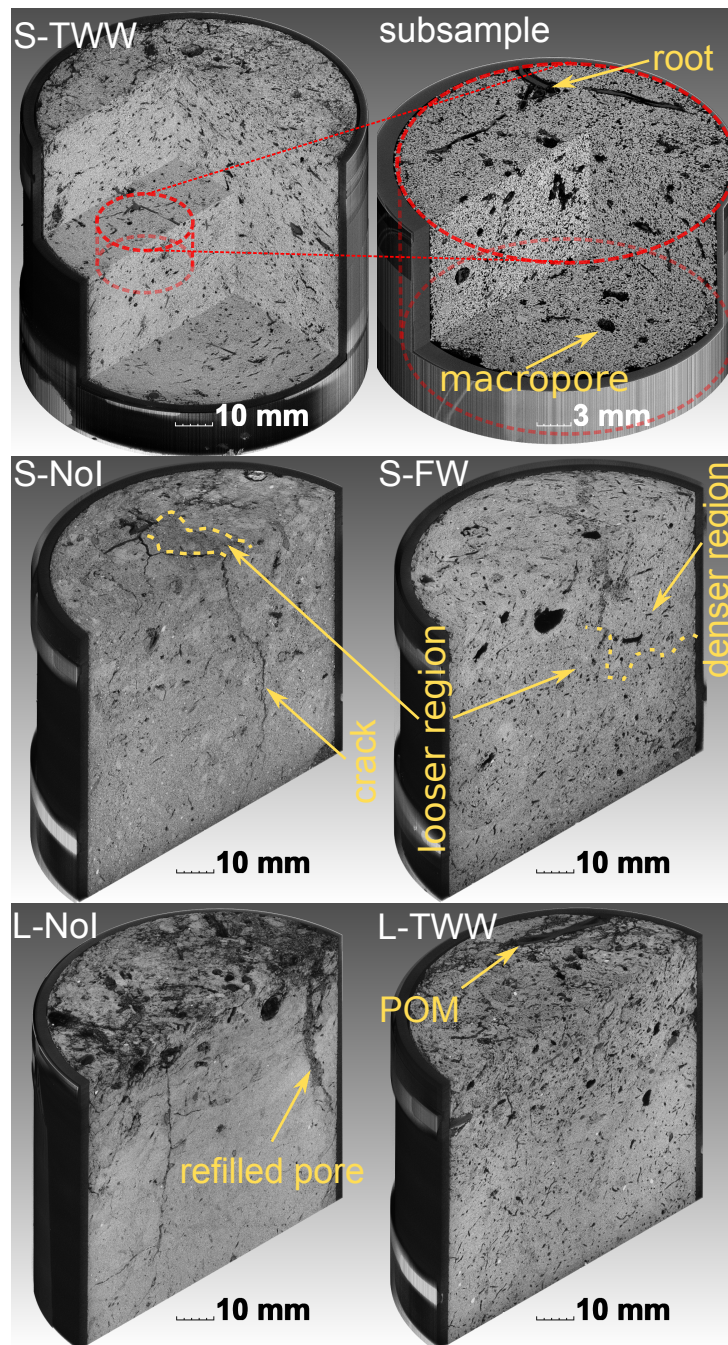
Figure 4.1: Reconstructed CT images of the topsoil at a spatial resolution of 60 μm, and, on the top right, of one sub sample at 19 μm (sites: S=loamy sand, L=sandy clay loam; treatments: NoI=non-irrigated control, FW=fresh water, TWW=treated wastewater). Grey values are related to material densities (black: pores, dark grey: organics, and light grey to white: soil matrix).
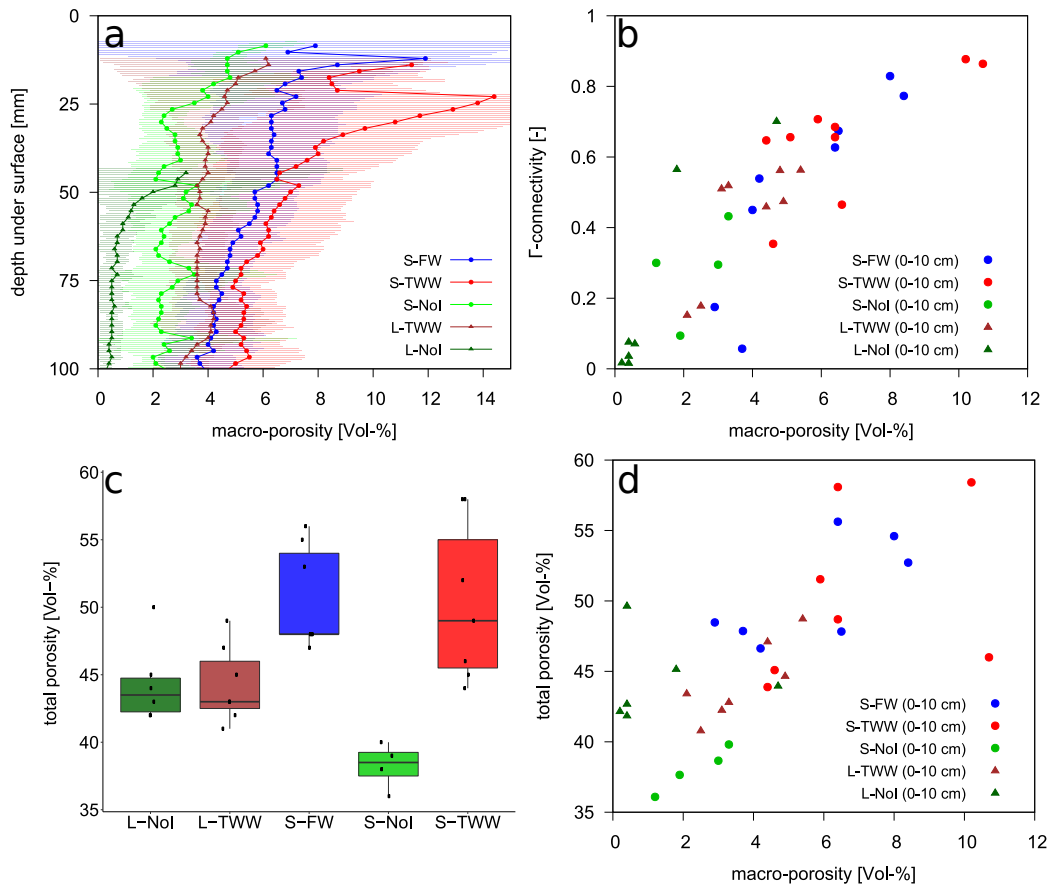
Figure 4.2: Pore network characteristics (sites: S=loamy sand, L=sandy clay loam; treatments: NoI=non-irrigated control, FW=fresh water, TWW=treated wastewater) determined at a resolution of $60\,\mu m$ (a, b), and total porosity determined by dry weight (c). The depth profile (a) shows the mean macro-porosities and the shaded area margins the 95 % confidence interval of the mean determined by two times standard deviation.
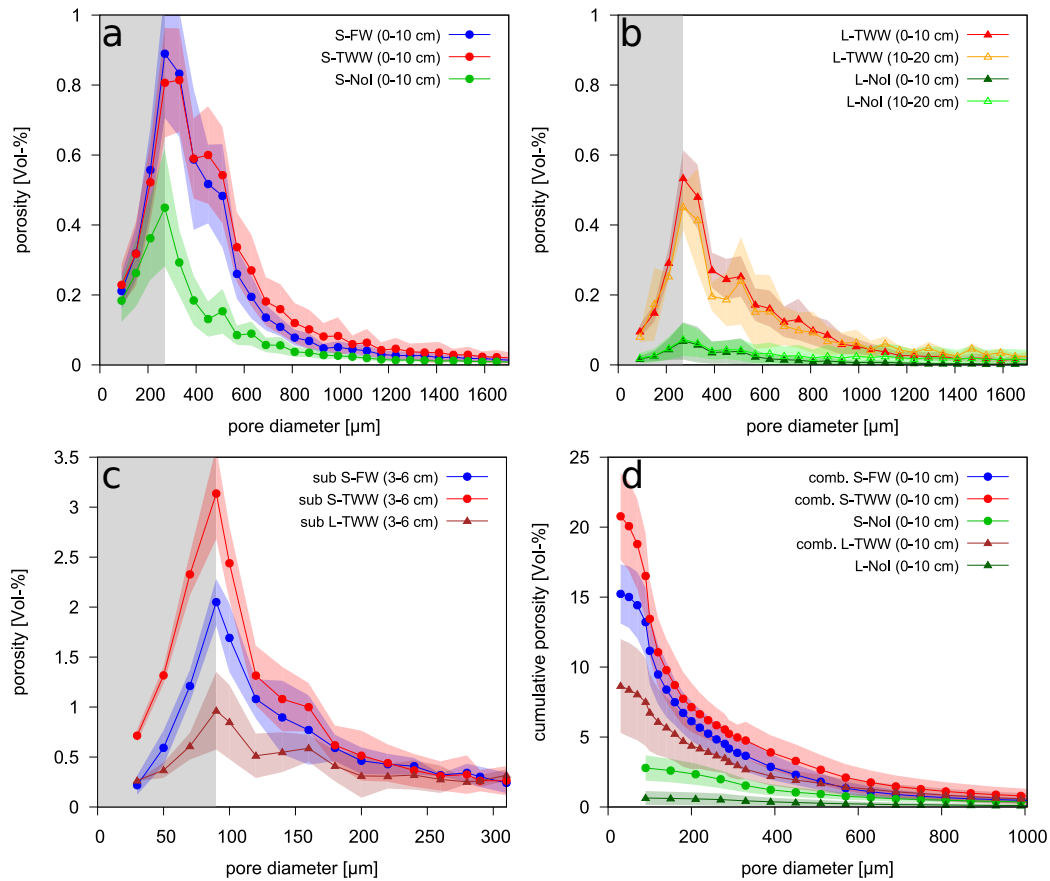
Figure 4.3: Mean distribution of classified pore sizes for loamy sand (NoI=non-irrigated control, FW=fresh water, TWW=treated wastewater) of the topsoil (a), for sandy clay loam at two depths (0 to 10 cm and 10 to 20 cm, b), and for the sub-samples (c). The grey background marks the range of uncertainty of the detection method, the shaded area of the lines margins two times standard error. The cumulative porosity based on 10 cm samples, which was combined with sub-samples porosity (comb.) for S-FW, S-TWW, and L-TWW.
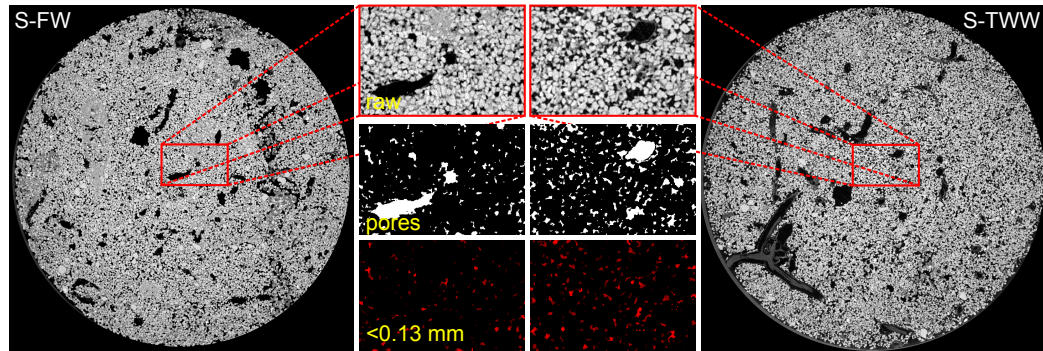
Figure 4.4: Raw X-ray microtomography images of a fresh water (S-FW) and treated wastewater (S-TWW) irrigated loamy sand sub-sample at a certain depth. The enlarged details of the pictures depict the segmented pore spectrum and pores smaller than 130 µm.

porosity had a strong influence on the total porosity ($R^2 = 0.52$), for the L-soil the total porosity did not change by increasing macro-porosity ($R^2 = 0.08$). The scatter plots also reveal the great heterogeneity within the treatments. Therefore, no significant differences in macro-porosity, connectivity or total porosity were determined between S-FW/S-TWW and L-NoI/L-TWW. Nevertheless, S-soil was significantly loosened ($p < 0.01$) in the irrigated area from S-NoI: 38.1 vol. % total porosity to S-FW: 50.5 vol. % and to S-TWW: 50.3 vol. %, while for the L-soil the mean bulk density did not change between the treatments, and remained at 44.3 vol. %. To determine specific changes inside the pore systems, a detailed look into the distribution of different pore sizes was necessary.

The averaged pore size distributions (PSD) for pores larger than 60 µm are depicted in Figure 4.3a) for the S-soil and in b) for the L-soil. The second row provides the PSD of the smaller sub-samples for pores larger than 19 µm (c) and the combined cumulative porosity after merging both scales (d). The grey background marks the range, where pores smaller than 4 voxels are expected to be systematically underestimated due to image processing (Vogel et al., 2010). The high resolution of the sub-samples expands the range of valid data from secondary pores (biopores) down to primary pores arising from the arrangement of soil particles. For both soils, the rise in macro-porosity under irrigation (FW and TWW) was distributed over a wide spectrum of pore sizes from 90 to 1700 µm, and was largest in a pore diameter range of 210 to 1000 µm. For the L-soil, within the different treatments no differences in PSD were determined between the two sampling depths (0 to 10 cm and 10 to 20 cm). Pores smaller than 130 µm, as detected by the sub-samples at higher resolution, were more abundant in the TWW irrigated S-soil resulting in greater cumulative macro-porosity.

TWW irrigation reduced the clay and silt content for S-soil (Tab. 4.2), hence more intergranular spaces were detected as pores instead of the embedding matrix of fines. Figure 4.4 shows two representative slices of the reconstructed X-ray microtomographies of a S-FW sub-sample (left side) and a S-TWW sub-sample (right side). For both treatments, we enlarged a section of the image to demonstrate the discussed differences in segmented pore classes, especially for pores smaller than 130 µm. Most sand grains of the S-FW sample were embedded in a fine textured material, whereas for S-TWW, the sand grains were surrounded by pores. In summary, it has been hypothesised that TWW irrigation could lead to a reduction of porosity due to enhanced clay swelling, organic coatings on pore walls, or pore clogging through suspension and translocation of clay particles and suspended solids in the wastewater. These parameters are well below our detection limit, but could have caused a shift of the pore size distribution towards smaller pores between S-TWW and S-FW, and between L-TWW 0 to 10 cm and L-TWW 10 to 20 cm respectively. In our study, neither the total porosity nor the visible macro-porosity indicated that the pore system was negatively affected by TWW irrigation. On the contrary, the macro-porosity was increased in terms of quantity and connectivity in the irrigated plots. This might be due to greater root activity, or due to soil fauna which was not limited by drought or nutrients. The higher resolution of the sub-samples enabled the detection of an increased macro-porosity for S-TWW, which might have been due to the loss of clay minerals previously filling the pores between the sand grains and by a greater density of fine roots.

Overall, for the S-soil the visible macro-porosity was positively correlated with total porosity and with their connectivity. This indicates that the micro- and meso-porosity was not affected by TWW compared to FW irrigation. For the L-soil, no significant differences were determined between the treatments in terms of porosity, macro-porosity, or connectivity. At both orchards, macro-porosity and visible POM were an important component of soil structure, mainly in 0 to 6 cm depth, and therefore might influence soil water dynamics.

4.4.3   Soil hydraulic properties

For the S-soil (Fig. 4.5a), water retention curves varied considerably with a tendency of steeper slopes (i.e. earlier drainage) in S-TWW samples. The unsaturated hydraulic conductivities (b) were greater in S-NoI samples which was consistent with a lower volume fraction of macro-pores derived by CT which were air filled at low water potentials. For the L-soil (c), water retention curves had similar slopes for both treatments. Differences in soil water content between -10 and -100 hPa were caused by different saturated water contents due to differences in porosity. The unsaturated hydraulic conductivities were not significantly different between both treatments (d).
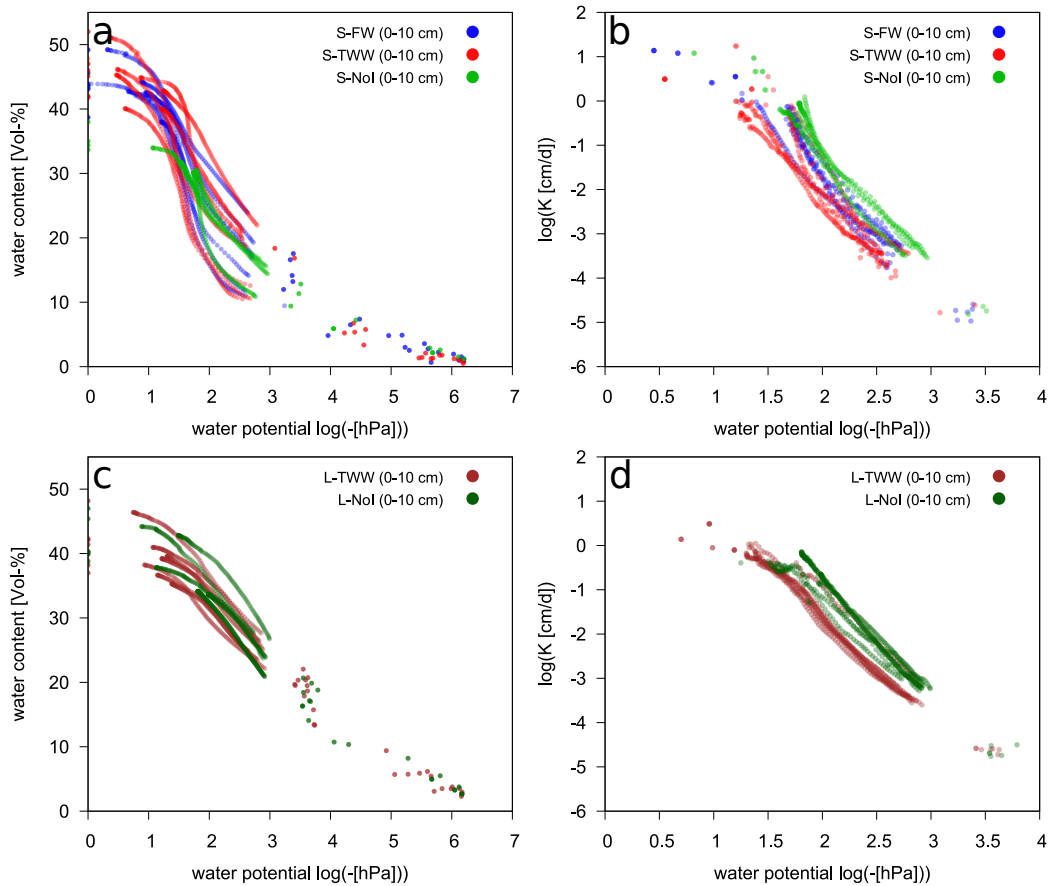
Figure 4.5: Soil water retention curve (SWRC) and hydraulic conductivity (sites: S=loamy sand, L=sandy clay loam; treatments: NoI=non-irrigated control, FW=fresh water, TWW=treated wastewater). Data points for SWRC were determined by HYPROP ($<$ log(-[4.5 hPa])) and WP4C ($>$ log(-[4.5 hPa])), for hydraulic conductivity by Multi-Step-Flux ($<$ log(-[1.5 hPa])) and HYPROP ($>$ log(-[1.4 hPa])) experiments.

Table 4.3: Results of a Partial Least Squares Regression analysis. Percentage of the variance in water content/hydraulic conductivity at -100 hPa explained by different predictor variables (EC=electrical conductivity, SAR=sodium absorption ratio, WDPT=water drop penetration time, CA=initial contact angle) for all samples and separated for both locations (S=loamy sand, L=sandy clay loam).

Water content at -100 hPa	All samples	S-samples	L-samples
Predictor variables:			
Texture: sand & clay	68.72 %	28.45 %	12.07 %
Water repellency: WDPT & CA	25.84 %	9.13 %	2.78 %
Salt: SAR & EC	2.49 %	1.00 %	1.00 %
Combined: sand & SAR & CA	70.93 %	32.60 %	21.40 %
Hydraulic conductivity at -100 hPa			
Predictor variables:			
Texture: sand & clay	17.48 %	5.47 %	32.48 %
Water repellency: WDPT & CA	50.69 %	22.23 %	64.41 %
Salt: SAR & EC	25.90 %	33.81 %	44.29 %
Combined: sand & SAR & CA	43.43 %	10.84 %	87.25 %
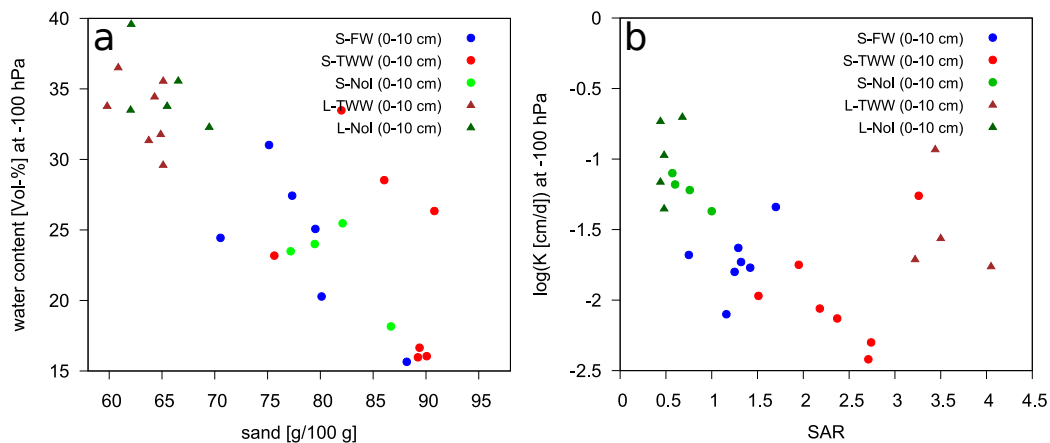
Figure 4.6: Water content and hydraulic conductivity (k) at -100 hPa (sites: S=loamy sand, L=sandy clay loam; treatments: NoI=non-irrigated control, FW=fresh water, TWW=treated wastewater).

According to Young-Laplace equation, the pore spectrum analysed via image analysis was drained at water potentials between 0 and -50 hPa for the large samples and at -158 hPa for the sub-samples. The differences in visible macro-porosity were therefore represented by the variance of the SWRCs close to saturation, but the highly sensitive range around -100 hPa was not covered for all treatments. Nevertheless, sub-samples of the S-soil indicated the loss of clay as an explanation for differences in the cumulative macro-porosity between S-FW and S-TWW (Fig. 4.3). Furthermore, a fast draining SWRC is typical for sandy soils.

To determine the sensitivity of hydraulic properties towards textural composition and physicochemical soil properties, their correlations with water contents at -100 hPa and their respective hydraulic conductivities were evaluated via Partial Least Squares Regression. In Table 4.3 we list the percentages of explained variability in the dependent variable by a set of predictors lumped into texture, water repellency, and salinity. Finally we combined the most influential parameters as a set of predictors. The greatest predictive power was found by including all samples for model calibration due to salient differences in hydraulic properties between the study sites. Also the predictive power for the hydraulic conductivity of L-samples was high due to low variability within the samples. The predictive power of the determined parameters was weak for the S-soil due to high variances.

For water retention at -100 hPa, soil texture was the best predictor. Considering all samples, variances in sand and clay content explained 69 % of the variability in water retention, but this was found to be weak when only looking at the samples from one specific site (Fig. 4.6a). Yet, the eluviation of fines may explain the overall lower water retention at -100 hPa. Using the sand content to predict the hydraulic conductivity at -100 hPa did not result in a comparatively good prediction. Here, water repellency and SAR provided the best predictive powers. The conductivity for the S-soil decreased with increasing concentration of sodium (Fig. 4.6b). Also the conductivity of the L-soil was reduced by SAR, but not that drastically. This could be an indicator that sodium had caused enhanced soil swelling and pore clogging by clay migration in the TWW-treatments, which was below under the detection limit by microtomography.

Causes of reduced hydraulic conductivity by TWW were reported to be related to entrapment of suspended solids originating from the TWW and decreased pore size distribution by adsorption of soluble organic molecules on soil particles (Lado and Ben-Hur, 2010). However, the effect of reduced hydraulic conductivity was mostly related to fine-textured soils and in most cases only the saturated hydraulic conductivity was considered which is highly sensitive to macro-pore flow. Our analysis of soil structure showed that the macro-porosity of the S-soil covered 30 to 40 % of the total porosity and the major differences were detected for small pores. Hence, significant differences in saturated hydraulic conductivity for the S-soil are not expected. For unsaturated field conditions, we could show that TWW irrigation

reduced the unsaturated hydraulic conductivity.

In summary, both parameters, sand content and SAR, did explain some variability of differences in water retention and unsaturated hydraulic conductivities. Nevertheless, outliers were found in both cases, especially for the S-soil. Besides textural compositions, other parameters can influence hydraulic properties, such as organic material, macro-pore-flow, swelling and shrinking, and reduced wettability.

4.5   Conclusion

Long-term irrigation with secondary treated wastewater (TWW) proved to have different effects on physicochemical characteristics of the topsoil. 7 years of TWW irrigation on a loamy sand already changed soil textural composition, acidity, salinity, and SAR, while 30 years of TWW irrigation on a sandy clay loam only increased the SAR of the soil. For both soils, organic carbon and nitrogen contents were mainly influenced by the accumulation of litter from the trees and not by the quality of irrigation water. By analysing the macro-pore network ($> 60\,\mu m$) it was shown that irrigation in general promoted the development of a macro-pore system in terms of volume and connectivity. No constriction of the macro- and meso-pores due to enhanced clay swelling or organic coatings was detected. On the contrary, for the loamy sand an increase of porosity by TWW compared to the replacing fresh water irrigation was detected due to the eluviation of dispersed clay minerals, which was reflected by a reduced soil water retention and greater visible porosity ($> 19\,\mu m$). The well developed macro-pore networks might promote water flow close to saturation, but when unsaturated, a reduction in hydraulic conductivity was found for both soils, suggesting that mainly primary pores and small macro-pores were affected by TWW irrigation. These small-scale changes in hydraulic properties might exacerbate instabilities in water infiltration promoting the formation of preferential flow. With regard to the long history of TWW application on the more fine textured soil, the detected changes for the topsoil were marginal.

Chapter 5

Synthesis and conclusions

5.1 A multiple analysis of soil structure alteration and hydraulic properties

The main objective of this thesis was to jointly analyse the effect of long-term irrigation with TWW on soil structure, wettability, and soil water dynamics in undisturbed soils. A multiple analysis of different soil characteristics and parameters on the same undisturbed samples required the usage of non-destructive methods to keep soil structure intact. Therefore, a new methodological approach to detect and quantify instabilities of water infiltration in undisturbed, cylindrical soil cores was developed.

The method enabled to analyse changes in water content via X-ray radiography without using chemical traces or destructing the sample after the experiment. It could be used over the full range of water contents and experiments were not limited in time by a shading corrections protocol. As samples remained intact, it was possible to run test series with different initial water contents to simulate different irrigation strategies. However, the method only provided a projection of mean changes in water content as an integral over the sample thickness. Therefore, it was difficult to assign single flow phenomena to structural features in the 3D-space. A 3D-reconstruction of changes in water contents was not possible due to the applied high water flux and a value conversion during filtered-back projection of the used software, where the quantitative information was lost. Another drawback of the method was, that it relays on the stability of soil structure. Changes in soil density due to particle transport or swelling and shrinking of clay minerals were detected as changes in water content. Nevertheless, the newly developed approach enabled to study the impact of TWW irrigation on water flow in undisturbed soil cores. An advantage over former studies using flat, quasi-two-dimensional Hele-Shaw cells with repacked soils.

It has been hypothesised that long-term irrigation with TWW may change water retention and flow regime in the topsoil due to

(i)   the alteration of wettability and herewith the development of preferential flow path,

(ii) the change in soil biological communities and their structure forming potential,

(iii) the physicochemical alteration due to higher loads of salts and organic material.

By using non-destructive methods of X-ray radiography and X-ray computed tomography, it was possible to address these hypotheses for two common soil textures in Israel: a sandy clay loam and a loamy sand. In conclusion, long-term irrigation with TWW affected the wettability of soil minerals, soil physicochemical characteristics, the pore-network, and consequently soil hydraulic properties. However, occurrence and severity were strongly dependent on soil texture and a result of different mechanisms enforced by the wide variety of chemicals, organics, and micro-pollutants introduced by the irrigation water. For both soils, it was shown that irrigation, independent of the water quality, supported the development of a connected macro-pore system. The minor water quality did not negatively affect soil biological activity. This is of great interest as bioturbation counteracts the formation of soil sealing, stabilises soil structure, enhances aeration, and promotes water flow close to saturation. Further, a higher input of organics did not consequently result in greater soil carbon concentrations. Considering all determined parameters and soil characteristics, it became apparent that the long-term effects of TWW irrigation had to be discussed soil specific rather than by the single hypotheses.

Impact on a sandy clay loam

A sandy clay loam irrigated for 30 years with TWW did not significantly change textural composition, soil acidity, and salinity compared to the non-irrigated control, whereas SAR was significantly increased. Despite the continous application of organics during irrigation, the mean carbon concentration was comparably low. As soil was kept moist over the year, biological activity was not limited by drought stress and hence decomposition of organics was not reduced. The only parameters that varied between the seasons were WDPT and CA to measure hydrophobicity. In October 2015, at the end of the dry season, soil was classified as slightly water repellent, whereas at the end of the rainy season, in February 2016, soil was predominant wettable. The slightly reduced wettability did not affect the stability of water infiltration for field moist samples. No effect was expected for lower

water contents as soil was predominant wettable. More specifically, the observed differences in water content changes along the sample profile could be explained by an increased macro-porosity in the upper part of the sample and the high flux rate which was applied. At a flux of $j = 8\,\mathrm{mm\,h^{-1}}$ the water was transported also through the detected macro-pores. Overall, a greater amount of secondary pores was detected for TWW samples compared to the non-irrigated control, which confirms the hypothesis of a stimulated biological activity resulting in reduced carbon concentrations. However, the total porosity of all sandy clay loam samples was not affected by TWW irrigation, concluding that the determined differences in macro-pores reflect only a minor part of the total pore network. Therefore, no differences in soil water retention curves were observed. A slight decrease in unsaturated hydraulic conductivity over a wide range of water potential were measured, which can be explained by clay mineral swelling due to higher sodium concentrations narrowing primary pores, and pore clogging by suspended solids. However, this was below the detection limit by microtomography and need to be further investigated. Overall, the sandy clay loam was highly resistant to soil alteration by long-term TWW irrigation.

Impact on a loamy sand

7 years of TWW irrigation on a loamy sand significantly increased soil sodicity, salinity, and carbon and nitrogen concentrations. Compared to the FW irrigated plots, the clay content was significantly decreased, resulting in a greater sand content. A reduced wettability of mineral surfaces was determined for both irrigated treatments, which was explained by the 3 years TWW irrigation history for the FW-soil. While FW-soil samples provided a seasonal dynamic in hydrophobicity, TWW irrigated plots were classified as severely water repellent over the analysed depth (0 to $-5\,\mathrm{cm}$) independent of the season. Furthermore, the measured CA dynamics indicated that for TWW-soil, the reorientation of hydrophobic molecules was slower when exposed to water. The reduced wettability resulted in water flow instabilities when water content dropped below 13 vol. %, and became even more severe when lowering the initial water content. After 7 days of drying, TWW samples significantly reduced their availability to re-wet and hence to store water. It is noted that the infiltration fronts at 1.5 vol. % initial water content followed the same paths as at 13 vol. %. The seasonal independence of water repellency and the occurrence of recurring patterns of flow paths indicated that hydrophobicity has become a persistent soil characteristics. This phenomenon could enhance the impact of TWW irrigation locally and promote the formation of preferential flow paths on an entire soil profile. The results demonstrated, that an appropriate irrigation strategy, which keeps soil moisture above a critical water content, could prevent the formation of preferential flow paths. Therefore, the applied amount of water has to be sufficient to keep soil moist over the soil profile during the entire

day. The effect on soil structure was mainly triggered by the loss of fine textured material increasing the determined porosity for pores smaller than $130\,\mu m$. The eluviation of clay minerals reduced the water retention of the loamy sand, while the phyicochemical alteration reduced the unsaturated hydraulic conductivity. It can be stated that the loss of fines and the input of hydrophobic organics made the loamy sand highly vulnerable to TWW irrigation.

5.2   Outlook and recommendations

The direct measurement of soil structure, soil hydraulic properties, infiltration characteristics, and physicochemical status of undisturbed soil cores provided evidence that the long-term irrigation with TWW had an impact on different soil properties of a loamy sand and a sandy clay loam. By using multivariate statistics it was possible to restrict potential drivers of TWW contaminants for changes in hydraulic properties. However, soil structural heterogeneity, the non-linearity of hydraulic properties, and the wide variety of TWW-composition resulted in a complex interplay of physical and chemical interactions. Therefore, the determined relations between soil textural composition and water retention as well as physicochemical alteration and unsaturated hydraulic conductivity provided uncertainties which have to be addressed in further studies. In the present thesis, it has been shown that the occurrence of water repellency on the soil surface measured by WDPT and initial CA would not consequently lead to instabilities of water infiltration. The persistence of water repellency on the small scale, i.e. the resistance of hydrophobic molecules to reorientation, and the impact over depth washed in by continuous irrigation seem to have caused the flow instabilities for the loamy sand.

The research objectives of this thesis concentrated on the topsoil, 0 to 20 cm below the irrigation drippers, which was considered as the most affected region by TWW irrigation. The topsoil is most important for water infiltration, biological activity, plant nutrition, and in areas with high evaporation influenced by the accumulation of salts and contaminants. Nevertheless, the impact on deeper soil layers should be investigated to address concerns about the leaching of water and chemicals below the root zone on the field scale. Furthermore, the effect of induced water repellency on water loss through evaporation could be another important factor for sustainable water management.

The search for new water resources for irrigation is a mandatory requirement in many arid and semiarid agroecosystems. Most likely, reclaimed water will be one of the water resources whose usage would further increase. The results of this study mainly provided experimental evidence that soil texture and water management should be evaluated for a sustainable usage of TWW for agricultural irrigation. In order to define appropriate guidelines for the usage of TWW, a detailed knowledge

about the wastewater composition, its availability, and the soil is required. Information about soil texture, calcium and magnesium availability to reduce the impact of sodium, and the nutrition level should be considered. Farmers should adjust their fertiliser application to the wastewater composition to prevent soil acidification and over-fertilisation. For sandy soils, the effect of reduced wettability due to organics should be monitored closely to prevent water loss, leaching of chemicals, and to keep its availability to store water. Technical solutions, like the application of surfactants, a third treatment stage, or further dilution of the effluent could reduce the impact on soil properties. Additionally, different water management strategies such as a rotation between FW and TWW application could prevent the formation of preferential flow, as demonstrated by the reclamation of infiltration properties by FW application. The findings of this study confirmed the concern that TWW irrigation may impair soil quality. However, compared to the known consequences by using untreated wastewater for irrigation or the overexploitation of potable water resources, the usage of TWW for agricultural irrigation is still a promising option for a sustainable water allocation in water scarce regions.

Bibliography

Adrover, M., Farrús, E., Moyà, G., Vadell, J., 2012. Chemical properties and biological activity in soils of Mallorca following twenty years of treated wastewater irrigation. J. Environ. Manage. 95, 188–192.

Aiello, R., Cirelli, G. L., Consoli, S., 2007. Effects of reclaimed wastewater irrigation on soil and tomato fruits: a case study in Sicily (Italy). Agr. Water Manage. 93, 65–72.

Allaire, S. E., Roulier, S., Cessna, A. J., 2009. Quantifying preferential flow in soils: A review of different techniques. J. Hydrol. 378, 179–204.

Arye, G., Tarchitzky, J., Chen, Y., 2011. Treated wastewater effects on water repellency and soil hydraulic properties of soil aquifer treatment infiltration basins. J. Hydrol. 397, 136–145.

Assouline, S., Narkis, K., 2011. Effects of long-term irrigation with treated wastewater on the hydraulic properties of a clayey soil. Water Resour. Res. 47, W08530.

Assouline, S., Narkis, K., 2013. Effect of long-term irrigation with treated wastewater on the root zone environment. Vadose Zone J. 12.

Assouline, S., Narkis, K., Gherabli, R., Sposito, G., 2016. Combined effect of sodicity and organic matter on soil properties under long-term irrigation with treated wastewater. Vadose Zone J. 15.

Assouline, S., Russo, D., Silber, A., Or, D., 2015. Balancing water scarcity and quality for sustainable irrigated agriculture. Water Resour. Res. 51, 3419–3436.

Bachmann, J., Ellies, A., Hartge, K. H., 2000. Development and application of a new sessile drop contact angle method to assess soil water repellency. J. Hydrol. 231-232, 66–75.

Bardhan, G., Russo, D., Goldstein, D., Levy, G. J., 2016. Changes in the hydraulic properties of a clay soil under long-term irrigation with treated wastewater. Geoderma 264, 1–9.

Bauters, T. W. J., Steenhuis, T. S., DiCarlo, D. A., Nieber, J. L., Dekker, L. W., Ritsema, C. J., Parlange, J.-Y., Haverkamp, R., 2000. Physics of water repellent soils. J. Hydrol. 231-232, 233–243.

Bayer, A., Vogel, H.-J., Roth, K., 2004. Direct measurement of the soil water retention curve using X-ray absorption. Hydrol. Earth Syst. Sc. 8, 2–7.

Becerra-Castro, C., Lopes, A. R., Vaz-Moreira, I., Silva, E. F., Manaia, C. M., Nunes, O. C., 2015. Wastewater reuse in irrigation: A microbiological perspective on implications in soil fertility and human and environmental health. Environ. Int. 75, 117–135.

Bedbabis, S., Rouina, B. B., Boukhris, M., Ferrara, G., 2014. Effect of irrigation with treated wastewater on soil chemical properties and infiltration rate. J. Environ. Manage. 133, 45–50.

Bedbabis, S., Trigui, D., Ahmed, C. B., Clodoveo, M. L., Camposeo, S., Vivaldi, G. A., Rouina, B. B., 2015. Long-terms effects of irrigation with treated municipal wastewater on soil, yield and olive oil quality. Agr. Water Manage. 160, 14–21.

Ben-Hur, M., 2004. Sewage water treatments and reuse in Israel. In: Zereini, F., Jaeschke, W. (Eds.), Water in the Middle East and in North Africa: Resources, Protection and Management. Springer, Berlin, Heidelberg, pp. 167–180.

Ben-Hur, M., Yolcu, G., Uysal, H., Lado, M., Paz, A., 2009. Soil structure changes: aggregate size and soil texture effects on hydraulic conductivity under different saline and sodic conditions. Soil Res. 47, 688–696.

Bisdom, E. B. A., Dekker, L. W., Schoute, J. F. T., 1993. Water repellency of sieve fractions from sandy soils and relationships with organic material and soil structure. In: Brussaard, L., Kooistra, M. J. (Eds.), Soil Structure/Soil Biota Interrelationships. Elsevier, Amsterdam, pp. 105–118.

Bottinelli, N., Jouquet, P., Capowiez, Y., Podwojewski, P., Grimaldi, M., Peng, X., 2015. Why is the influence of soil macrofauna on soil structure only considered by soil ecologists? Soil Till. Res. 146, 118–124.

Bughici, T., Wallach, R., 2016. Formation of soil–water repellency in olive orchards and its influence on infiltration pattern. Geoderma 262, 1–11.

Carrillo, M. L. K., Letey, J., Yates, S. R., 2000. Unstable water flow in a layered soil ii. effects of an unstable water-repellent layer. Soil Sci. Soc. Am. J. 64, 456–459.

Chen, W., Wu, L., Frankenberger, W. T., Chang, A. C., 2008. Soil enzyme activities of long-term reclaimed wastewater-irrigated soils. J. Environ. Qual. 37, 36–42.

Clothier, B. E., Vogeler, I., Magesan, G. N., 2000. The breakdown of water repellency and solute transport through a hydrophobic soil. J. Hydrol. 231-232, 255–264.

Coppola, A., Santini, A., Botti, P., Vacca, S., Comegna, V., Severino, G., 2004. Methodological approach for evaluating the response of soil hydrological behavior to irrigation with treated municipal wastewater. J. Hydrol. 292, 114–134.

DeBano, L. F., 1981. Water repellent soils: a state-of-the-art. Gen. Tech. Rep. PSW-GTR-46. Berkeley, CA: U.S. Department of Agriculture, Forest Service, Pacific Southwest Forest and Range Experiment Station.

Dekker, L. W., Ritsema, C. J., 1994. How water moves in a water repellent sandy soil: 1. Potential and actual water repellency. Water Resour. Res. 30, 2507–2517.

Dekker, L. W., Ritsema, C. J., 2000. Wetting patterns and moisture variability in water repellent Dutch soils. J. Hydrol. 231-232, 148–164.

Diamantopoulos, E., Durner, W., Reszkowska, A., Bachmann, J., 2013. Effect of soil water repellency on soil hydraulic properties estimated under dynamic conditions. J. Hydrol. 486, 175–186.

Díaz-Zorita, M., Perfect, E., Grove, J., 2002. Disruptive methods for assessing soil structure. Soil Till. Res. 64, 3–22.

DIN ISO 11277, 2002. Soil quality - Determination of particle size distribution in mineral soil material - Method by sieving and sedimentation. Beuth.

Doerr, S. H., 1998. On standardizing the 'water drop penetration time' and the 'molarity of an ethanol droplet' techniques to classify soil hydrophobicity: a case study using medium textured soils. Earth Surf. Proc. Land. 23, 663–668.

Doerr, S. H., Ritsema, C. J., Dekker, L. W., Scott, D. F., Carter, D., 2007. Water repellence of soils: new insights and emerging research needs. Hydrol. Process. 21, 2223–2228.

Doerr, S. H., Shakesby, R. A., Walsh, R. P. D., 2000. Soil water repellency: its causes, characteristics and hydro-geomorphological significance. Earth-Sci. Rev. 51, 33–65.

Doerr, S. H., Thomas, A. D., 2003. Soil moisture: a controlling factor in water repellency? In: Ritsema, C., Dekker, L. (Eds.), Soil Water Repellency. Elsevier, Amsterdam, pp. 137 – 149.

Doube, M., Klosowski, M. M., Arganda-Carreras, I., Cordelières, F. P., Dougherty, R. P., Jackson, J. S., Schmid, B., Hutchinson, J. R., Shefelbine, S. J., 2010. Bonej: Free and extensible bone image analysis in ImageJ. Bone 47, 1076–1079.

Elifantz, H., Kautsky, L., Mor-Yosef, M., Tarchitzky, J., Bar-Tal, A., Chen, Y., Minz, D., 2011. Microbial activity and organic matter dynamics during 4 years of irrigation with treated wastewater. Microb. Ecol. 62, 973–981.

Elliott, E. T., Coleman, D. C., 1988. Let the soil work for us. Ecol. Bull. 39, 23–32.

Feigin, A., Ravina, I., Shalhevet, J., 1991. Irrigation with Treated Sewage Effluent: Management for Environmental Protection. Springer, Berlin, Heidelberg.

Frenk, S., Hadar, Y., Minz, D., 2014. Resilience of soil bacterial community to irrigation with water of different qualities under Mediterranean climate. Environ. Microbiol. 16, 559–569.

Ganz, C., Bachmann, J., Lamparter, A., Woche, S. K., Duijnisveld, W. H. M., Göbel, M.-O., 2013. Specific processes during in situ infiltration into a sandy soil with low-level water repellency. J. Hydrol. 484, 45–54.

Gharaibeh, M. A., Ghezzehei, T. A., Albalasmeh, A. A., Alghzawi, M. Z., 2016. Alteration of physical and chemical characteristics of clayey soils by irrigation with treated waste water. Geoderma 276, 33–40.

Gonçalves, R. A. B., Folegatti, M. V., Gloaguen, T. V., Libardi, P. L., Montes, C. R., Lucas, Y., Dias, C. T. S., Melfi, A. J., 2007. Hydraulic conductivity of a soil irrigated with treated sewage effluent. Geoderma 139, 241–248.

González-Peñaloza, F. A., Cerdà, A., Zavala, L. M., Jordán, A., Giménez-Morera, A., Arcenegui, V., 2012. Do conservative agriculture practices increase soil water repellency? A case study in citrus-cropped soils. Soil Till. Res. 124, 233–239.

Graber, E. R., Tagger, S., Wallach, R., 2007. Do surface active substances from water repellent soils aid wetting? Eur. J. Soil Sci. 58, 1393–1399.

Hadas, E., Kislev, Y., 2011. Economic aspects of irrigation with treated wastewater. In: Levy, G. J., Fine, P., Bar-Tal, A. (Eds.), Treated Wastewater in Agriculture: Use and Impacts on the Soil Environment and Crops. Wiley-Blackwell, Oxford, pp. 113–127.

Hainsworth, J. M., Aylmore, L. A. G., 1983. The use of computer assisted tomography in determine spatial distribution of soil water content. Aust. J. Soil Res. 21, 435–443.

Halliwell, D. J., Barlow, K. M., Nash, D. M., 2001. A review of the effects of wastewater sodium on soil physical properties and their implications for irrigation systems. Aust. J. Soil Res. 39, 1259–1267.

Hendrickx, J. M. H., Flury, M., 2001. Uniform and preferential flow mechanisms in the vadose zone. In: Conceptual models of flow and transport in the fractured vadose zone. The National Academies Press, Washington, D.C., pp. 149–187.

Hillel, D., 1998. Environmental soil physics: Fundamentals, applications, and environmental considerations. Academic press, San Diego, London.

Horne, D. J., McIntosh, J. C., 2000. Hydrophobic compounds in sands in New Zealand - extraction, characterisation and proposed mechanisms for repellency expression. J. Hydrol. 231-232, 35–46.

Iannelli, R., Giraldi, D., 2011. Sources and composition of sewage effluent; treatment systems and methods. In: Levy, G. J., Fine, P., Bar-Tal, A. (Eds.), Treated Wastewater in Agriculture: Use and Impacts on the Soil Environment and Crops. Wiley-Blackwell, Oxford, pp. 3–50.

Ibekwe, A. M., Gonzalez-Rubio, A., Suarez, D. L., 2018. Impact of treated wastewater for irrigation on soil microbial communities. Sci. Total Environ. 622-623, 1603–1610.

Jahn, R., Blume, H. P., Asio, V. B., Spaargaren, O., Schad, P., 2006. Guidelines for soil description, 4th Edition. FAO, Rome.

Jarvis, N. J., 2007. A review of non-equilibrium water flow and solute transport in soil macropores: principles, controlling factors and consequences for water quality. Eur. J. Soil Sci. 58, 523–546.

Jueschke, E., Marschner, B., Tarchitzky, J., Chen, Y., 2008. Effects of treated wastewater irrigation on the dissolved and soil organic carbon in Israeli soils. Water Sci. Technol. 57, 727–733.

Jury, W. A., Gardner, W. R., Gardner, W. H., 1991. Soil physics, 5th Edition. John Wiley & Sons, New York.

Kaestner, A. P., Trtik, P., Zarebanadkouki, M., Kazantsev, D., Snehota, M., Dobson, K. J., Lehmann, E. H., 2016. Recent developments in neutron imaging with applications for porous media research. Solid Earth 7, 1281–1292.

Kobayashi, M., Shimizu, T., 2007. Soil water repellency in a Japanese cypress plantation restricts increases in soil water storage during rainfall events. Hydrol. Process. 21, 2356–2364.

Kuka, K., Illerhaus, B., Fritsch, G., Joschko, M., Rogasik, H., Paschen, M., Schulz, H., Seyfarth, M., 2013. A new method for the extraction of undisturbed soil samples for X-ray computed tomography. J. Nondestr. Test. 8.

Lado, M., Bar-Tal, A., Azenkot, A., Assouline, S., Ravina, I., Erner, Y., Fine, P., Dasberg, S., Ben-Hur, M., 2012. Changes in chemical properties of semiarid soils under long-term secondary treated wastewater irrigation. Soil Sci. Soc. Am. J. 76, 1358–1369.

Lado, M., Ben-Hur, M., 2009. Treated domestic sewage irrigation effects on soil hydraulic properties in arid and semiarid zones: A review. Soil Till. Res. 106, 152–163.

Lado, M., Ben-Hur, M., 2010. Effects of irrigation with different effluents on saturated hydraulic conductivity of arid and semiarid soils. Soil Sci. Soc. Am. J. 74, 23–32.

Lado, M., Ben-Hur, M., Assouline, S., 2005. Effects of effluent irrigation on seal formation, infiltration, and soil loss during rainfall. Soil Sci. Soc. Am. J. 69, 1432–1439.

Lamparter, A., Deurer, M., Bachmann, J., Duijnisveld, W. H. M., 2006. Effect of subcritical hydrophobicity in a sandy soil on water infiltration and mobile water content. J. Plant Nutr. Soil Sc. 169, 38–46.

Lenth, R. V., 2016. Least-squares means: The R package lsmeans. J. Stat. Softw. 69, 1–33.

Letey, J., Carrillo, M. L. K., Pang, X. P., 2000. Approaches to characterize the degree of water repellency. J. Hydrol. 231-232, 61–65.

Leuther, F., Weller, U., Wallach, R., Vogel, H.-J., 2018. Quantitative analysis of wetting front instabilities in soil caused by treated waste water irrigation. Geoderma 319, 132–141.

Levy, G., Goldstein, D., Mamedov, A., 2005. Saturated hydraulic conductivity of semiarid soils: Combined effects of salinity, sodicity, and rate of wetting. Soil Sci. Soc. Am. J. 69, 653–662.

Levy, G. J., 2011. Impact of long-term irrigation with treated wastewater on soil-structure stability - the Israeli experience. Isr. J. Plant Sci. 59, 95–104.

Levy, G. J., Assouline, S., 2011. Physical aspects. In: Levy, G. J., Fine, P., Bar-Tal, A. (Eds.), Treated Wastewater in Agriculture: Use and Impacts on the Soil Environment and Crops. Wiley-Blackwell, Oxford, pp. 306–327.

Levy, G. J., Rosenthal, A., Tarchitzky, J., Shainberg, I., Chen, Y., 1999. Soil hydraulic conductivity changes caused by irrigation with reclaimed waste water. J. Environ. Qual. 28, 1658–1664.

Lipsius, K., Mooney, S. J., 2006. Using image analysis of tracer staining to examine the infiltration patterns in a water repellent contaminated sandy soil. Geoderma 136, 865–875.

Luo, L., Lin, H., Halleck, P., 2008. Quantifying soil structure and preferential flow in intact soil using X-ray computed tomography. Soil Sci. Soc. Am. J. 72, 1058–1069.

Mace, J. E., Amrhein, C., 2001. Leaching and reclamation of a soil irrigated with moderate SAR waters. Soil Sci. Soc. Am. J. 65, 199–204.

Marschner, H., Römheld, V., Horst, W. J., Martin, P., 1986. Root-induced changes in the rhizosphere: Importance for the mineral nutrition of plants. Z. Pflanz. Bodenkunde 149, 441–456.

Mathan, K. K., 1994. Studies on the influence of long-term municipal sewage-effluent irrigation on soil physical properties. Bioresour. Technol. 48, 275–276.

Minz, D., Karyo, R., Gerstl, Z., 2011. Effects of treated municipal wastewater irrigation on soil microbiology. In: Levy, G. J., Fine, P., Bar-Tal, A. (Eds.), Treated Wastewater in Agriculture: Use and Impacts on the Soil Environment and Crops. Wiley-Blackwell, Oxford, pp. 77–111.

Mooney, S. J., 2002. Three-dimensional visualization and quantification of soil macroporosity and water flow patterns using computed tomography. Soil Use Manage. 18, 142–151.

Moradi, A. B., Carminati, A., Vetterlein, D., Vontobel, P., Lehmann, E., Weller, U., Hopmans, J. W., Vogel, H.-J., Oswald, S. E., 2011. Three-dimensional visualization and quantification of water content in the rhizosphere. New Phytol. 192, 653–663.

Mori, Y., Maruyama, T., Mitsuno, T., 1999. Soft X-ray radiography of drainage patterns of structured soils. Soil Sci. Soc. Am. J. 63, 733–740.

Müller, K., Carrick, S., Meenken, E., Clemens, G., Hunter, D., Rhodes, P., Thomas, S., 2016. Is subcritical water repellency an issue for efficient irrigation in arable soils? Soil Till. Res. 161, 53–62.

Müller, K., Magesan, G. N., Bolan, N. S., 2007. A critical review of the influence of effluent irrigation on the fate of pesticides in soil. Agr Ecosyst Environ 120, 93–116.

Murray, R. S., Grant, C. D., 2007. The impact of irrigation on soil structure. The National Program for Sustainable Irrigation (Land & Water Australia), Canberra, Austalia.

Oades, J. M., 1993. The role of biology in the formation, stabilization and degradation of soil structure. In: Brussaard, L., Kooistra, M. J. (Eds.), Soil Structure/Soil Biota Interrelationships. Elsevier, Amsterdam, pp. 377–400.

OECD, 2015. Water resources allocation: Sharing risks and opportunities. OECD Publishing, Paris.

Or, D., Lehmann, P., Shahraeeni, E., Shokri, N., 2013. Advances in soil evaporation physics - A review. Vadose Zone J. 12.

Or, D., Tuller, M., 2005. Capillarity. In: Hillel, D., Rosenzweig, C., Powlson, D., Scow, K., Singer, M., Sparks, D. (Eds.), Encyclopedia of Soils in the Environment. Elsevier, Oxford, pp. 155–164.

Paranychianakis, N. V., Salgot, M., Angelakis, A. N., 2011. Irrigation with recycled water: Guidelines and regulations. In: Levy, G. J., Fine, P., Bar-Tal, A. (Eds.), Treated Wastewater in Agriculture: Use and Impacts on the Soil Environment and Crops. Wiley-Blackwell, Oxford, pp. 77–111.

Paudel, I., Cohen, S., Shaviv, A., Bar-Tal, A., Bernstein, N., Heuer, B., Ephrath, J., 2016. Impact of treated wastewater on growth, respiration and hydraulic conductivity of citrus root systems in light and heavy soils. Tree Physiol. 36, 770–785.

Pedrero, F., Kalavrouziotis, I., Alarcón, J. J., Koukoulakis, P., Asano, T., 2010. Use of treated municipal wastewater in irrigated agriculture - Review of some practices in Spain and Greece. Agr. Water Manage. 97, 1233–1241.

Qadir, M., Wichelns, D., Raschid-Sally, L., McCornick, P. G., Drechsel, P., Bahri, A., Minhas, P. S., 2010. The challenges of wastewater irrigation in developing countries. Agr. Water Manage. 97, 561–568.

Rabot, E., Wiesmeier, M., Schlüter, S., Vogel, H.-J., 2018. Soil structure as an indicator of soil functions: A review. Geoderma 314, 122–137.

Rahav, M., Brindt, N., Yermiyahu, U., Wallach, R., 2017. Induced heterogeneity of soil water content and chemical properties by treated wastewater irrigation and its reclamation by freshwater irrigation. Water Resour. Res. 53, 4756–4774.

Rahman, M. Z., Riesbeck, F., Dupree, S., 2018. The Opportunity Versus Risks in Wastewater Irrigation. In: Hettiarachchi, H., Ardakanian, R. (Eds.), Safe Use of Wastewater in Agriculture: From Concept to Implementation. Springer, Cham, pp. 13–25.

Renard, P., Allard, D., 2013. Connectivity metrics for subsurface flow and transport. Adv. Water Resour. 51, 168–196.

Rengasamy, P., 2010. Soil processes affecting crop production in salt-affected soils. Funct. Plant Biol. 37, 613–620.

Rogasik, H., Crawford, J. W., Wendroth, O., Young, I. M., Joschko, M., Ritz, K., 1999. Discrimination of soil phases by dual energy X-ray tomography. Soil Sci. Soc. Am. J. 63, 741–751.

Rowell, D. L., 1994. Soil science: methods and applications. Harlow Longman Scientific & Technical, London.

Rye, C. F., Smettem, K. R. J., 2017. The effect of water repellent soil surface layers on preferential flow and bare soil evaporation. Geoderma 289, 142–149.

Rye, C. F., Smettem, K. R. J., 2018. Seasonal variation of subsurface flow pathway spread under a water repellent surface layer. Geoderma 327, 1–12.

Sato, T., Qadir, M., Yamamoto, S., Endo, T., Zahoor, A., 2013. Global, regional, and country level need for data on wastewater generation, treatment, and use. Agr. Water Manage. 130, 1–13.

Schacht, K., Chen, Y., Tarchitzky, J., Lichner, L., Marschner, B., 2014. Impact of treated wastewater irrigation on water repellency of Mediterranean soils. Irrigation Sci. 32, 369–378.

Schacht, K., Marschner, B., 2015. Treated wastewater irrigation effects on soil hydraulic conductivity and aggregate stability of loamy soils in Israel. J. Hydrol. Hydromech. 63, 47–54.

Schindelin, J., Arganda-Carreras, I., Frise, E., Kaynig, V., Longair, M., Pietzsch, T., Preibisch, S., Rueden, C., Saalfeld, S., Schmid, B., Tinevez, J.-Y., White, D. J., Hartenstein, V., Eliceiri, K., Tomancak, P., Cardona, A., 2012. Fiji: an open-source platform for biological-image analysis. Nat. Meth. 9, 676–682.

Schindler, U., Durner, W., von Unold, G., Müller, L., 2010. Evaporation method for measuring unsaturated hydraulic properties of soils: Extending the measurement range. Soil Sci. Soc. Am. J. 74, 1071–1083.

Schlüter, S., Leuther, F., Vogler, S., Vogel, H.-J., 2016. X-ray microtomography analysis of soil structure deformation caused by centrifugation. Solid Earth 7, 129–140.

Schlüter, S., Sheppard, A., Brown, K., Wildenschild, D., 2014. Image processing of multiphase images obtained via X-ray microtomography: A review. Water Resour. Res. 50, 3615–3639.

Scott, D., 2000. Soil wettability in forested catchments in South Africa; as measured by different methods and as affected by vegetation cover and soil characteristics. J. Hydrol. 231-232, 87–104.

Seis, W., Lesjean, B., Maaßen, S., Balla, D., Hochstrat, R., Düppenbecker, B., 2016. Rahmenbedingungen für die umweltgerechte Nutzung von behandeltem Abwasser zur landwirtschaftlichen Bewässerung. Umweltbundesamt, Dessau-Roßlau.

Shokri, N., Lehmann, P., Or, D., 2008. Effects of hydrophobic layers on evaporation from porous media. Geophys Res. Lett. 35.

Singer, A., 2007. The Soils of Israel. Springer, Berlin, Heidelberg.

Snehota, M., Jelinkova, V., Sobotkova, M., Sacha, J., Vontobel, P., Hovind, J., 2015. Water and entrapped air redistribution in heterogeneous sand sample: Quantitative neutron imaging of the process. Water Resour. Res. 51, 1359–1371.

Suarez, D. L., Gonzalez-Rubio, A., 2017. Effects of the dissolved organic carbon of treated municipal wastewater on soil infiltration as related to sodium adsorption ratio and pH. Soil Sci. Soc. Am. J. 81, 602–611.

Tarchitzky, J., Golobati, Y., Chen, Y., Keren, R., 1999. Wastewater effects on montmorillonite suspensions and hydraulic properties of sandy soils. Soil Sci. Soc. Am. J. 63, 554–560.

Tarchitzky, J., Lerner, O., Shani, U., Arye, G., Lowengart-Aycicegi, A., Brener, A., Chen, Y., 2007. Water distribution pattern in treated wastewater irrigated soils: hydrophobicity effect. Eur. J. Soil Sci. 58, 573–588.

Tarchouna, L. G., Merdy, P., Raynaud, M., Pfeifer, H.-R., Lucas, Y., 2010. Effects of long-term irrigation with treated wastewater. Part I: Evolution of soil physico-chemical properties. Appl. Geochem. 25, 1703–1710.

The World Bank, 2012. Renewable energy desalination: an emerging solution to close the water gap in the Middle East and North Africa. World Bank Publications, Washington, D.C.

Toze, S., 2006. Reuse of effluent water - benefits and risks. Agr. Water Manage. 80, 147–159.

Tracy, S. R., Daly, K. R., Sturrock, C. J., Crout, N. M. J., Mooney, S. J., Roose, T., 2015. Three-dimensional quantification of soil hydraulic properties using X-ray Computed Tomography and image-based modeling. Water Resour. Res. 51, 1006–1022.

Vinten, A. J. A., Mingelgrin, U., Yaron, B., 1983. The effect of suspended solids in wastewater on soil hydraulic conductivity: II. Vertical distribution of suspended solids. Soil Sci. Soc. Am. J. 47, 408–412.

Vogel, H.-J., Weller, U., Schlüter, S., 2008. Quantim- c/c++ library for scientific image processing. http://www.quantim.ufz.de (accessed 15 Mai 2017).

Vogel, H.-J., Weller, U., Schlüter, S., 2010. Quantification of soil structure based on Minkowski functions. Comput. Geosci. 36, 1236–1245.

Wallach, R., Ben-Arie, O., Graber, E. R., 2005. Soil water repellency induced by long-term irrigation with treated sewage effluent. J. Environ. Qual. 34, 1910–1920.

Wallach, R., Graber, E. R., 2007. Infiltration into effluent irrigation-induced repellent soils and the dependence of repellency on ambient relative humidity. Hydrol. Process. 21, 2346–2355.

Wallach, R., Jortzick, C., 2008. Unstable finger-like flow in water-repellent soils during wetting and redistribution – The case of a point water source. J. Hydrol. 351, 26–41.

Wallach, R., Margolis, M., Graber, E. R., 2013. The role of contact angle on unstable flow formation during infiltration and drainage in wettable porous media. Water Resour. Res. 49, 6508–6521.

Wang, Z., Wu, Q. J., Wu, L., Ritsema, C. J., Dekker, L. W., Feyen, J., 2000. Effects of soil water repellency on infiltration rate and flow instability. J. Hydrol. 231-232, 265–276.

Wehrens, R., Mevik, B.-H., 2007. The pls package: Principal component and partial least squares regression in R. J. Stat. Softw. 18, 1–23.

Weller, U., Leuther, F., Schlüter, S., Vogel, H.-J., 2018. Quantitative analysis of water infiltration in soil cores using X-ray. Vadose Zone J. 17.

Weller, U., Vogel, H.-J., 2012. Conductivity and hydraulic nonequilibrium across drainage and infiltration fronts. Vadose Zone J. 11.

Wildenschild, D., Sheppard, A. P., 2013. X-ray imaging and analysis techniques for quantifying pore-scale structure and processes in subsurface porous medium systems. Adv. Water Resour. 51, 217–246.

Winpenny, J., Heintz, I., Koo-Oshima, S., 2010. The wealth of waste: the economics of wastewater use in agriculture. FAO Water Reports, Roma.

WWAP, 2017. The United Nations World Water Development Report 2017: Wastewater, the untapped resource. UNESCO, Paris.

Xiong, Y., Furman, A., Wallach, R., 2012. Moment analysis description of wetting and redistribution plumes in wettable and water-repellent soils. J. Hydrol. 422, 30–42.

Zavala, L. M., González, F. A., Jordán, A., 2009. Intensity and persistence of water repellency in relation to vegetation types and soil parameters in Mediterranean SW Spain. Geoderma 152, 361–374.

Appendix

Supplementary material

A) Infiltration experiments

The following figures show changes in water content (vol. %) during infiltration experiments of all field moist soil columns, and with reduced initial water contents. The mean initial water contents were reduced to 13 vol. % after 3 days of drying, and 1.5 vol. % after 7 days of drying. The columns of the figures separate samples from different sampling locations and their treatments, the rows show the progress of infiltrating water after certain time steps. Individual exceptions of time steps (designated with additional times) were chosen for better illustration of the infiltration front. For the loamy sand, column S and T provide the results of 20 cm heigh samples, as for the sandy clay loam columns G and J.
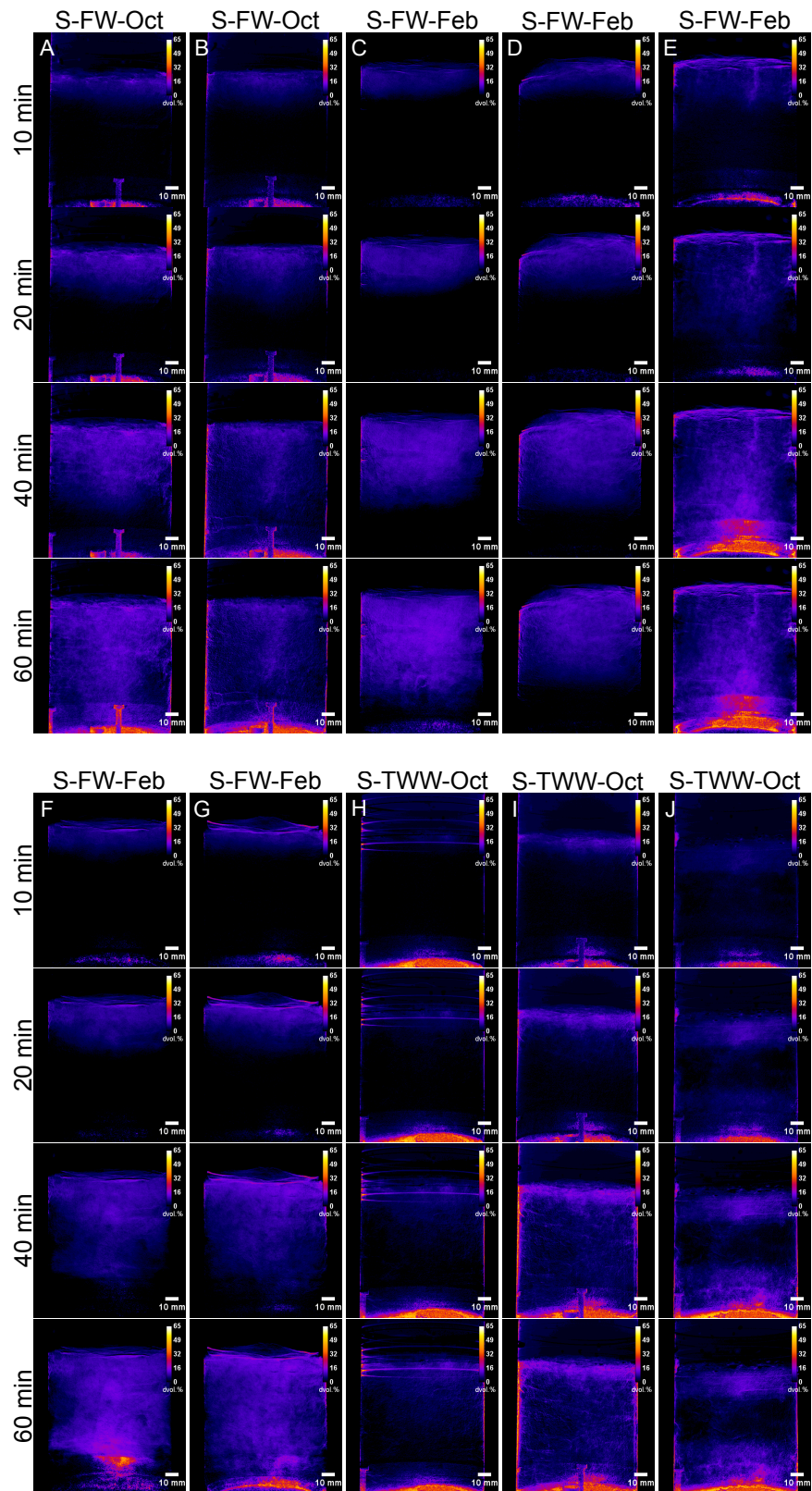
Figure A1: Loamy sand - changes in water content $\Delta\theta$ (vol. %) at field moisture (FW=fresh water, TWW= treated wastewater, NoI=non-irrigated control).
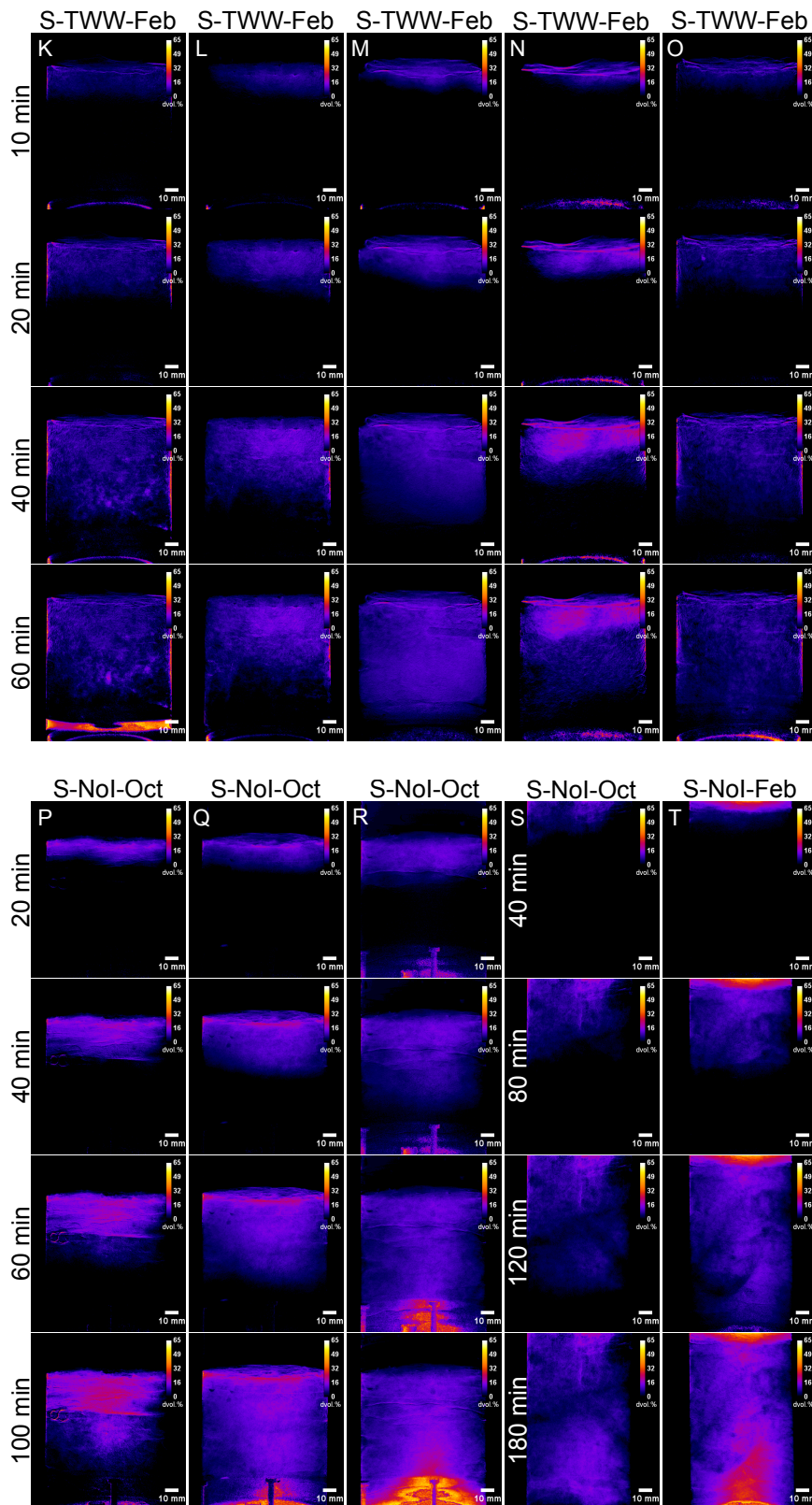
Figure A2: Loamy sand - changes in water content $\Delta\theta$ (vol. %) at field moisture (FW=fresh water, TWW= treated wastewater, NoI=non-irrigated control).
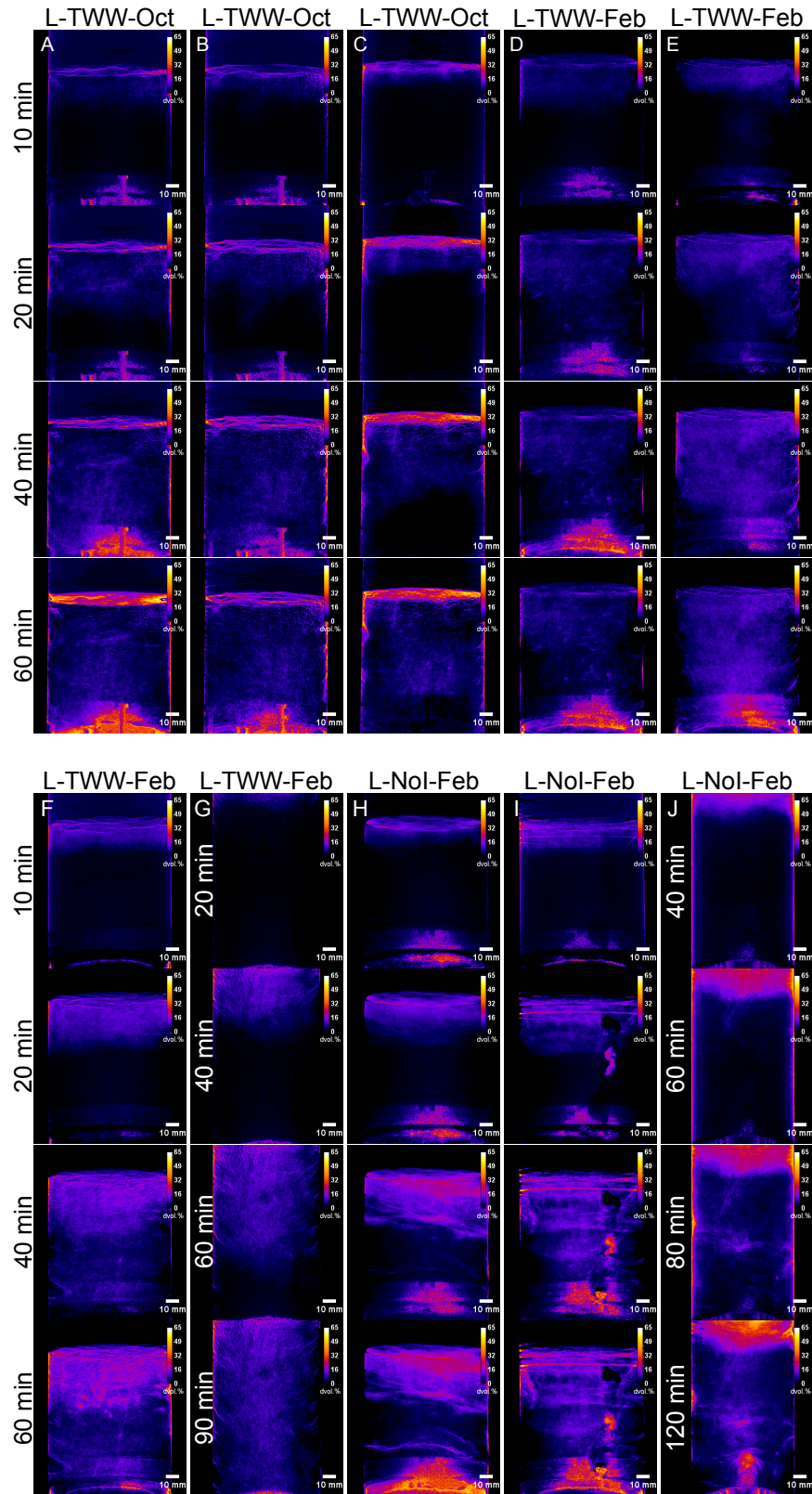
Figure A3: Sandy clay loam - changes in water content Δθ (vol. %) at field moisture (TWW= treated wastewater, NoI=non-irrigated control).
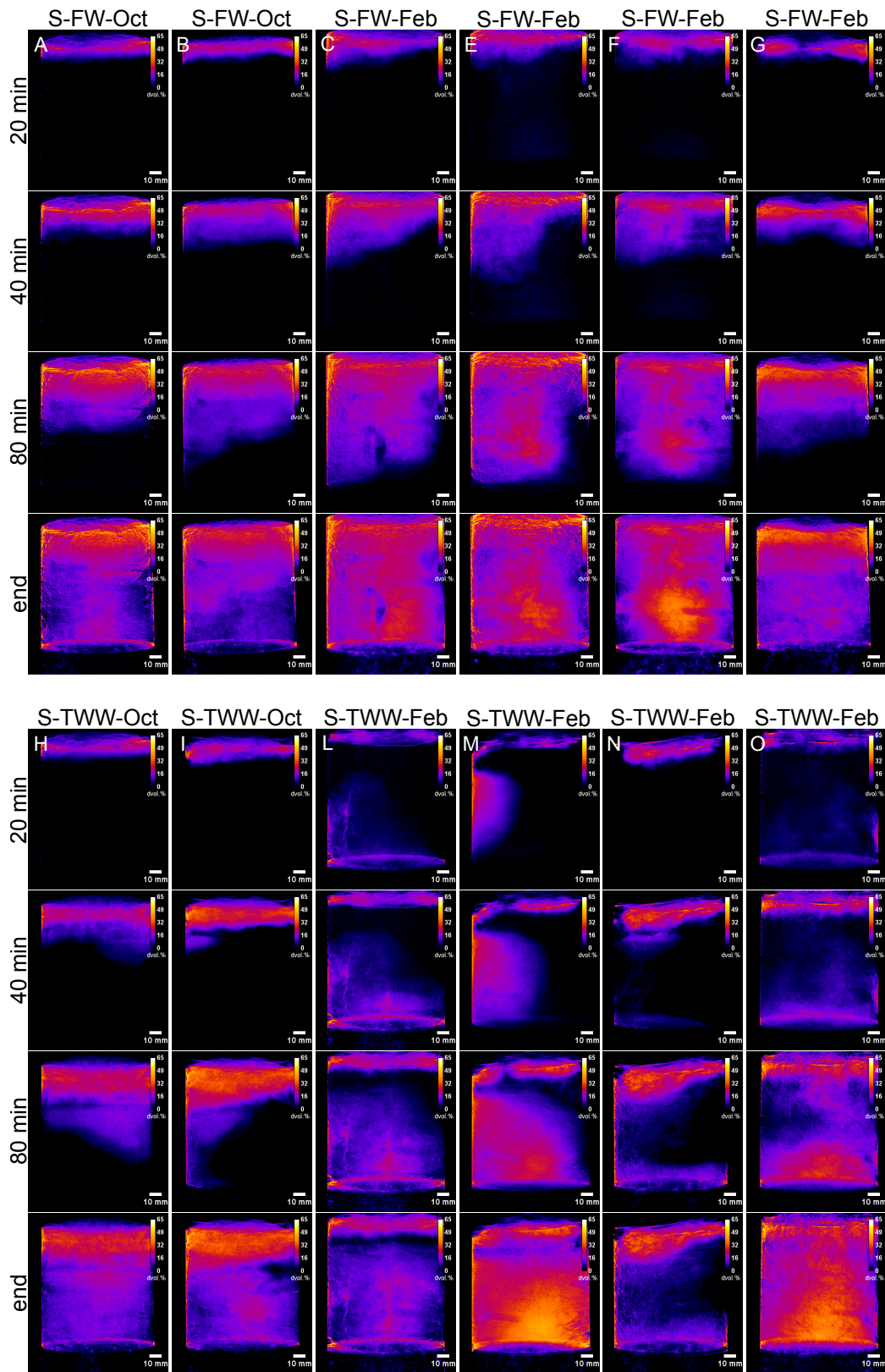
Figure A4: Loamy sand - changes in water content Δθ (vol. %) after 3 days of drying (FW=fresh water, TWW= treated wastewater).
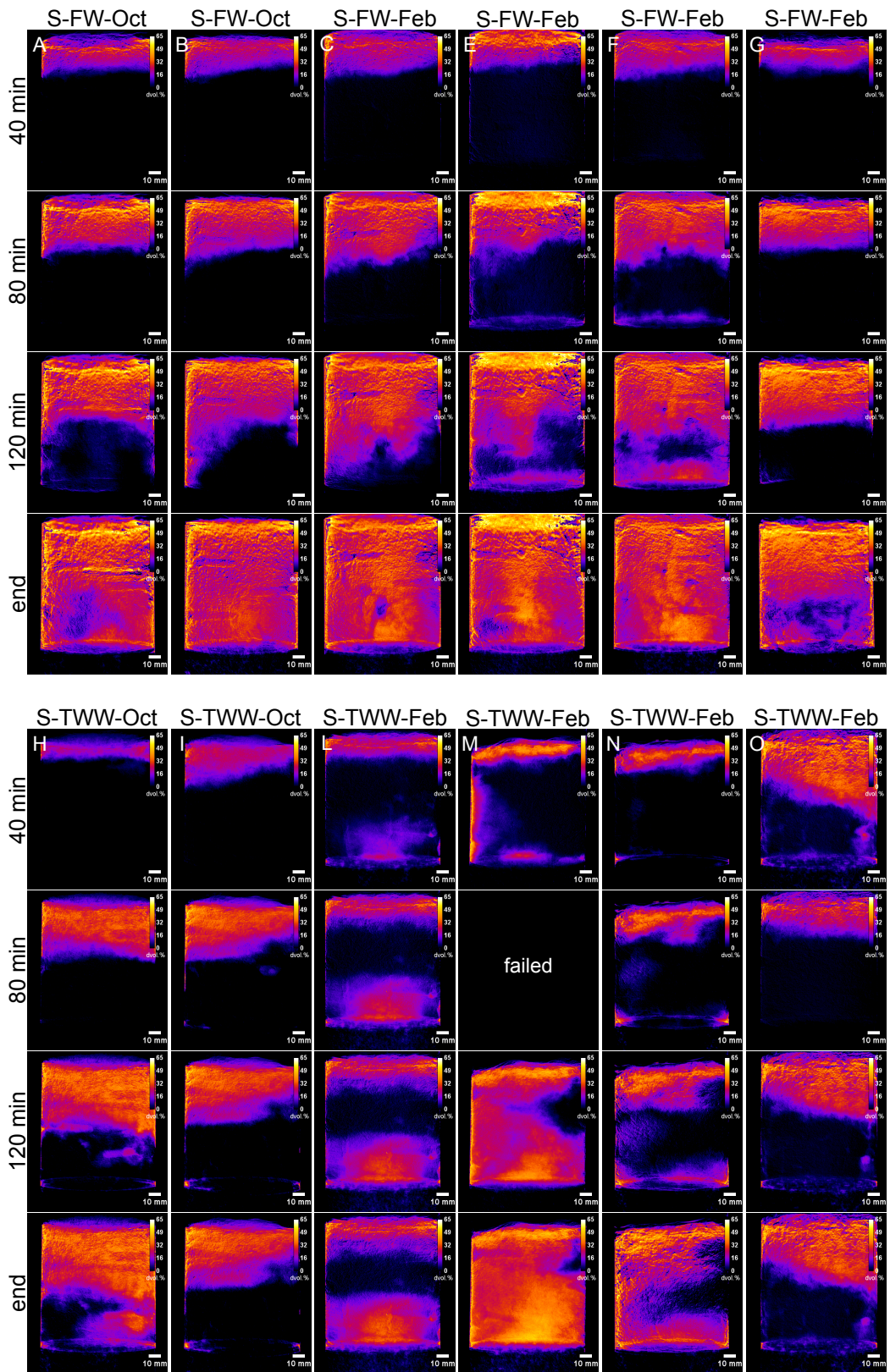
Figure A5: Loamy sand - changes in water content $\Delta\theta$ (vol. %) after 7 days of drying (FW=fresh water, TWW= treated wastewater).

B) Particulate organic matter and physicochemical soil properties

Figure A6 provides the information about particulate organic matter (POM), that was classified for all treatments except for S-NoI where no roots nor litter larger 2 voxels could be found. Except for the absence of visible POM for S-NoI, differences in visible POM content between the other treatments were marginal. The segmented POM covered a volume fraction of 2 to 3 vol. % in S-FW and S-TWW samples, and around 1 vol. % in L-TWW and L-NoI samples. In Figure A6a), POM is shown as depth profiles of the averaged volumetric POM contents for every treatment except for S-NoI. For L-NoI, the soil matrix of the upper 3 cm was mixed with organic litter smaller than the detection limit, so that a clear segmentation of the images was not possible. Therefore, this part was excluded for image analysis. The boxplots in Figure A6b) show the volumetric POM contents of the topmost 10 cm for every sample.

Figure A7 provides the information about the determined physicochemical soil properties illustrated as boxplots: clay content (a), sand content (b), soil acidity (c), salinity (d), and sodicity (e). The ratios of carbon and nitrogen contents are depicted in Figure A7f).
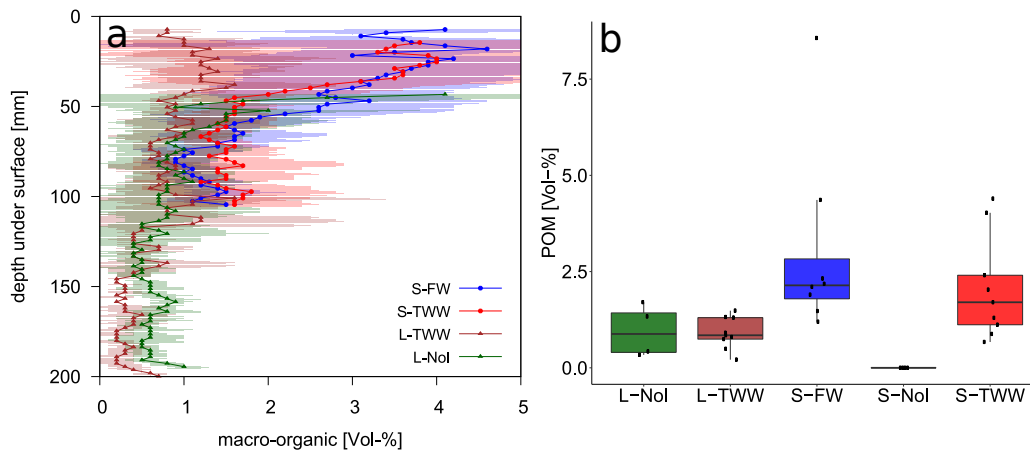
Figure A6: Particulate organic matter (POM) $> 120\,\mu m$ as depth profile (a) and as total volumetric POM content of the 10 cm samples (b). The shaded area margins the 95 % confidence interval of the mean determined by two times standard deviation.
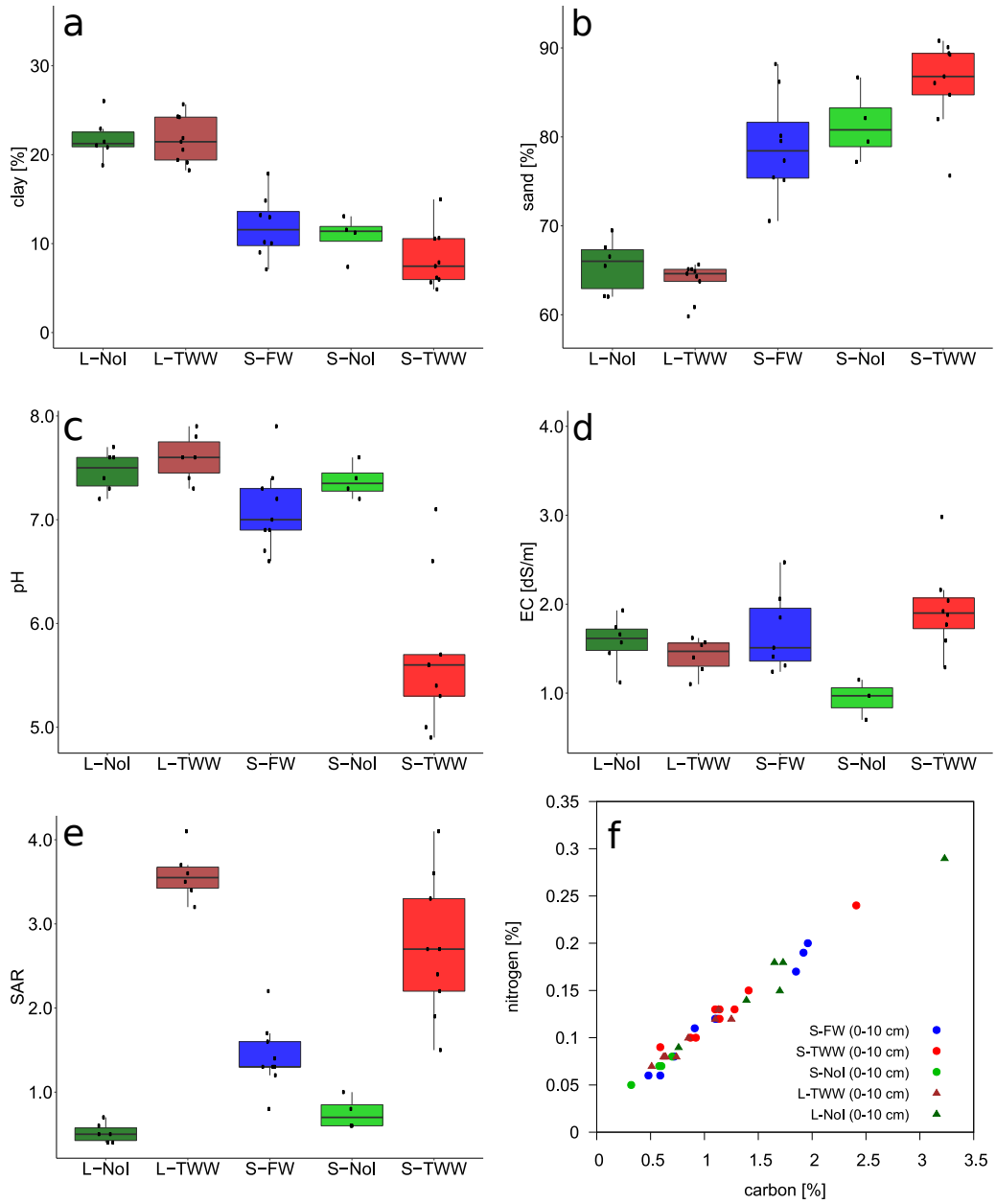
Figure A7: Physicochemical soil properties under different irrigation treatments (sites: S=loamy sand, L=sandy clay loam; treatments: NoI= non-irrigated control, FW=fresh water, TWW=treated wastewater; chemical soil parameters: EC=electrical conductivity, SAR=sodium absorption ratio).

Danksagung/Acknowledgement

Curriculum vitae

Name Frederic Leuther

Ausbildung

2011-2014 M. Sc. Management natürlicher Ressource an der Martin-Luther-Universität Halle-Wittenberg

2013 Masterstudent am International Rice Research Institute Los Banos, Philippinen (Stipendium von der deutschen Gesellschaft für internationale Zusammenarbeit)

2008-2011 B. Sc. Umweltmanagement an der Justus-Liebig-Universität Gießen

2010-2011 Auslandssemester an der Universidad Polytechnica de Valencia, Spanien (ERASMUS-Stipendium)

Beruflicher Werdegang

seit 2018 wissenschaftlicher Mitarbeiter am Helmholtz-Zentrum für Umweltforschung - UFZ in Halle

2015-2018 Doktorand am Helmholtz-Zentrum für Umweltforschung - UFZ in Halle

Halle (Saale), August 21, 2018 . . . .

List of Publications

2019 Leuther, F., Schlüter, S., Wallach, R., Vogel, H.-J. (2019) Structure and hydraulic properties in soils under long-term irrigation with treated wastewater. Geoderma 333. 90-98

2018 Geistlinger, H., Leuther, F. (accepted July 24, 2018) Evaporation study for real soils (sandy soil, loamy sand) based on HYPROP-hydraulic functions and micro-CT-measured pore-size distribution. Vadose Zone J.

Leuther, F., Weller, U., Wallach, R., Vogel, H.-J. (2018) Quantitative analysis of wetting front instabilities in soil caused by treated waste water irrigation. Geoderma 319. 132-141

Weller, U.*, Leuther, F.*, Schlüter, S, Vogel, H.-J. (2018) Quantitative analysis of water infiltration in soil cores using X-ray. Vadose Zone J. 17
(* co-first authorship)

2016 Schlüter, S., Leuther, F., Vogler, S. and Vogel, H.-J. (2016) X-ray microtomography analysis of soil structure deformation caused by centrifugation. Solid Earth 7. 129-140

2015 Klotzbücher, T., Leuther, F., Marxen, A., Vetterlein, D., Horgan, F. G., Jahn, R. (2015) Forms and fluxes of potential plant-available silicon in irrigated lowland rice production (Laguna, the Philippines). Plant Soil 393. 177-191

Eidesstattliche Erklärung / Declaration under oath

Ich erkläre an Eides statt, dass ich die Arbeit selbstständig und ohne fremde Hilfe verfasst, keine anderen als die von mir angegebenen Quellen und Hilfsmittel benutzt und die den benutzten Werken wörtlich oder inhaltlich entnommenen Stellen als solche kenntlich gemacht habe.
I declare under penalty of perjury that this thesis is my own work entirely and has been written without any help from other people. I used only the sources mentioned and included all the citations correctly both in word or content.

Halle (Saale), August 21, 2018   . . . .